



Universität für Bodenkultur Wien  
University of Natural Resources and Life Sciences, Vienna  
Department of Biotechnology

# A comparative study of vector propagation for Lymphocytic Choriomeningitis virus in different mammalian cell lines

Master Thesis

Submitted by  
Andre Philipp, BSc  
Vienna, October 2017

In collaboration with  
HOOKIPA Biotech AG

Supervisor at BOKU: Kunert Renate, Univ.Prof. Dipl.-Ing. Dr.nat.techn.

Supervisor at HOOKIPA: Aspöck Andreas, Dipl.-Ing



# Acknowledgements

Writing this master thesis was one of the biggest steps towards my master's degree in biotechnology. Therefor I really appreciated the opportunity to accomplish this in collaboration with Hookipa Biotech AG, by enabling the work on this interesting topic and also by providing a highly professional working environment. I want to thank my external supervisor Andreas Aspöck, for introducing me to the upstream department, where he provided the perfect supervision and encouragement. In this context I also want to thank my colleague Clemens Schimek for his support during the thesis. Both willingly shared their time to answer all my questions and created a positive atmosphere, which made it a pleasure to work.

I am further especially thankful to my supervisor Professor Renate Kunert, for her experience and support with valuable remarks, engagements and constructive comments through the development of this master thesis.

Last but not least I want to thank my family, friends and especially my parents, which always supported me over many years and encouraged me in my decisions. Without them I wouldn't have achieved all of this.

# Abstract

The development of new therapeutics and vaccines constantly pushes the boundaries of successful treatments against malignant diseases. With increasing understanding of mechanisms in virus biology, the use of viral vectors earned a place in the spotlight as a sophisticated vaccine and therapy platform. An efficient production process has to be established which assures the supply in satisfactory quality and quantities. In order to perpetually improve and optimize the process outcome it is from utmost importance to evaluate promising process alternatives for their suitability for viral vector production. In this master thesis a process using suspension human embryonic kidney (HEK) -293 cells is compared to a possible microcarrier and Fibracel based approach, using adherently growing African green monkey kidney (Vero) cells for the production of Lymphocytic Choriomeningitis virus (LCMV). To increase process knowledge the accurate determination of selected metabolite concentrations is important. Samples containing replication competent virus require inactivation, if measured in biosafety level (BSL) 1 surroundings. The robustness of selected metabolite concentrations for a thermal inactivation protocol for LCMV in different cultivation media was assessed. Further an infection protocol for Vero cells with LCMV has been established in the course of this master thesis. Both evaluations were supported by a Design of Experiment approach. The successful cultivation and infection of Vero cells on Cytodex 1 microcarrier beads was demonstrated and a cell attachment and growth inhibiting factor was found for Vero cells on microcarriers. Subsequently cell growth and LCMV - infection characteristics of Vero cells on said microcarriers and discs were determined and compared to an established infection protocol using suspension HEK-293 cells. From all here introduced cultivation modes the best performing and most suitable process for virus production was evaluated.

# Zusammenfassung

Die Entwicklung neuer Therapeutika und Impfstoffe erweitert laufend die Grenze erfolgreicher Behandlungen gegen heimtückische Krankheiten. Mit dem steigenden Wissen über Virusbiologie haben sich Virale Impfstoffe einen Platz im Rampenlicht als ausgeklügelte Impf- und Therapieplattformen verdient. Um Produktqualität als auch -quantität sicherzustellen muss ein effizienter Produktionsprozess geschaffen werden. Um dabei eine ständige Prozessverbesserung und -optimierung zu gewährleisten ist es von äußerster Wichtigkeit vielversprechende Prozessalternativen für deren Eignung zur viralen Vektorproduktion zu evaluieren. In dieser Masterarbeit wird ein Prozess zur Produktion von Lymphozytären Choriomeningitis Virus (LCMV), mit „Human Embryonic Kidney (HEK) -293“ Suspensionszellen, ursprünglich isoliert aus menschlichen embryonalen Nierenzellen, mit möglichen Microcarrier- und Fibracel-Ansätzen verglichen. Diese verwenden adherent wachsende Vero Zellen, ursprünglich isoliert aus Nierenzellen von Grünen Meerkatzen. Um bestehendes Prozesswissen zu erweitern ist die akkurate Bestimmung von Metaboliten wichtig. Proben, welche replikationsfähigen Virus enthalten, dürfen nicht in einer Umgebung mit Biologischer Schutzstufe 1 gemessen werden, weshalb eine Inaktivierung nötig ist. Die Robustheit der Metabolitenkonzentrationen mit einem thermischen Inaktivierungsprotokoll wurde dafür für verschiedene Kultivierungsmedien beurteilt. Weiters wurde ein Infektionsprotokoll für Vero Zellen mit LCMV etabliert. Beide Auswertungen wurden dabei durch Statistische Versuchplanung unterstützt. Es wurde die erfolgreiche Kultivierung von Vero Zellen auf Cytodex 1 Microcarriern demonstriert und ein Faktor identifiziert, welcher Zellattachement und -wachstum von Vero Zellen auf Microcarriern hemmt. Darauf folgend wurden Zellwachstums- und LCMV-Infektionscharakteristiken auf Microcarriern und Fibracel-Discs bestimmt und mit einem etablierten Infektionsprotokoll mit HEK-293 Suspensionszellen verglichen. Von den hier vorgestellten Kultivierungen wurde der leistungsfähigste Prozess für die LCMV-Virusproduktion evaluiert.

# Content

1 Abbreviations and Units.....	1
1.1 Abbreviations.....	1
1.2 Units.....	3
1.3 Variables .....	3
2 Introduction.....	4
2.1 Vaccine history & viral vectors.....	4
2.2 Lymphocytic choriomeningitis virus .....	5
2.3 Viral vector production.....	7
2.4 Cells .....	8
2.4.1 HEK-293 cells .....	9
2.4.2 Vero cells .....	9
2.5 Adherent cultivation versus suspension cultivation for viral vaccine production .....	10
3 Aim .....	12
4 Material and Methods .....	13
4.1 Material .....	13
4.1.1 Equipment.....	13
4.1.2 Disposables.....	13
4.1.3 Software .....	14
4.1.4 Reagents.....	14
4.1.5 Buffer .....	15
4.1.6 Kits .....	15
4.1.7 Enzymes .....	15
4.1.8 Medium .....	15
4.2 Methods.....	15
4.2.1 Host cell lines .....	15

4.2.1.1 HEK-293 cells .....	15
4.2.1.2 Vero cells .....	16
4.2.2 Preparations .....	16
4.2.2.1 Medium preparation .....	16
4.2.2.2 Microcarrier preparation .....	16
4.2.2.3 Support growth matrix preparation .....	17
4.2.3 Cell culture methods .....	17
4.2.3.1 Passaging of suspension cells .....	17
4.2.3.2 Passaging of adherent cells .....	17
4.2.4 Sampling scheme .....	18
4.2.4.1 Sampling of suspension cultivation .....	18
4.2.4.2 Sampling of adherent cultivation .....	19
4.2.5 Infection of cells with LCMV .....	19
4.2.6 Thermal inactivation of replication competent LCMV samples for metabolite assays .....	20
4.2.7 Experimental set-ups .....	20
4.2.7.1 Alteration of metabolite concentrations of PF26#278 during thermal inactivation of LCMV for metabolite assays I .....	21
4.2.7.2 Alteration of metabolite concentrations of PF26#278 during thermal inactivation of LCMV for metabolite assays II .....	23
4.2.7.3 Alteration of metabolite concentrations of VP-SFM and PF26#280 during thermal inactivation of LCMV for metabolite assays .....	23
4.2.7.4 Influence of Glutamine and L-alanyl-L-glutamine on Vero cell growth characteristics .....	24
4.2.7.5 Determination of an optimized MOI and SCD of adherently growing Vero cells .....	25
4.2.7.6 Proof of Concept for infection of adherently growing Vero cells with LCMV .....	26

4.2.7.7 Initial cultivation and infection of Vero cells on microcarriers in shake flasks .....	27
4.2.7.8 Evaluation of cell growth inhibiting factors on Vero cells in microcarrier cultivation.....	27
4.2.7.9 Adapted cultivation and infection of Vero cells on microcarriers in shake flasks .....	28
4.2.7.10 Cultivation and infection of Vero cells on Fibracel in shaker flasks ..	29
4.2.7.11 Current infection protocol using suspension HEK-293 cells.....	30
4.2.8 Analytical methods .....	30
4.2.8.1 pH and dissolved gas analysis via Stat Profile® pHox® Analyzer .....	30
4.2.8.2 Cell count via LUNA™ Automated Cell Counter .....	31
4.2.8.3 Nuclei count of Vero cells on microcarrier via LUNA™ Automated Cell Counter .....	31
4.2.8.4 Nuclei count of Vero cells on Fibracel discs via LUNA™ Automated Cell Counter .....	32
4.2.8.5 Metabolite assay .....	32
4.2.8.6 Focus Forming Unit Assay .....	33
4.2.9 Calculations.....	34
4.2.9.1 Passaging of suspension cells .....	34
4.2.9.2 Passaging of adherent cells .....	35
4.2.9.3 Viral infection volume for suspension cells .....	35
4.2.9.4 Viral infection volume for adherent cells .....	35
4.2.9.5 Specific growth rate .....	36
4.2.9.6 Specific metabolic rates for suspension cells.....	36
4.2.9.7 Specific metabolic rates for adherent cells.....	37
4.2.9.8 Specific viral titer of suspension cells.....	37
4.2.9.9 Specific viral titer of adherent cells .....	37
4.2.9.10 Viral yield .....	38
5 Results.....	39

5.1 Alteration of metabolite concentrations of PF26#278 during thermal inactivation of LCMV for metabolite assays I.....	39
5.2 Alteration of metabolite concentrations of PF26#278 during thermal inactivation of LCMV for metabolite assays II.....	41
5.3 Alteration of metabolite concentrations of VP-SFM and PF26#280 during thermal inactivation of LCMV for metabolite assays.....	43
5.4 Influence of Glutamine and L-alanyl-L-glutamine on Vero cell growth characteristics .....	45
5.5 Determination of an optimized MOI and SCD of adherently growing Vero cells .....	51
5.6 Proof of Concept for infection of adherently growing Vero cells with LCMV ....	53
5.7 Initial cultivation and infection of Vero cells on microcarriers in shake flasks ..	55
5.8 Evaluation of cell growth inhibiting factors on Vero cells in microcarriers cultivation .....	57
5.9 Cultivation and infection of Vero cells on microcarriers in shake flasks.....	60
5.10 Cultivation and infection of Vero cells on Fibracel discs .....	65
5.11 Suspension infection process using HEK-293 cells.....	69
6 Discussion .....	72
6.1 Alteration of metabolite concentrations of PF26#278 during thermal inactivation of LCMV for metabolite assays I.....	72
6.2 Alteration of metabolite concentrations of PF26#278 during thermal inactivation of LCMV for metabolite assays II.....	72
6.3 Alteration of metabolite concentrations of VPSFM and PF26#278 during thermal inactivation of LCMV for metabolite assays.....	73
6.4 Influence of Glutamine and L-alanyl-L-glutamine on Vero cell growth characteristics .....	73
6.5 Determination of an optimized MOI and SCD of adherently growing Vero cells .....	75
6.6 Proof of Concept for infection of adherently growing Vero cells with LCMV ....	75
6.7 Initial cultivation and infection of Vero cells on microcarriers in shake flasks ..	76



6.8 Evaluation of cell growth inhibiting factors on Vero cells in microcarriers cultivation .....	76
6.9 Cultivation and infection of Vero cells on microcarriers in shake flasks.....	77
6.10 Cultivation and infection of Vero cells on FibraCel discs in shake flasks.....	78
6.11 Suspension infection process using HEK-293 cells.....	78
6.12 Viral titers of different cultivation modes .....	79
6.13 General considerations regarding the production process .....	80
6.13.1 Timeframes for production .....	80
6.13.2 Required amount of cell substrate.....	81
6.13.3 Product quality & Safety aspects.....	82
6.13.4 Amount of process steps.....	82
6.14 General considerations regarding experimental set-ups .....	83
6.14.1 Choice of medium .....	83
6.14.2 Process changes which may affect the design space .....	83
6.14.3 Comparison between cell counting methods.....	84
6.14.4 Performance of FibraCel discs .....	84
6.15 Future prospective.....	84
6.16 Conclusio.....	86
7 References .....	88
7.1 List of Figures.....	88
7.2 List of Tables .....	94
7.3 List of Pictures.....	94
7.4 Bibliography.....	95
8 Appendix.....	98

# 1 Abbreviations and Units

## 1.1 Abbreviations

ATCC	American Type Culture Collection
BSL	Biosafety level
CTL	Cytotoxic T lymphocytes
DMEM	Dulbecco's Modified Eagle Medium
DoE	Design of Experiment
ECACC	European Collection of Authenticated Cell Cultures
EMA	European Medicines Agency
FCS	Fetal Calf Serum
FFU	Foci Forming Unit
G-6-P	Glucose-6-phosphate
G-6-PDH	Glucose-6-phosphate dehydrogenase
GMP	Good Manufacturing Practice
GOD	L-glutamate oxidase
GP	Glycoprotein
HEK	Human Embryo Kidney
HK	Hexokinase
hpi	Hours post infection
hps	Hours post seeding
HRP	Horse radish peroxidase
IGR	Intergenic region
L	Large Segment
LCMV	Lymphocytic choriomeningitis virus
Ln(...)	Natural logarithm
LOD	Lactate oxidase
Log(...)	Decadic logarithm
L-ORF	RNA-dependent RNA polymerase
MC	Microcarrier
MCB	Master cell bank
MOI	Multiplicity of infection
NP	Nucleoprotein

## Abbreviations and Units

ORF	Open reading frame
PBS	Phosphate buffered saline
pCO <sub>2</sub>	Dissolved carbon dioxide partial pressure
pO <sub>2</sub>	Dissolved oxygen partial pressure
PoC	Proof of Concept
POD	Peroxidase
Q <sub>2</sub>	Estimate for the future prediction
R <sup>2</sup>	Coefficient of determination
rLCMV	Replication-deficient LCMV
RNA	Ribonucleic acid
SA	Surface area
SCD	Seeding cell density
UTR	Untranslated region
VCD	Viable cell density
Vero	African green monkey cells
VP-SFM	Virus production serum free medium
vRNP	Viral ribonucleoprotein
WCB	Working cell bank
WV	Working volume
Z	Small RING finger protein

## 1.2 Units

°C	Degree Celsius
μL	Microliter [ $10^{-6}$ L]
μm	Micrometer [ $10^{-6}$ m]
cm	Centimeter [ $10^{-2}$ m]
FFU/mL	Foci forming units per milliliter
g	Gram
g/L	Mass concentration
h	Hours
M	Molarity [mol/L]
mg	Milligram [ $10^{-3}$ g]
min	Minute
mM	Millimolar [ $10^{-3}$ mol/L]
rpm	Rounds per minute
s	Seconds
x g	Times earth gravitational force

## 1.3 Variables

$\mu$	Specific growth rate	$\text{h}^{-1}$
$q_{\text{Glc}}$	Specific Glucose consumption rate	mol/cell/hour
$q_{\text{Gln}}$	Specific Glutamine consumption rate	mol/cell/hour
$q_{\text{Lac}}$	Specific Lactate production rate	mol/cell/hour
$q_{\text{NH}_4}$	Specific Ammonia production rate	mol/cell/hour
$Y_{\text{Lac/Glc}}$	Lactate to Glucose Yield	mol/mol
$Y_{\text{NH}_3/\text{Gln}}$	Ammonia to Glutamine Yield	mol/mol

## 2 Introduction

### 2.1 Vaccine history & viral vectors

The first vaccines used were whole live virus, derived from human-to human or animal-to-human transfer, such as Edward Jenner's cowpox pus inoculation in 1796, intended to immunize against the more pathogenic smallpox in humans. The word vaccination (Latin: vaccinus = cow) originated from this first vaccine, since it was derived from virus affected cows. Production methods then advanced to live attenuated virus vaccines produced in vivo or in ovo (Josefsberg and Buckland, 2012). The beginnings of modern cell culture based industry were marked by the first in vitro cultivation of a viral vaccine against polio virus in non-neural human cells by Enders in 1949, followed by Salk's inactivated polio vaccine in primary monkey kidney cells in 1955 (Aunins et al., 2011).

Recent discoveries that led to increased understanding of viral molecular biology and genetics has rendered the use of viruses as vaccine platforms and as cancer therapies (Choi and Chang, 2013). The concept of the viral vector was introduced in 1972 by Jackson et al. Since then several types of viral vectors have been developed, and they have been used in animal studies and clinical trials (Ura et al., 2014). Viral vectors used as live recombinant vectored vaccines are live viruses (the vector) that express a heterologous antigen(s). A live recombinant vectored vaccine can also be genetically modified for other reasons, e.g. attenuation (EMA, 2010). The specific properties of a vector are determined by the virus from which it derives (Ura et al., 2014). Viral vector utility is based on the ability of viruses to infect cells. In general, the advantages of viral vectors are as follows: (a) high efficiency gene transduction for production; (b) highly specific delivery of genes to target cells after vaccination; and (c) induction of robust immune responses, and increased cellular immunity (Ura et al., 2014). Viral vectors allow simultaneous expression of multiple antigenic determinants while avoiding the safety risks associated with the use of the whole pathogenic virus (Lininger et al., 2007). Viral vectors have the advantage of being capable of inducing both antibody and T-cell-mediated immunity in the absence of an adjuvant, do not require complex purification development, may be able to generate antigens with native conformation, and may be able to deliver more than one gene (Li et al., 2007). With potential targets ranging from different manifestations of cancer to a vast number of infectious diseases, the benefits resulting from successful application of viral vectors to prevent and treat

human diseases can be immense (Choi and Chang, 2013). The development of viral vectors requires a high biological safety level in order to gain public acceptance. Therefore, non- (or low-) pathogenic viruses are often selected. In most cases, viruses are genetically engineered to reduce or eliminate pathogenicity. Additionally, most viral vectors are replication-defective (Ura et al., 2014).

## 2.2 Lymphocytic choriomeningitis virus

Arenaviruses are divided into two groups, Old World and New World arenaviruses (see Figure 1), based on geographical, serological, and phylogenetic differences (Urata and Yasuda, 2012). Lymphocytic choriomeningitis virus (LCMV) was the first isolated arenavirus, discovered in 1933, during the study of samples from a St. Louis encephalitis epidemic. As outlined in Figure 1 it belongs to the Old World arenaviruses. Since more than 80 years, arenaviruses have provided important model systems for the study of host–virus interactions. The study of these models has illuminated a wide range of principles in virus biology and pathogenicity, including persistent infection, virus-induced immunopathologic disease, cytotoxic T-cell recognition, and immunological memory. Natural hosts are *Mus domesticus* and *Mus musculus*. The clinical picture of an infection is usually recognized as aseptic meningitis. Its most rarely diagnosed clinical form is febrile illness without neurologic involvement. More severe central nervous system disease occasionally occurs (Knipe and Howley, 2013).

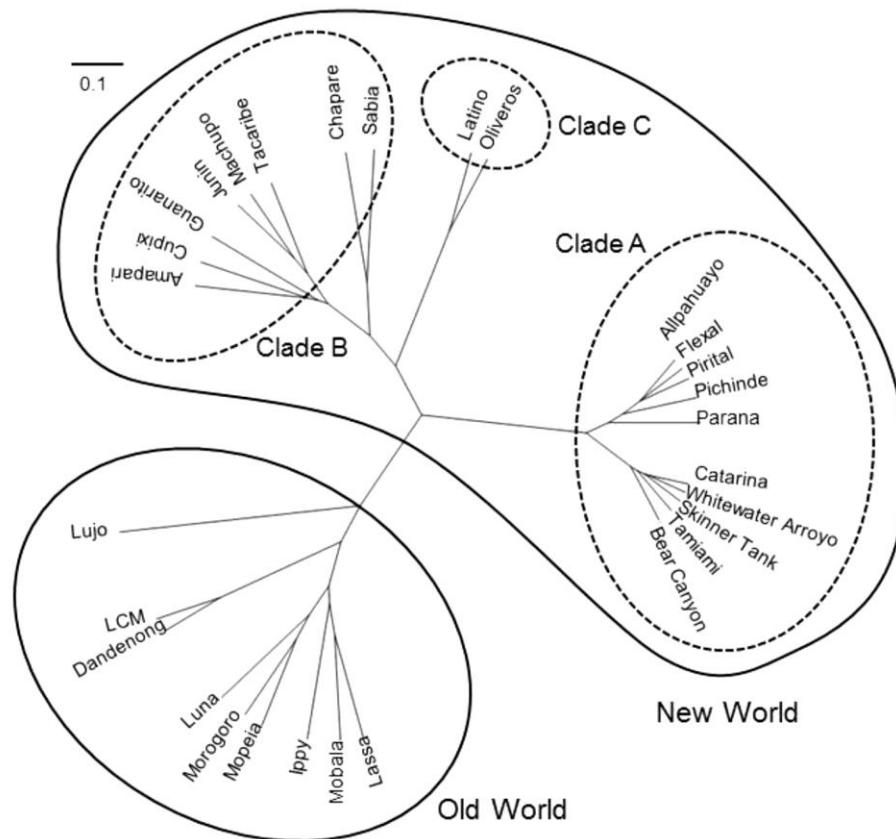


Figure 1: Phylogenetic tree of arenavirus Z protein (from Urata and Yasuda, 2012)

Arenavirus virions are pleomorphic ranging in size from 40 to more than 200 nm in diameter and contain a surface envelope that is studded with evenly spaced spikes that correspond to glycoprotein (GP) (Knipe and Howley, 2013). They contain a bi-segmented negative stranded RNA genome. Each RNA segment uses an ambisense coding strategy to direct the expression of two viral proteins in opposite orientations which are separated by a non-coding intergenic region (IGR). The large segment (L-Segment; 7.2 kb) encodes the L protein, a RNA-dependent RNA polymerase, and the small RING finger protein Z, which serves as a matrix protein. The small segment (S-Segment; 3.5 kb) encodes the viral nucleoprotein (NP) and surface glycoprotein (GP) (Ortiz-Riano et al., 2013). The segments are each enclosed by the 5' and 3' untranslated region (UTR).

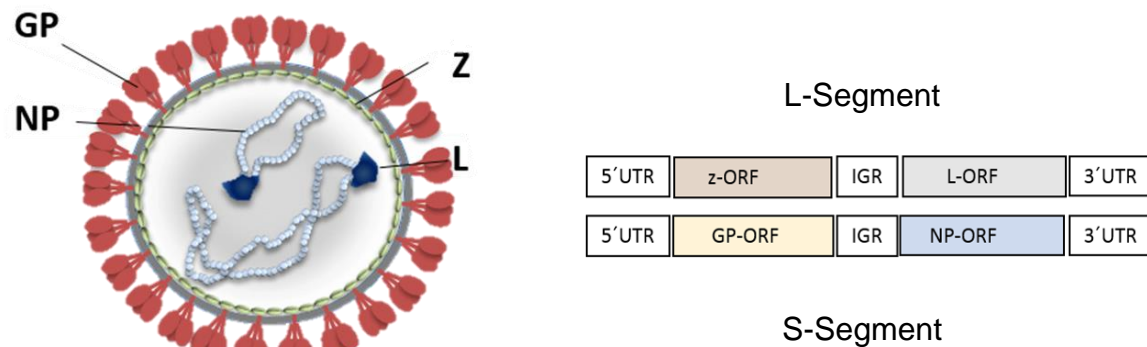


Figure 2: Left: Schematic graphic of LCMV; Right: RNA genome of LCMV (graphic by Klaus Orlinger, PhD, Hookipa Biotech AG)

Consistent with the broad host range and cell-type tropism, the highly conserved and widely expressed cell-surface protein  $\alpha$ -dystroglycan has been identified as the main receptor for LCMV. Upon receptor binding, arenavirus virions are internalized by smooth-walled vesicles into a low-pH subcellular environment that triggers a pH-dependent membrane fusion step between cell and viral membranes which results in the release of the viral ribonucleoprotein (vRNP) into the cytoplasm of the cell where viral RNA synthesis, transcription and replication take place (Knipe and Howley, 2013). Translated NP, L, and Z are gathered together with vRNP and cellular surface GP, and then pinched off from the surface of infected cells (Urata and Yasuda, 2012).

LCMV-induced T cell responses are broad and long-lived, and LCMV infection has been widely studied as a model of cytotoxic T lymphocytes (CTL) - mediated protection. Possible applications for a replication-deficient LCMV (rLCMV) include protective vaccines, for example, against HIV, hepatitis C virus, tuberculosis and malaria, as well as cancer immunotherapy. rLCMV represents an attractive vector for stimulating both cellular and humoral immunity. Thus, it provides a platform that may be used to prevent or treat malignant and infectious diseases for which other existing viral vector vaccination strategies, which were compared by Flatz et al. in 2010, have yet to confer protection.

## 2.3 Viral vector production

Viral vectors are derived from viruses that naturally infect human cells or other mammalian cells, thus their production is essentially using animal cell cultures and for



some systems, insect cell cultures. Therefore, animal cell culture processes, involving cell culture bioreactors are needed for the industrial production of viral vectors (Merten et al., 2014).

In a conventional batch setting, the production of viral vectors involves the following steps: growing the cells to a desired cell density for infection, infecting with a virus seed stock at predetermined optimal multiplicity of infection (MOI), the ratio of infective particle to host, and finally harvesting the virus at an optimal time post infection. With respect to the particular design of the upstream process some steps may change accordingly. In order to minimize the amount of virus stock and to get batch-to-batch reproducibility, it is recommended to determine the lowest possible MOI to obtain the optimal virus yields (Merten et al., 2014).

## 2.4 Cells

Many viral vaccines were originally produced in primary cell lines, which are cells obtained directly from animal organs and tissues. This primary cell cultures had been subjected to a very limited number of subcultures owing the very short lifespan of such cultures. The main sources of primary cells were primates, chicken or duck embryos, hamsters and rabbits. Primary cell culture systems suffered from the disadvantage of inconsistent starting material and concerns about contamination with adventitious agents. Cells have been used for the production of Salk's inactivated poliovirus vaccine (Barrett et al., 2009). With the exception of primary chick embryo cells, the use of primary cells should be avoided or their use fully justified (EMA, 2010).

As a next step in the development of cell culture for vaccine production human diploid cell lines were used to avoid the difficulties associated with the use of primary tissue (Barrett et al., 2009). Diploid cells are derived from primary cultures and can be serially passaged, although they retain their anchorage dependence and limited lifespans (40–60 passages) (Sureau, 1987). Diploid cell lines are defined as having a finite in vitro lifespan in which the chromosomes are paired and are structurally identical to those of the species from which they are derived. Diploid cell lines have been used for the manufacture of a number of vaccines, such as hepatitis A, rubella and rabies. (Barrett et al., 2009).

Continuous cell lines originate from diploid cells that have undergone a chromosomal transformation to allow them to divide indefinitely (Josefsberg and Buckland, 2012).

For many years these cell lines were not considered to be suitable substrates for the production of human medicine products, due to their indefinitely lifespan and as such tumorigenic potential. As new techniques in immunology, virology and molecular biology were developed, a WHO Study Group concluded in 1986, that continuous cell lines were acceptable for the production of biologicals (Barrett et al., 2009). In the topic of this master thesis HEK-293 and Vero cells were compared for their virus production performance.

### 2.4.1 HEK-293 cells

The original 293 cells were derived in 1973 from the kidney of an aborted human embryo of unknown parenthood by transformation with sheared Adenovirus 5 DNA (Lin et al., 2014). The HEK-293 cell line has been widely used for over 30 years by the scientific community, mainly for the production of viral vectors used for gene and cell therapy. HEK-293 cells have also been validated as an efficient platform for the large-scale production of r-proteins and viral vectors by transient transfection in serum-free suspension culture (Durocher et al., 2002; Pham et al., 2005). It offers the advantage to be easily grown in suspension at high cell density (up to  $10^7$  cells/mL in batch mode) and in serum-free medium (Côté et al., 1998). Numerous viral vectors produced in HEK-293 cells are currently evaluated in phase II/III clinical trials. This is an indication of a good safety profile and possibly fast regulatory clearance for use of HEK-293 cell in manufacturing of biologics (Le Ru et al., 2010).

### 2.4.2 Vero cells

Vero cells were originally isolated from the kidney of a normal (i.e., non-diseased) adult African green monkey on March 27, 1962 by Y. Yasumura and Y. Kawakita at the Chiba University in Chiba, Japan. At its 93rd passage, the cell line was brought to the National Institute of Allergy and Infectious Diseases at the National Institutes of Health in the United States, and was provided to the American Type Culture Collection (ATCC) in 1966. By the end of the 1960s, Vero cell lines were being used across the globe, primarily in virology laboratories (Ammerman et al., 2008). It is currently the most widely accepted cell substrate by regulatory authorities for vaccine development due to the fact that Vero-derived human vaccines have been in use for nearly 30 years (Josefsberg and Buckland, 2012). They can be grown and infected on microcarrier beads in large-scale fermenters (6,000 L reported) and in serum-free medium with no loss in productivity (Barrett et al., 2009). Several innovative vaccines produced in Vero

cells have been licensed including the smallpox vaccine ACAM2000 (Sanofi Pasteur, Lyon, France) and the pediatric rotavirus vaccines Rotateq (Merck, Whitehouse Station, NJ) and Rotarix (GSK, Brentford, Middlesex, UK), all of which are live attenuated virus vaccines. Also produced from Vero cells is the H5N1 pandemic influenza vaccine Preflucel (Baxter, Deerfield, IL) and the Japanese encephalitis vaccine Ixiaro (Valneva, Vienna, Austria), both produced from inactivated virus (Josefsberg and Buckland, 2012).

## 2.5 Adherent cultivation versus suspension cultivation for viral vaccine production

The key difference between anchorage dependent and suspension cells from a process standpoint is the way of subculturing or passaging the cells. This can be as simple as dilution of the suspension cells in fresh medium or as complicated as detaching the anchorage dependent cells from a surface and plating them on a new surface in fresh medium (Merten et al., 2014). The benefit of using adherent cells lies in the easy medium exchange, but comes at the cost of the growth surface being a limiting factor (Genzel, 2015).

Some viruses need cell-to-cell contact to spread, and some viruses that spread via syncytia need an orientation of cells. In these cases, a process with adherent cell growth is advantageous. For all other viruses, suspension cell growth allows for easier and faster scale-up, and limits costs and the risk of contamination by microcarrier handling (Genzel, 2015).

Certain applications, such as vaccine production, may require the scale-up of Vero cell cultures. There are numerous growth systems used for the scale-up of anchorage-dependent cell lines: roller bottles, T-Flasks, cell factories, microcarriers, and fixed bed reactors. Roller bottles are cylindrical vessels, and the cells grow on the inner surface of the tube. The bottles slowly revolve to continually bathe the cells in growth medium. T-Flasks are rectangular flasks, where cells are cultivated in static conditions, on the bottom surface of the flask. This cultivation concept can be scaled up by increasing the number of bottom layers per flask. These cell factories can contain up to 40 surface layers and a surface of 2.6 m<sup>2</sup> per vessel. The surface area available for cell attachment can be even further increased by growing the cells on microcarrier beads.

The beads, usually around 0.2 mm in diameter, can be made of dextran, cellulose, gelatin, glass, silica and plastic (Ammerman et al., 2008).

The main disadvantages are certainly the fact that surface adherent cells can only be cultured in the stirred tank reactor system either after adaptation to growth in suspension or after establishment of a microcarrier culture system which is less straightforward to use in comparison to suspension cell cultures. Adverse hydrodynamic effects on cells grown on microcarriers in stirred tank bioreactor can lead to cell removal from the carriers, reduced cell growth, and cell death and may impact the cell metabolism. In such a case, other systems, in which the cells are protected from hydrodynamic stress, such as fixed bed reactor systems, are used (Merten et al., 2014). Possible drawbacks of the use of microcarrier are labor intensive preparing and washing steps before use and the high cell density (*Microcarrier Cell Culture Principles and Methods*, 2013). Finally cells can be cultivated in packed bed reactors, where cells attach to a fixed support growth matrix. With the high amount of already retained cells this cultivation mode is often operated in perfusion mode. In this master thesis the production of LCMV using HEK-293 cells adapted to growth in suspension and anchorage dependent Vero cells are compared. The performance of Vero cells will be investigated in static, on T-flasks, and dynamic cultivation, on microcarriers.

### 3 Aim

The generation of a high viral titer determines heavily the final amount of obtainable vaccine doses per production run. To accomplish such a task it is important to evaluate the performance of other promising cell platform alternatives to maximize the product yield and optimize the production process, as different cell lines and cultivation modes show advantages and disadvantages. The aim of this master thesis is to compare the performance of a suspension cultivation approach using HEK-293 cells for the production of LCMV versus a promising microcarrier based approach using African green monkey kidney cells. The determination of selected metabolite concentrations is important to increase process knowledge. Samples containing replication competent virus require inactivation, if measured in BSL 1 surroundings. The robustness of the metabolites Glucose, Glutamine, Lactate, and Ammonia during thermal inactivation was assessed in this master thesis.

## 4 Material and Methods

### 4.1 Material

#### 4.1.1 Equipment

Aspirator	Integra
Balance	Kern
Cedex Bio Analyzer	Roche
Cell Culture Incubator	Binder
Celltron	InforsHT
Centrifuge	Hettich
4°C Fridge	Liebherr
-20°C Freezer	Liebherr
-80°C Freezer	Panasonic
50 mL Glass Bottle	Schott Duran
100 mL Glass Bottle	Schott Duran
250 mL Glass Bottle	Schott Duran
Laminar Flow Hood	Kojar
Luna Automated Cell Counter	Logos
Microscope TS100	Nikon
Pipet boy	Integra
Stat Profile® pHox® Analyzer	Nova Biomedical
Stirrer	2Mag
Vortex	IKA
Water bath	VWR

#### 4.1.2 Disposables

Aspiration pipette 2 mL	Corning, Inc.	9099
Cell culture Flask 175 cm <sup>2</sup>	NUNC	155910
Cell culture Flask 75 cm <sup>2</sup>	PPT	90076
15 mL Conical Centrifuge Tubes	Corning, Inc.	352196
50 mL Conical Centrifuge Tubes	Corning, Inc.	352070
Cryo Vials	NUNC	375418

## Material and Methods

Cytodex 1 microcarrier beads	GE Healthcare	M1292-9984
Easy Tear Cleansteam Bag	Pall	TH1ET6P0000-0003
Fibra-Cel® Disks	Eppendorf	M1292-9984
LUNA™ Cell Counting Slides	Logos	L12001
Pipette tips 1000 µL	Eppendorf	022491253
Pipette tips 20 µL	Eppendorf	022491270
Pipette tips 200 µL	Eppendorf	022491296
Serological pipette 10 mL	Corning, Inc.	357551
Serological pipette 100 mL	Corning, Inc.	357600
Serological pipette 2 mL	Corning, Inc.	357507
Serological pipette 5 mL	Corning, Inc.	357543
Serological pipette 25 mL	Corning, Inc.	357525
Serological pipette 50 mL	Corning, Inc.	357550
125 mL Shaker Flask	Corning, Inc.	431143
250 mL Shaker Flask	Corning, Inc.	431144
500 mL Shaker Flask	Corning, Inc.	431147

### 4.1.3 Software

Cedex Bio V2.1.1.1630	Roche
Luna 2.5.4	Logos
MODDE 10.1.1 (Build 1193) , Nov 2014	Umetrics AB
ProgRes® CapturePro 2.10.0.0	Jenoptik

### 4.1.4 Reagents

Citric Acid	Sigma-Aldrich	25127-500G
Crystal violet	Sigma-Aldrich	V5265-250ML
L-alanyl-L-glutamine	Gibco	35050061
Glutamine	Gibco	25030081
Sigmacote®	Sigma-Aldrich	SL2-100ML
Sodium Hydroxide, 0.5 M	Sigma Aldrich	06203-1KG
Triton X-100	Sigma-Aldrich	T8787-250ML

Trypan blue solution 0.4%	Sigma-Aldrich	T8154
---------------------------	---------------	-------

### 4.1.5 Buffer

Nuclei Counting Solution	In-house	<ul style="list-style-type: none"> <li>○ Citric Acid 0.1 M</li> <li>○ Crystal Violet 0.1 %</li> <li>○ Triton X-100 1%</li> <li>○ 0.2 µm filtration</li> <li>○ Storage at 4 °C</li> </ul>
--------------------------	----------	------------------------------------------------------------------------------------------------------------------------------------------------------------------------------------------

PBS Buffer (1x)	PAA	H15-002
-----------------	-----	---------

### 4.1.6 Kits

Glucose Bio	Roche	06 343 732 001
Glutamine	Roche	06 408 150 001
Lactate Bio	Roche	06 343 759 001
NH3 Bio	Roche	06 343 775 001

### 4.1.7 Enzymes

StemPro® Accutase® Cell Dissociation Reagent	Gibco	A6964-100ML
-------------------------------------------------	-------	-------------

### 4.1.8 Medium

VP-SFM (1X)	Gibco	11681020
PF26#278	In-house	n/a
PF26#280	In-house	n/a

## 4.2 Methods

### 4.2.1 Host cell lines

#### 4.2.1.1 HEK-293 cells

Cells were sourced from a bank established at the ATCC (American Type Culture Collection) at passage 34. One vial was thawed, adapted to serum free conditions and



eventually banked as GMP-MCB and WCB. Cells derived from the WCB were used for these experiments.

### 4.2.1.2 Vero cells

Vero cells (*Vero (AC-free) (ECACC 08011101)*) were obtained from the ECACC (European Collection of Authenticated Cell Cultures) at passage 21. 5 passages post thawing a WCB was generated in house. Cells derived from this WCB (Passage 21.5) were used for experiments in this master thesis. By supplier information Vero cells were adapted to grow adherently in animal component free medium. A certificate of analysis by ECACC can be found in 8 Appendix Figure 42 to Figure 44.

## 4.2.2 Preparations

### 4.2.2.1 Medium preparation

Each medium used for the routine cell culture and experiments was supplemented with L-Alanyl-L-Glutamine up to a final concentration of 4 mM. Upon sterile formulation in the laminar flow hood, the supplemented medium was stored at 4 °C. Prior use the medium was tempered to 37 °C using a water bath.

### 4.2.2.2 Microcarrier preparation

Cytodex 1 microcarrier are based on a cross-linked dextran matrix which is substituted with positively charged N, N-diethylaminoethyl groups. Swollen they have an average diameter of 190 µm and an approximately area of 4400 cm<sup>2</sup>/g dry weight (*Microcarrier Cell Culture Principles and Methods*, 2013). For preparation, Schott glass bottles were treated with Sigmacote®, a chlorinated organopolysiloxane in heptane, which reacts with surface silanol (Si-OH) groups on glass to produce a neutral, hydrophobic film to prevent adsorption of microcarriers to the glass surface (Sigma-Aldrich Co. LLC, 2016). The dry and clean inner surface of the bottle was covered in Sigmacote®, after the instantaneous reaction excess solution was removed and the surface allowed to dry. The siliconized products were then rinsed repeatedly with water to remove HCl byproducts before use.

After siliconizing, Cytodex 1 microcarriers were added and swollen in Ca<sup>2+</sup>, Mg<sup>2+</sup>-free PBS (50 mL/g Cytodex 1) overnight on a shaker at 37 °C in an incubator. On the next day the supernatant was decanted and replaced with fresh Ca<sup>2+</sup>, Mg<sup>2+</sup>-free PBS (50

mL/g Cytodex 1). Microcarriers were then sterilized by autoclaving. Afterwards the microcarriers were allowed to settle, the supernatant was discarded and the microcarriers were rinsed with 37 °C culture medium three times, to replace trapped PBS between the microcarriers. After resuspending in culture medium (20 mL/g Cytodex 1), microcarriers were placed overnight in an incubator at 37 °C on a shaker with 140 rpm before use.

### *4.2.2.3 Support growth matrix preparation*

Fibra-Cel® disks were added at the required amount to a clean and dry Schott glass bottle and sterilized by autoclaving. The prepared, sterile disks were stored at room temperature until use.

## 4.2.3 Cell culture methods

### *4.2.3.1 Passaging of suspension cells*

For passaging of suspension cells 1 mL of cell suspension was transferred aseptically into an Eppendorf tube. Then pH, O<sub>2</sub>-saturation and CO<sub>2</sub>-saturation were measured, according to *4.2.8.1 pH and dissolved gas analysis via Stat Profile® pHox® Analyzer*. Cell density was determined according to *4.2.8.2 Cell count via LUNA™ Automated Cell Counter*. For a seeding density of  $3 \times 10^5$  cells/mL the required cell and medium volumes were calculated (*Equation 9 & Equation 10*). The shaker flask was filled with 37 °C pre-warmed medium and the required cell suspension volume was added. Remaining cells were discarded. The cells were incubated in an incubator at 37 °C with 5% CO<sub>2</sub>-atmosphere in humid atmosphere on a shaker with 140 rpm. Passaging occurred every 3 to 4 days.

### *4.2.3.2 Passaging of adherent cells*

Adherent cells were passaged by first examining the confluence of the cell layer using a light microscope. Aseptically 1 mL of supernatant was sampled in an Eppendorf tube for pH, O<sub>2</sub>-saturation and CO<sub>2</sub>-saturation analysis according to *4.2.8.1 pH and dissolved gas analysis via Stat Profile® pHox® Analyzer*. Remaining supernatant was discarded by using an aspiration pipette. The adherent cell layer was washed with a defined volume of pre-warmed to 37 °C PBS and discarded with another aspiration pipette. Afterwards a defined volume of 4 to 8°C cold Accutase was added for cell detachment. Accutase is a proteolytic and collagenolytic enzyme of marine origin

which shows enzyme activity inhibition at 37 °C (ThermoFisher Scientific, 2014). For an animal component free production process the detachment using trypsin and fetal calf serum for enzyme inhibition is not applicable. Cells were incubated for 3 to 5 minutes at 37 °C in an incubator until cells started to detach by firm but cautious shaking by hand. Detached cells were rinsed of the surface with a defined volume of pre-warmed to 37 °C culture medium supplemented with 4 mM GlutaMAX (see Table 1). A sample of 1 mL of detached cell suspension was transferred into an Eppendorf tube and the cell count was determined according to 4.2.8.2 *Cell count via LUNA™ Automated Cell Counter*. Depending on the incubation duration of 3 or 4 days cells were seeded with  $5 \times 10^4$  cells/cm<sup>2</sup> or  $3 \times 10^4$  cells/cm<sup>2</sup>, respectively. The required amount of cell suspension and culture medium volume was calculated according to Equation 10 & Equation 11. Pre-warmed medium supplemented with 4 mM GlutaMAX was filled in an appropriate T-Flask and the required cell suspension was added. Remaining cells were discarded. The cells were incubated in an incubator at 37 °C with 5% CO<sub>2</sub>-Atmosphere in humid atmosphere. Passaging occurred every 3 or 4 days respectively.

Table 1: Specification of volumes used for passaging of adherent cells.

	Washing volume [mL]	Detachment volume [mL]	Suspension volume [mL]	Working volume [mL]
T-Flask 75 cm <sup>2</sup>	5	1	5	20
T-Flask 175 cm <sup>2</sup>	10	3	10	45

### 4.2.4 Sampling scheme

#### 4.2.4.1 Sampling of suspension cultivation

At each sampling point 1 mL of cell suspension was transferred into an Eppendorf tube for determination of pH, O<sub>2</sub>-saturation and CO<sub>2</sub>-saturation and viable cell density according to 4.2.8.1 *pH and dissolved gas analysis via Stat Profile® pHox® Analyzer* and 4.2.8.2 *Cell count via LUNA™ Automated Cell Counter*. In case of LCMV infected cells, an aliquot of cell suspension was transferred into a 15 mL falcon tube and centrifuged at 4 °C, 300 g for 5 min. An amount of 4 - 5 cryovials were then filled with 0.5 mL supernatant and immediately stored at -80 °C for later viral titer determination.

One Eppendorf tube containing 0.5 mL supernatant was stored at -20 °C for further metabolite analysis. The remaining cell pellet was discarded.

### *4.2.4.2 Sampling of adherent cultivation*

The sampling of the adherent cultivations showed differences in the determination of the cell/nuclei count, which are explained below. Sampling of supernatant was similar for all shown cultivation and is described in the last paragraph. For the determination of the cell density in T-Flasks a detachment of the cell layer was required. This was not applicable for each sampling point in every experimental set-up. Normally on the last sampling point the cell density was determined using the same detachment procedure as described in *4.2.3.2 Passaging of adherent cells*.

For microcarrier containing samples about 1 mL of homogenous suspension was transferred in an Eppendorf tube for determination of the nuclei counts according to *4.2.8.3 Nuclei count of Vero cells on microcarrier via LUNA™ Automated Cell Counter*.

For the nuclei count determination of Vero cells on FibraCel discs, two discs were transferred into an Eppendorf tube for determination of the nuclei counts according to *4.2.8.4 Nuclei count of Vero cells on FibraCel discs via LUNA™ Automated Cell Counter*.

The supernatant of LCMV infected cells was transferred in 0.5 mL aliquots into 2 - 5 cryovials, which were then immediately stored at -80 °C. Two times 0.5 mL supernatant were distributed into Eppendorf tubes. One tube was used for determination of pH, O<sub>2</sub>-saturation and CO<sub>2</sub>-saturation according to *4.2.8.1 pH and dissolved gas analysis via Stat Profile® pHox® Analyzer*. The other one was stored at -20°C for further metabolite analysis.

### **4.2.5 Infection of cells with LCMV**

When infecting cells with LCMV the cell count was determined according to *4.2.8.2 Cell count via LUNA™ Automated Cell Counter* or in case of microcarriers or FibraCel discs according to *4.2.8.3 Nuclei count of Vero cells on microcarrier via LUNA™ Automated Cell Counter*. For experiments performed in T-Flasks an additional flask was cultivated for determination of the viable cell density at the time of infection.

The MOI is an important parameter for propagation kinetics of a viral infection. It is defined as the ratio of infective particle to infection host. For example a MOI of 0.01

would result in one virus particle for every 100 cells. The MOI has the unit foci forming units (FFU) /cell or, if the nuclei count instead of the cell count was determined, FFU/nuclei.

The required infection volume was calculated using *Equation 12* for suspension cultivations and *Equation 13* for adherent cultivation. The virus seed was stored at -80 °C, thawed at ambient temperature and then kept on ice until needed. Given the low MOI and therefore the low infection volume an appropriate dilution was chosen to reach an infection volume of 100 – 200 µL to reduce pipetting errors. The required dilution was achieved by consecutive 1:10 dilutions (e.g. 100 µL + 900 µL) in cold culture medium. After mixing by inverting the vial repeatedly, the cells were infected with a micropipette.

### 4.2.6 Thermal inactivation of replication competent LCMV samples for metabolite assays

The required thermal inactivation of replication competent LCMV samples for metabolite measurements using the Cedex bio analyzer was performed with samples stored at -20 °C in Eppendorf tubes at 66 °C for 1 hour in a water bath using a polystyrol swimming aid. This set-point was elaborated in *5.3 Alteration of metabolite concentrations of VP-SFM and PF26#280 during thermal inactivation* of LCMV for metabolite assays. Afterwards the virus inactivated samples were stored at -20 °C until further use for metabolite assays.

### 4.2.7 Experimental set-ups

In the herein presented work various experiments have been performed. This flowchart (*Figure 3*) should provide an overview for a better understanding of the order of events.

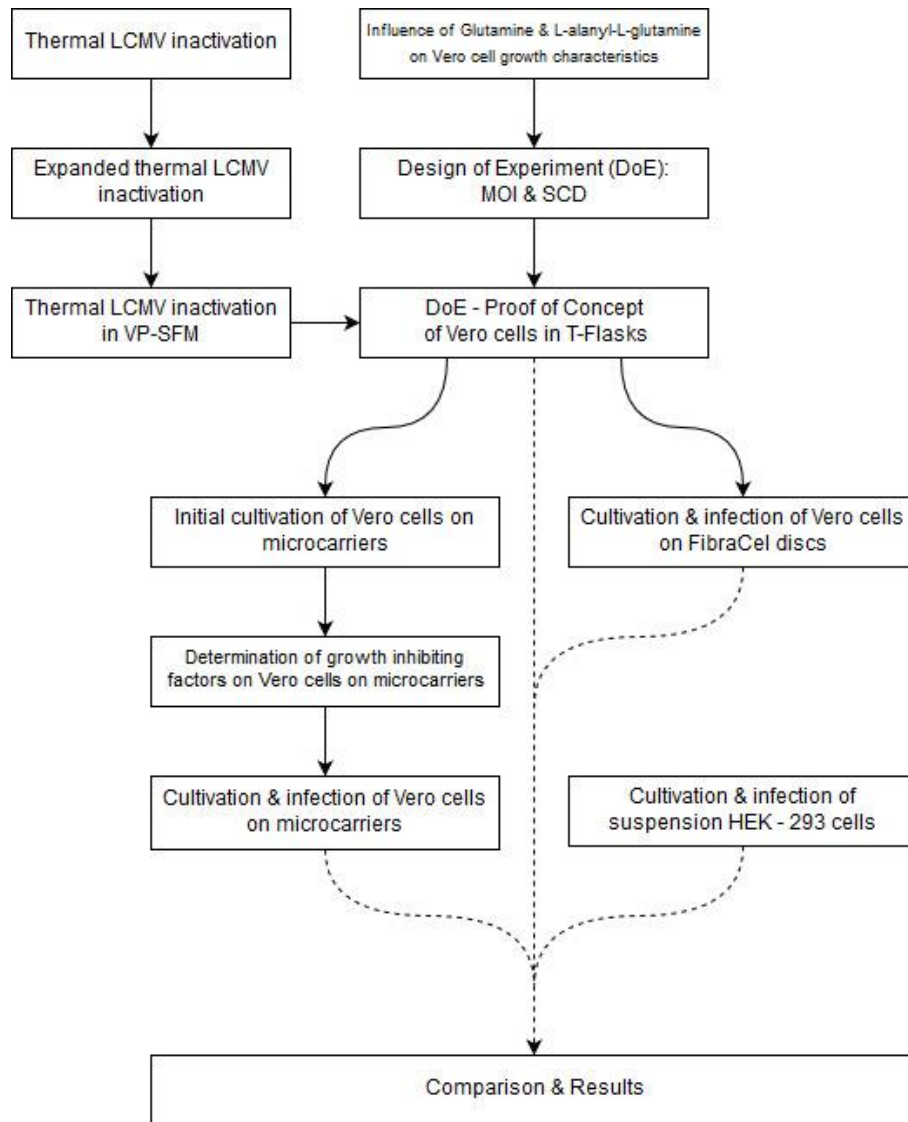


Figure 3: Flowchart of performed experiments

### 4.2.7.1 Alteration of metabolite concentrations of PF26#278 during thermal inactivation of LCMV for metabolite assays I

Due to the self-replicating ability of LCMV, it is classified as a BSL 2 agent and open handling without using an isolator or a laminar flow hood is prohibited. The automated pipetting mechanism of the Cedex Bio analyzer requires open handling vials to perform the analysis. The sample volume in the Eppendorf tube are therefore in contact with its surrounding. Because of space and size limitations, a containment (e.g. Laminar Air Flow or an Isolator) only for the analyzer was not possible. Therefore, samples containing a replication competent virus are required to be inactivated. Thermal inactivation via a water bath was selected, due to its relatively fast and safe handling, which did not require manipulation on the vials during the inactivation procedure (e.g.

opening of the container). At Hookipa Biotech AG no thermal inactivation protocol for LCMV has yet been established. A  $3^2$  - full factorial central composite face Design of Experiment approach with temperature and inactivation time as factors was used to find a suitable set point for a viral titer reading, lower than the detection limit of 5 FFU/mL of the most sensitive assay at Hookipa Biotech AG, the *Focus Forming Unit Assay* described in 4.2.8.6. Some metabolites are not stable at elevated temperatures. For example Glutamine decomposes spontaneously, which results in Ammonia formation (Tritsch and Moore, 1962). This would result in an incorrectly measured concentrations. To assess the robustness of the metabolite concentrations after the inactivation, supernatant of consumed medium without virus particles was treated with the same time and temperature set points, where a virus titer reading was lower than the detection limit. The concentrations will then be compared to an untreated sample. For future inactivation procedures, only metabolites will be analyzed which showed no alteration in concentration at these set point.

For the first approach levels for the factor "Temperature" were chosen to be 36 / 46 / 56 °C, whereas the levels for the factor "Inactivation time" were 5 / 25 / 45 minutes (see *Figure 4*). LCMV was propagated on HEK-293 cells with an established protocol. The supernatant containing the virus particles was harvested by cell removal through centrifugation, at 300 g for 5 minutes, and stored at -80 °C until further use. As the experiment was performed in singlets 9 samples were treated as follows; the samples were transferred in a -20 °C freezer 3 hours prior the experiment start, for the same temperature starting point as for later stored metabolite analysis samples. For the inactivation, the samples were inserted into a floating aid and put directly in the pre-heated water bath. At reaching the given inactivation time samples were immediately stored at -80 °C to avoid further deactivation. The viral titer was determined according to the *Focus Forming Unit Assay* described in 4.2.8.6.

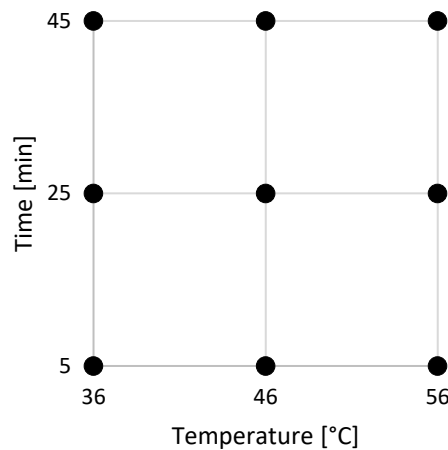


Figure 4: The  $3^2$ -full factorial central composite face design of experimental set-up with inactivation time (5, 25, and 45 minutes) and temperature (36, 46, and 56 °C) as factors for the thermal inactivation of LCMV in PF26#278 for metabolite assays with foci forming units per mL as response. The design was conducted in singlets.

#### 4.2.7.2 Alteration of metabolite concentrations of PF26#278 during thermal inactivation of LCMV for metabolite assays II

As the previous thermal inactivation experiment (5.1 *Alteration of metabolite concentrations of PF26#278 during thermal inactivation of LCMV for metabolite assays I*) did not deliver satisfactory results a follow-up experiment was conducted. For this purpose 3 new temperature set-points, 56, 66, and 76 °C and an inactivation time of 60 minutes were chosen. The experiment was performed in singlets. Remaining virus samples generated for the first thermal inactivation were re-used. Preparation and operation were performed as described previously in 4.2.7.1. The difference in metabolite concentrations for obtained set points, where the virus concentration was lower than the detection limit of the FFU - assay, was determined with uninfected consumed medium samples, which were treated with the same setpoints. Glucose, Lactate, Glutamine, and Ammonia were compared to an untreated sample of uninfected consumed medium. The metabolites were analyzed with the Cedex Bio Analyzer.

#### 4.2.7.3 Alteration of metabolite concentrations of VP-SFM and PF26#280 during thermal inactivation of LCMV for metabolite assays

For the cultivation as for the virus production VP-SFM was used as growth medium for Vero cells. Further was the medium, for future HEK-293 suspension processes



switched to a different formulation, from PF26#278 to PF26#280. It had to be demonstrated that the previously determined result held true also for these media. The experimental set-up examined the same temperatures as in 4.2.7.2. Virus material in PF26#280 was produced with the same set points as in 4.2.7.1 but with a production period of 72 hours. As no results for virus propagation with Vero cells in VP-SFM were determined at this time the MOI was set to  $1 \times 10^{-3}$  FFU/cell for the production of crude virus harvest. The harvesting procedure was the same as in 4.2.7.1. The experiment was performed in singlets, the virus titer was analyzed with the FFU assay. Afterwards uninfected consumed medium samples were treated with the same set points, where the virus titer read out was below the detection limit. Glucose, Lactate, Glutamine and Ammonia concentrations were compared to an untreated sample of uninfected consumed medium. Samples were analyzed by the Cedex Bio Analyzer.

#### *4.2.7.4 Influence of Glutamine and L-alanyl-L-glutamine on Vero cell growth characteristics*

As a first encounter with adherently growing Vero cells for the Upstream Department at Hookipa Biotech AG growth characteristics had not been investigated. With the aim to gain insight into the growth and substrate consumption characteristics of Vero cells, which allows choosing a suitable time point for a later viral infection, an experiment in T-Flasks was conducted. Therefore cells were seeded with  $3 \times 10^4$  cells/cm<sup>2</sup> in 75 cm<sup>2</sup> T-Flasks containing cultivation medium supplemented with 4 mM Glutamine instead of L-Alanyl-L-glutamine. Flasks were incubated at 37 °C in humid, 5 % CO<sub>2</sub>-atmosphere. As pH dropped below 7, a total medium exchange was carried out. Determination of the pH, the viable cell density and selected metabolites, consisting of Glucose, Glutamine, Lactate and Ammonia, occurred every 24 hours until 168 hours post seeding (hps). Due to the nature of the cell count determination, see 4.2.4.2 *Sampling of adherent cultivation*, one flask had to be harvested for each sampling point. As the last 4 sampling points were measured in duplicates in sum 11 flasks were prepared.

Furthermore the influence of the commonly used L-glutamine alternative, L-alanyl-L-glutamine on the cell density and the aforementioned selected metabolites, was determined by adding 4 mM L-alanyl-L-glutamine instead of Glutamine to the cultivation medium of 3 additional T-Flask. With the same seeding and cultivation treatment as described above one flask was harvested after 72 hours, whereas the other two were harvested as duplicates 168 hps.

#### 4.2.7.5 Determination of an optimized MOI and SCD of adherently growing Vero cells

The optimal MOI and SCD still had to be determined. For this cause a randomized,  $3^2$ -full factorial central composite face experiment design was applied. The levels for the MOI were chosen to be  $10^{-1}$ ,  $10^{-3}$  and  $10^{-5}$ . To assess the influence of the confluence, and therefore the state of metabolic activity of the cells on the viral titer production, SCD levels were set to  $2 \times 10^4$ ,  $3.5 \times 10^4$  and  $5 \times 10^4$  cells/cm<sup>2</sup>. All points were determined in duplicates, the center point in quadruplicates, resulting in 20 T75-flasks (see Figure 5 & Table 2). For determination of the cell density at the time of infection three additional flasks were cultivated with the respective SCD. Vero cells were prepared as described in 4.2.3.2 *Passaging of adherent cells*. Required cell suspension and medium volumes for the different seeding densities were calculated using Equation 10 & Equation 11. According to the results of the growth characteristics of Vero cells (5.4 *Influence of Glutamine and L-alanyl-L-glutamine on Vero cell growth characteristics*) cells were infected 72 hps. Infection was performed as described in 4.2.5 *Infection of cells with LCMV*. Sampling (see 4.2.4.2 *Sampling of adherent cultivation*) occurred every 24 hours after the infection for a total post infection time of 96 hours. Flasks were incubated at 37 °C in humid, 5 % CO<sub>2</sub>-atmosphere.

Table 2:  $3^2$ -full factorial central composite face experiment design set-up for the determination of an optimal MOI and SCD of adherently growing Vero cells.

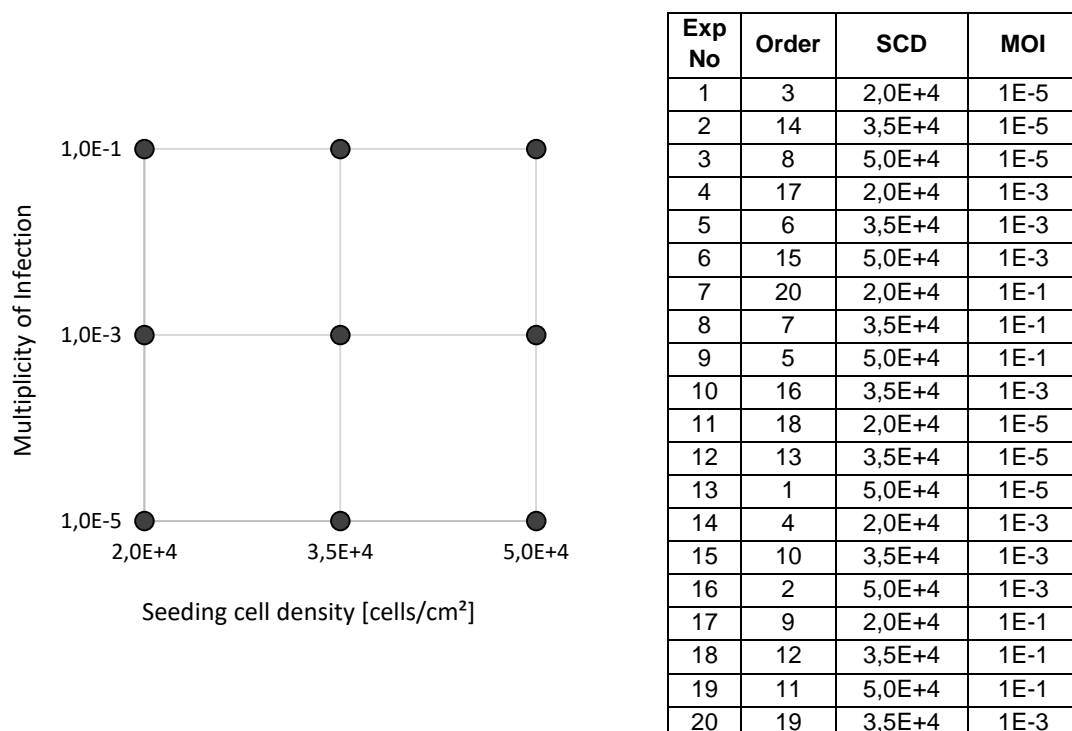


*Figure 5: DoE set-up for determination of an optimized MOI of adherently growing Vero cells*

### *4.2.7.6 Proof of Concept for infection of adherently growing Vero cells with LCMV*

In order to confirm or reject the established models in the previous experiment a Proof of Concept (PoC) was conducted. For this purpose, three points in the design space of experiment 4.2.7.5. were chosen and the virus titers for each sampling point were predicted by the generated models:

- The first point (see *Figure 6*: red point) had optimal setpoints for the highest titer, with a SCD of  $2 \times 10^4$  cells/cm<sup>2</sup> and a MOI of  $3 \times 10^{-3}$  FFU/cell.
- The second point (see *Figure 6*: blue point) was expected to have a low titer, with a SCD of  $2.5 \times 10^4$  cells/cm<sup>2</sup> and an MOI of  $1 \times 10^{-4}$  FFU/cell.
- The last point (see *Figure 6*: green point) should yield a similar titer as the first one, but required a higher SCD of  $4.5 \times 10^4$  cells/cm<sup>2</sup> and the same MOI of  $3 \times 10^{-3}$  FFU/cell.

Each point was performed in triplicates, for the determination of the cell density at the time of infection one additional flask was cultivated for each cell density. Two additional flasks with the optimal setpoints were sampled 96 hpi for determination of the cell density at the expected peak for the calculation of the specific titer. Preparation, execution, and sampling was handled the same way as described in 5.5 *Determination of an optimized MOI and SCD of adherently growing Vero cells*. An additional read-out for this experiment was to assess the virus stability post peak. Therefore sampling of not harvested flasks was continued 48 hours post the expected titer peak resulting in a 144 hour post infection duration. Flasks were incubated at 37 °C in humid, 5 % CO<sub>2</sub>-atmosphere.

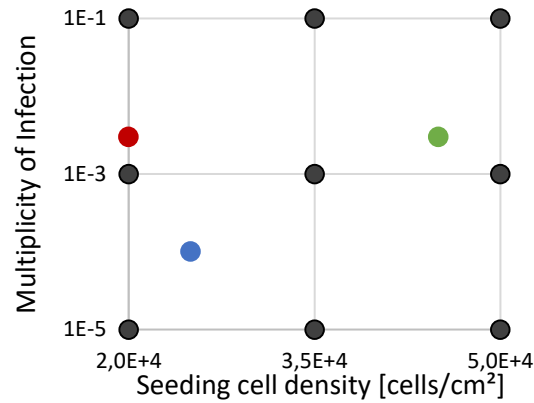


Figure 6: Design space of the SCD and MOI optimization experiment. Black dots show the initial determined setpoints. Colored dots show the investigated setpoints for the proof of concept.

#### 4.2.7.7 Initial cultivation and infection of Vero cells on microcarriers in shake flasks

To shed light on the growth behavior of Vero cells on Cytodex 1 microcarrier an initial cultivation was conducted. A concentration of 3 g/L Cytodex 1 was considered to be optimal for a general cultivation (Clark and Hirtenstein, 1981). Vero cells were cultivated with microcarrier concentrations of 1 and 3 g/L in duplicates. Microcarriers were prepared as described in 4.2.2.2 *Microcarrier preparation*. Cells were seeded with a seeding density of  $2 \times 10^4$  cells/cm<sup>2</sup> in a 125 mL shaker flask with a working volume of 40 mL containing 1 or 3 g/L Cytodex 1 microcarrier. Flasks were incubated at 37 °C in humid, 5 % CO<sub>2</sub>-atmosphere. After 72 hours 60 % medium was replaced by allowing the microcarriers to settle and cells were infected with LCMV with a MOI of 0.003 FFU/cell, as described in 4.2.5 *Infection of cells with LCMV*. Every 24 hours samples were taken to determine cell morphology and cell count until 168 hps. To reduce shear stress agitation was set to 100 rpm with a 2.5 cm shaking radius, which kept microcarrier nearly in suspension.

#### 4.2.7.8 Evaluation of cell growth inhibiting factors on Vero cells in microcarrier cultivation

Three possible influences on cell attachment and growth were investigated in this experiment. A reduced volume at seeding and intermittent stirring for two hours after seeding were hypothesized to allow a higher interaction between cells and microcarriers. As third influence the removal of self-deactivated Accutase after cell preparation by centrifugation and suspending the pellet in fresh medium, was

illuminated. A  $2^3$ -full factorial screening design resulting in 8 shake flasks was applied. Due to low quantity of available cells this experiment was performed in singlets. The DoE set-up is illustrated in *Table 3* & *Figure 7*. Microcarriers were prepared as described in *4.2.2.2 Microcarrier preparation*. Cells were seeded with a seeding density of  $2 \times 10^4$  cells/cm<sup>2</sup> in a 125 mL shaker flask with a working volume of 40 mL containing 3 g/L pre-treated Cytodex 1 microcarrier. Flasks were incubated at 37 °C in humid, 5 % CO<sub>2</sub>-atmosphere. After 72 hours, cultivation medium was replaced and cells were infected with LCMV applying a MOI of 0.003 FFU/cell, as described in *4.2.5 Infection of cells with LCMV*. Every 24h samples were taken to determine cell morphology, cell count and viral titer until 168 hps. Agitation was set to 100 rpm with a 2.5 cm shaking radius, which kept microcarrier nearly in suspension.

*Table 3: DoE set-up for evaluation of cell growth inhibiting factors on Vero cells in microcarrier cultivation*

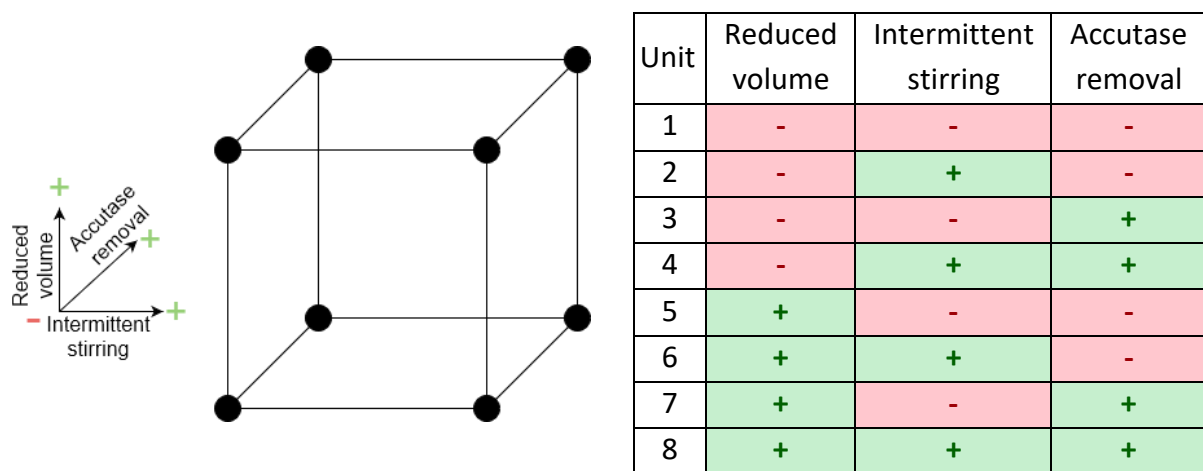


*Figure 7: DoE set-up for evaluation of cell growth inhibiting factors on Vero cells in microcarrier cultivation*

### *4.2.7.9 Adapted cultivation and infection of Vero cells on microcarriers in shake flasks*

After the adaption of the cultivation preparation, resulting in a successful attachment and growth, a final cultivation was performed to compare the microcarrier cultivation to the current suspension cultivation. Microcarriers were prepared as described in *4.2.2.2 Microcarrier preparation*. Cells were obtained as described in *4.2.3.2 Passaging of adherent cells*. To remove cell growth inhibiting Accutase, cells were centrifuged for 5 minutes at 300 g, the supernatant was replaced with fresh pre-warmed medium and cells were resuspended. Afterwards they were seeded with a seeding density of  $2 \times 10^4$  cells/cm<sup>2</sup> in a 250 mL shaker flask with a working volume of 80 mL containing

3 g/L Cytodex 1. Cells were cultivated at 37 °C and 5 % CO<sub>2</sub> atmosphere, and agitated at 100 rpm and an amplitude of 2.5 cm. After 72 hours 60 % medium was exchanged by allowing the microcarrier to sediment. Cells were infected with LCMV using an MOI of 0.003, as described in 4.2.5 *Infection of cells with LCMV*. Sampling, described in 4.2.4.2 *Sampling of adherent cultivation*, occurred every 24 hour until 96 hpi. This experiment was performed in duplicates. For further comparison also an MOCK cultivation, which was treated the same way except the there was no infection, was performed in duplicates.

#### 4.2.7.10 *Cultivation and infection of Vero cells on FibraCel in shaker flasks*

During this master thesis, additional to microcarrier, FibraCel was investigated as an alternative growth-supporting matrix. The possible future use in a single use perfusion bioreactor after a first successful cultivation should be evaluated by this experiment.

As no small scale bioreactor units for a perfusion mode were available at the time conducting the experiment, it was decided to simulate this process with shaker flasks to get an idea of the performance. For initial seeding conditions, with the same disc/volume ratio of the perfusion reactor, cells were seeded with a seeding density of  $2 \times 10^4$  cells/cm<sup>2</sup> and cultivated for the first 24 hours in 125 mL shaker flasks with 1 g previously autoclaved FibraCel discs with a working volume of 25 mL. Cells were obtained as described in 4.2.3.2 *Passaging of adherent cells*. To remove cell growth inhibiting Accutase, cells were centrifuged for 5 minutes at 300 g, the supernatant was replaced with fresh pre-warmed medium and cells were resuspended. Flasks were incubated at 37 °C in humid, 5 % CO<sub>2</sub>-atmosphere. Agitation was set to 140 rpm with a 2.5 cm shaking radius. After 24 hours cells on discs were transferred into a 500 ml shaker flask with a working volume of 200 mL. A medium exchange during the growth phase was performed if necessary. As an initial cultivation with this new method, it was chosen to infect cells at a sub confluent cell density, which was used in previous T-Flask growth studies. Cells were infected with LCMV with MOI of 0.003 FFU/cell. During the infection phase no medium exchange was performed. Sampling points were 48 / 72 / 96 hours after infection. The nuclei count was determined according to 4.2.8.4 *Nuclei count of Vero cells on FibraCel discs via LUNA™ Automated Cell Counter*,  $2 \times 0.5$  ml of supernatant were frozen at -80°C for titer determination,  $1 \times 0.5$  mL were stored at -20°C for metabolite analysis. The experiment was performed in duplicates.

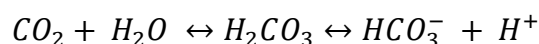
### 4.2.7.11 Current infection protocol using suspension HEK-293 cells

For comparison of the different investigated processes the standard infection process at the time of the experiment conduction was performed. This process used suspension HEK-293 cells, cultivated in PF26#278. Suspension cells were obtained as described in 4.2.3.1 *Passaging of suspension cells*. They were infected concurrently at seeding at  $3 \times 10^5$  cells/mL with LCMV with a MOI of  $10^{-5}$  FFU/cell, as described in 4.2.5 *Infection of cells with LCMV*. For optimal comparability 250 mL shaker flasks with a working volume of 80 mL were used. To show the effect of infection on the cells an uninfected experiment unit was cultivated. The experiment was performed in duplicates, resulting in 4 units. Flasks were incubated at 37 °C in humid, 5 % CO<sub>2</sub>-atmosphere. Agitation was set to 140 rpm with a 2.5 cm shaking radius. Sampling, mentioned in 4.2.4.1 *Sampling of suspension cultivation*, was performed every 24 hours until 96 hours after infection.

## 4.2.8 Analytical methods

### 4.2.8.1 pH and dissolved gas analysis via Stat Profile® pHox® Analyzer

To measure pH, pO<sub>2</sub>-saturation and pCO<sub>2</sub>-saturation, a volume of 300 µL cell suspension was aspirated by the Stat Profile® pHox® Analyzer. For an accurate result the sample has to be analyzed immediately after sampling to minimize dissipation of soluble O<sub>2</sub> and CO<sub>2</sub> and therefore a shift in the equilibrium of the Bicarbonate buffer system of the cultivation medium.



Equation 1

pH is measured using a hydrogen ion selective glass membrane, which is in contact with a solution of constant pH and the solution with the to be determined pH. A potential change is proportional to the pH difference of this solution and is measured against a reference electrode of constant potential (Nova Biomedical, 2001).

Partial Pressure of Carbon Dioxide (pCO<sub>2</sub>) is measured using a modified pH sensor. Carbon dioxide diffuses across a gas permeable membrane into a thin layer of electrolyte solution, becomes hydrated and results in a change in hydrogen ion activity (*Equation 1*). This change is then measured with the same principle as the pH measurement (Nova Biomedical, 2001).

The partial pressure of oxygen is measured amperometrically. As oxygen diffuses through the gas permeable membrane it gets reduced at the cathode and consumes 4 electrons for each oxygen molecule. This electron flow is then measured and directly proportional to the partial pressure of oxygen (Nova Biomedical, 2001).

### *4.2.8.2 Cell count via LUNA™ Automated Cell Counter*

For determination of the viable cell density the LUNA™ Automated Cell Counter was used. It is an image-based cell counter which utilizes image analysis software to extract information regarding the brightness, circularity and diameter of suspension cells. The measurable cell concentration ranges from  $5 \times 10^4 - 1 \times 10^7$  cells/mL with a 3 – 60  $\mu\text{m}$  cell diameter. Clusters are counted as individual cells by a declustering algorithm. With a Trypan Blue Exclusion test the software distinguishes live and dead cells from debris (Logos biosystems, 2014). A homogenous cell suspension sample of 100  $\mu\text{L}$  was diluted with 100  $\mu\text{L}$  0.4 % Trypan blue, vortexed and an aliquot was placed in a disposable LUNA™ Cell counting slide and inserted into the device.

Following counting parameters were applied:

- Noise reduction 7/10
- Roundness 7/10
- Min. cell size 8  $\mu\text{m}$
- Max. cell size 30  $\mu\text{m}$

For each sample two counts were performed and the arithmetic mean was calculated.

### *4.2.8.3 Nuclei count of Vero cells on microcarrier via LUNA™ Automated Cell Counter*

A homogenous microcarrier containing aliquot of 100  $\mu\text{L}$  was transferred in an Eppendorf tube and diluted with 100  $\mu\text{L}$  nuclei staining solution, vortexed 1 minute and an aliquot was placed in a disposable LUNA™ Cell counting slide and inserted into the device.

Following counting parameters were applied:

- Noise reduction 5/10
- Roundness 5/10
- Min. cell size 6  $\mu\text{m}$



- Max. cell size 15 µm

For each sample two counts were performed and the arithmetic mean was calculated.

### 4.2.8.4 Nuclei count of Vero cells on FibraCel discs via LUNA™ Automated Cell Counter

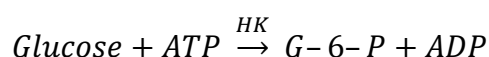
Two Fibra-Cel discs were transferred in an Eppendorf tube and mixed with 1 mL of the nuclei staining solution, vortexed for one minute and an aliquot was transferred in a disposable LUNA™ Cell counting slide and inserted into the device. The same counting parameters as in 4.2.8.3 Nuclei count of Vero cells on microcarrier via LUNA™ Automated Cell Counter were applied. For each sample two counts were performed and the arithmetic mean was calculated.

### 4.2.8.5 Metabolite assay

Metabolite assays of virus free or heat inactivated virus containing samples (4.2.7.1) were performed with the Cedex Bio Analyzer (Roche), an automated computerized analyzer that determines analyte concentrations photometrically. Samples were thawed and tests to be performed were added using the CEDEX software. The sample was mixed with a vortex, placed in a holding tube and inserted in the sampling retainer. Upon finishing of the tests the sampling tube was removed and stored at -20 °C. Then the next test was added and the next sample was placed.

#### 4.2.8.5.1 Glucose

The Glucose assay is based on the phosphorylation of Glucose by ATP in presence of Hexokinase (HK) to Glucose-6-phosphate (G-6-P), which is oxidized by NADH in presence of Glucose-6-phosphate dehydrogenase (G-6-PDH). The rate of NADPH formation is measured UV-photometrically and is directly proportional to the Glucose concentration.



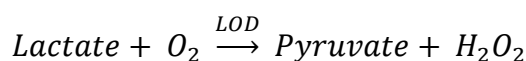
Equation 2



Equation 3

### 4.2.8.5.2 Lactate

Lactate is oxidized by the specific Lactate oxidase (LOD) to pyruvate and H<sub>2</sub>O<sub>2</sub>, which generates in presence of peroxidase (POD) a coloured dye. The photometrically measured absorbance of the dye is directly proportional to the Lactate concentration.



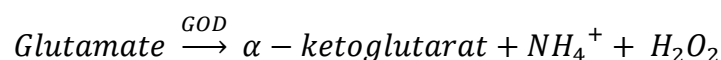
Equation 4



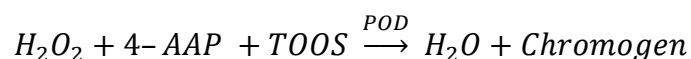
Equation 5

### 4.2.8.5.3 Glutamine

Glutamine is deaminated by glutaminase to Glutamate. In presence of Glutamate oxidase (GOD) Glutamate is oxidized to α-ketoglutarat, NH<sub>4</sub><sup>+</sup> and H<sub>2</sub>O<sub>2</sub>, which then generates a coloured quinine dye in presence of peroxidase (POD). The dye formation is measured photometrically and is directly proportional to the glutamate concentration.



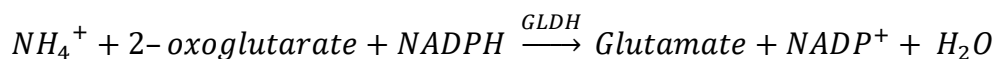
Equation 6



Equation 7

### 4.2.8.5.4 Ammonia

Solved ammonia in presence of glutamate dehydrogenase (GLDH) reacts with 2-oxoglutarate and NADPH in a reductive amination to form Glutamate and NADP<sup>+</sup>. The decrease of NADPH is directly proportional to the ammonia concentration and is measured photometrically.



Equation 8

### 4.2.8.6 Focus Forming Unit Assay

This assay was performed by the Analytic Development Department of Hookipa Biotech AG.

The biological FFU Assay employs immune-staining for determination of the viral titer of LCMV. Adherent HEK-293T cells, cultivated in DMEM High Glucose Medium including additives e.g. fetal calf serum, are seeded with a cell concentration of  $8 \times 10^5$  cells/mL in 24 well plates. To promote attachment the plates were pre-coated with Poly-L-Lysine. The virus samples were serially diluted over a 6-log range in 96-well plates and were transferred to the attached HEK-293T cells using a multichannel pipette. The mixture was incubated for two to 4 hours at 37 °C allowing infection of the cells. To prevent spreading of the virus throughout the well methylcellulose in cell culture medium was added at a final concentration of 2 % to the cell layer. The plates were incubated at 37 °C for 38-44 hours. Afterwards the liquid content was disposed and the cell layer was fixated with 4 % Paraformaldehyde, washed once with 1 % Triton X-100 in Gey's Balanced Salt Solution and blocked with 5 % FCS. Then the primary anti NP antibody VL-4 was added at a concentration of 1 mg/mL to the wells and incubated for 1 hour. After another washing step a horse radish peroxidase (HRP)-linked secondary antibody was added and also incubated for one hour. The plates were washed and a 3-3' diaminobenzidine tetrahydrochloride / nickel ammonium sulfate solution was added. The resulting color reaction after 5-10 minutes incubation created a dark brown precipitate over infected cell which were counted visually after a last washing step. The amount of created spots, or foci, multiplied by the serial dilution and averaged over the countable range of foci (10-150) then was calculated as final FFU/mL result, under the assumption that one infective virus particle creates one foci. The lower detection limit of the assay is 5 FFU/mL.

### 4.2.9 Calculations

#### 4.2.9.1 Passaging of suspension cells

$$V_{cells} = \frac{SCD \times WV}{VCD} = [mL]$$

Equation 9

$$V_{Medium} = WV - V_{cells}$$

Equation 10

*SCD* ...seeding cell density [cells/mL]

*VCD* ...viable cell density [cells/mL]

$V_{cells}$  ...volume of cell suspension [mL]

$V_{Medium}$  ...volume of medium [mL]

$WV$  ... working volume [mL]

#### 4.2.9.2 Passaging of adherent cells

$$V_{cells} = \frac{SCD \times SA}{VCD} = [mL]$$

Equation 11

$SA$  ... surface area [cm<sup>2</sup>]

$SCD$  ...seeding cell density [cells/cm<sup>2</sup>]

$VCD$  ...viable cell density [cells/mL]

$V_{cells}$  ...volume of cell suspension [mL]

#### 4.2.9.3 Viral infection volume for suspension cells

$$V_{infection} = \frac{VCD \times MOI \times WV}{Titer_{seed}} = [mL]$$

Equation 12

$MOI$  ...multiplicity of infection [FFU/cells]

$Titer_{seed}$  ...titer of LCMV seed [FFU/mL]

$VCD$  ...viable cell density [cells/mL]

$V_{infection}$  ...infection volume [mL]

$WV$  ... working volume [mL]

#### 4.2.9.4 Viral infection volume for adherent cells

$$V_{infection} = \frac{VCD \times MOI \times SA}{Titer_{seed}} = [mL]$$

Equation 13

$MOI$  ...multiplicity of infection [FFU/cell]

$SA$  ... surface area [cm<sup>2</sup>]

$Titer_{seed}$  ...titer of LCMV seed [FFU/mL]

$VCD$  ...viable cell density [cells/cm<sup>2</sup>]

$V_{infection}$  ...infection volume [mL]

#### 4.2.9.5 Specific growth rate

$$\mu = \frac{[\ln(x_1) - \ln(x_0)]}{dt} = [h^{-1}]$$

Equation 14

$\mu$  ...specific growth rate [h<sup>-1</sup>]

$dt$  ...time difference between sampling points [h]

$x_0$  ...cell density [cells/mL, respectively cells/cm<sup>2</sup>] at previous sampling point

$x_1$  ...cell density [cells/mL, respectively cells/cm<sup>2</sup>] at sampling point

#### 4.2.9.6 Specific metabolic rates for suspension cells

$$q = -\frac{1}{\frac{x_0 + x_1}{2}} \times \frac{1}{1000} \times \frac{dS}{dt} \text{ or } \frac{1}{\frac{x_0 + x_1}{2}} \times \frac{1}{1000} \times \frac{dP}{dt} = [\text{mol/cell/hour}]$$

Equation 15

$dP$  ...molar product concentration difference [mol/L]

$dS$  ...molar substrate concentration difference [mol/L]

$dt$  ...time difference between sampling points [h]

$q$  ...specific metabolic consumption rate ( $q_{Glc}$ ,  $q_{Gln}$ ), or specific metabolic production rate ( $q_{Lac}$ ,  $q_{NH_4^+}$ ) [mol/cell/h]

$x_0$  ...cell density [cells/mL, respectively cells/cm<sup>2</sup>] at previous sampling point

$x_1$  ...cell density [cells/mL, respectively cells/cm<sup>2</sup>] at sampling point

#### 4.2.9.7 Specific metabolic rates for adherent cells

$$q = -\frac{1}{\frac{x_0 + x_1}{2}} \times \frac{WV}{SA} \times \frac{1}{1000} \times \frac{dS}{dt} \text{ or } \frac{1}{\frac{x_0 + x_1}{2}} \times \frac{WV}{SA} \times \frac{1}{1000} \times \frac{dP}{dt} = [\text{mol/cell/hour}]$$

Equation 16

$dP$	...molar product concentration difference [mol/L]
$dS$	...molar substrate concentration difference [mol/L]
$dt$	...time difference between sampling points [h]
$q$	...specific metabolic consumption rate ( $q_{Glc}$ , $q_{Gln}$ ), or specific metabolic production rate ( $q_{Lac}$ , $q_{NH_4^+}$ ) [mol/cell/h]
$SA$	...surface area [cm <sup>2</sup> ]
$x_0$	...cell density [cells/cm <sup>2</sup> ] at the first sampling point
$x_1$	...cell density [cells/cm <sup>2</sup> ] at the second sampling point
$WV$	...working volume [mL]

#### 4.2.9.8 Specific viral titer of suspension cells

$$\text{specific titer} = \frac{\text{titer}}{VCD} = [FFU/cell]$$

Equation 17

$\text{titer}$	...viral titer at sampling point [FFU/mL]
$VCD$	...viable cell density [cells/mL]

#### 4.2.9.9 Specific viral titer of adherent cells

$$\text{specific titer} = \frac{\text{titer}}{VCD} \times \frac{WV}{SA} = [FFU/cell]$$

Equation 18

$\text{titer}$	...viral titer at sampling point [FFU/mL]
$VCD$	...viable cell density [cells/cm <sup>2</sup> ]
$SA$	...surface area [cm <sup>2</sup> ]

*WV* ...working volume [mL]

#### 4.2.9.10 Viral yield

$$\text{viral yield} = \frac{\text{specific titer}}{\text{MOI}} = [\text{FFU}/\text{FFU}]$$

Equation 19

*specific titer* ...specific titer [FFU/cell]

*MOI* ...Multiplicity of infection [FFU/cell]

## 5 Results

### 5.1 Alteration of metabolite concentrations of PF26#278 during thermal inactivation of LCMV for metabolite assays I

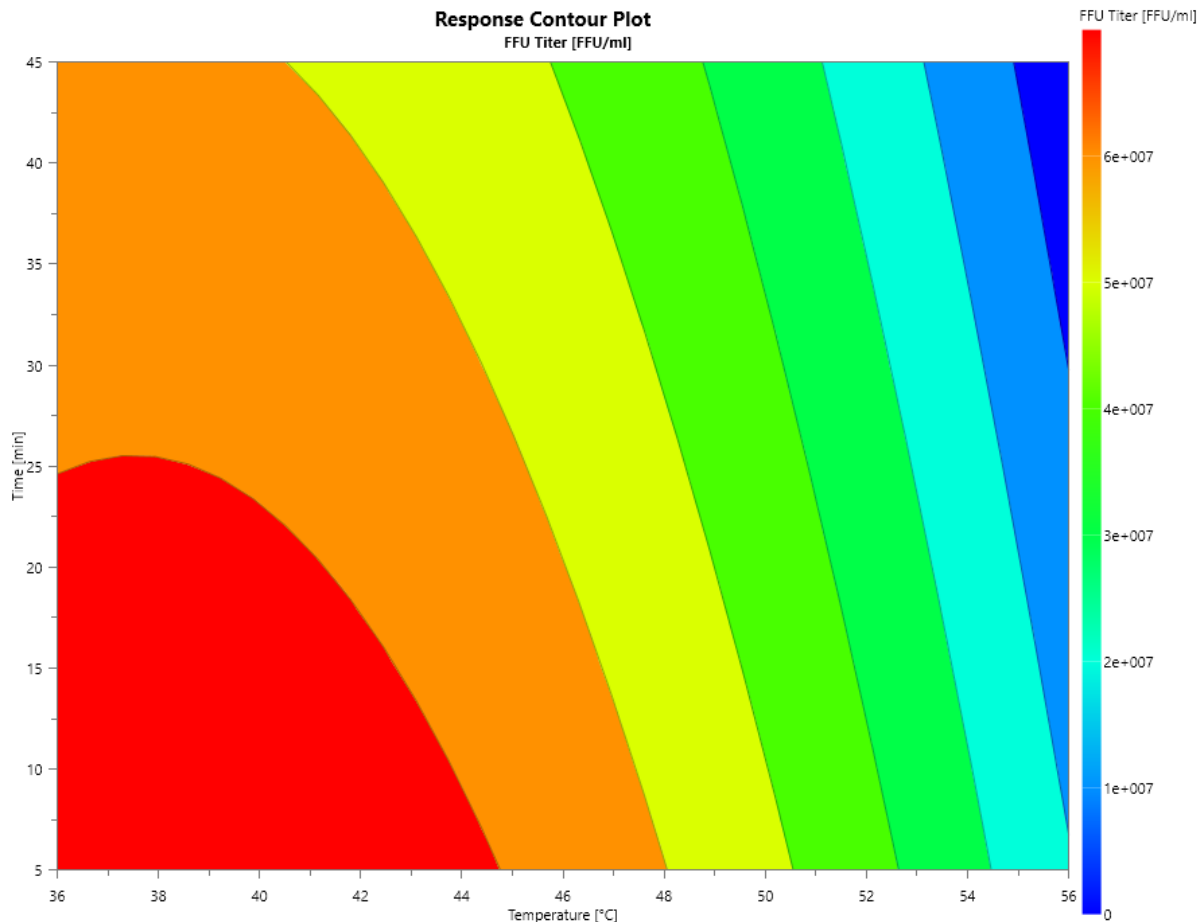


Figure 8: Response Contour Plot of foci forming units per mL for thermal inactivation of LCMV in PF26#278, generated with a  $3^2$ -full factorial design of experimental set-up with temperature (36 to 56 °C) on the x-axis and inactivation time (5 to 45 minutes) on the y-axis as factors. Red areas indicate highest responses and blue areas lowest.  $R^2$ : 0.94825;  $Q^2$ : 0.795

Figure 8 shows the Response Contour Plot for the set-up described in 4.2.6. The factors temperature on the x-axis and inactivation time on the y-axis show the influence on the response viral titer in FFU/mL. Red areas indicate highest and blue areas lowest virus concentration. The coefficient of determination  $R^2$  is the measure how close the fitted regression line is to the measured data. A value higher than 0.68 is a significant model. The coefficient of determination for this model was with 0.94825 highly significant. The estimate for the future prediction is reflected in  $Q^2$ . A value higher than 0.5, here 0.795, indicates a good model. In the plot the decrease in viral titer over time



and temperature is modeled. The influence of temperature on virus inactivation is clear, recognizable at the higher amount of increments along the x-axis than the y-axis for the inactivation time. The highest inactivation was achieved at the highest combination of inactivation time and temperature. In contrast to the model, which proposes no detectable virus concentration at the highest settings, it is evident in Figure 9 that this does not hold true as the virus titer still had a concentration of 100 FFU/mL. As no set point was able to produce a result lower than the detection limit of the FFU-assay, no additional samples of virus free, consumed medium samples were treated, to assess the alteration of metabolite concentrations during the inactivation procedure. This led to follow-up experiment, *4.2.7.2 Alteration of metabolite concentrations of PF26#278 during thermal inactivation of LCMV for metabolite assays II* with increased temperature and inactivation time.

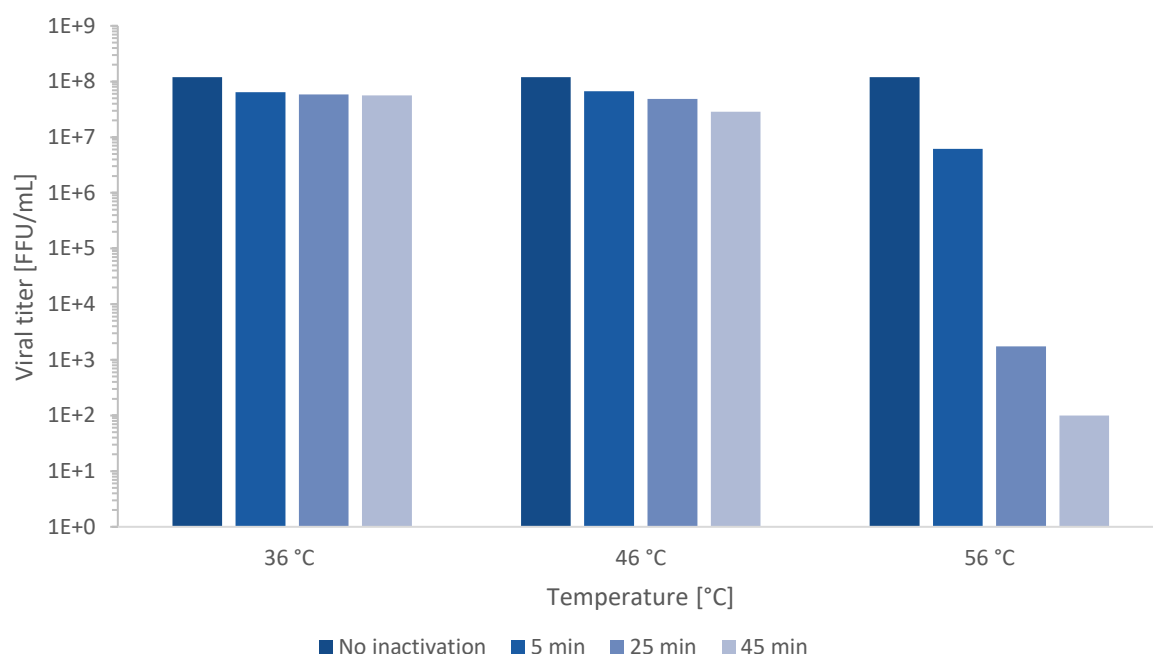


Figure 9: Foci forming units per mL of PF26#278 samples containing LCMV samples after 5, 25, and 45 minutes and 36, 46, and 56 °C thermal inactivation following a full factorial design of experimental set-up.

## 5.2 Alteration of metabolite concentrations of PF26#278 during thermal inactivation of LCMV for metabolite assays II

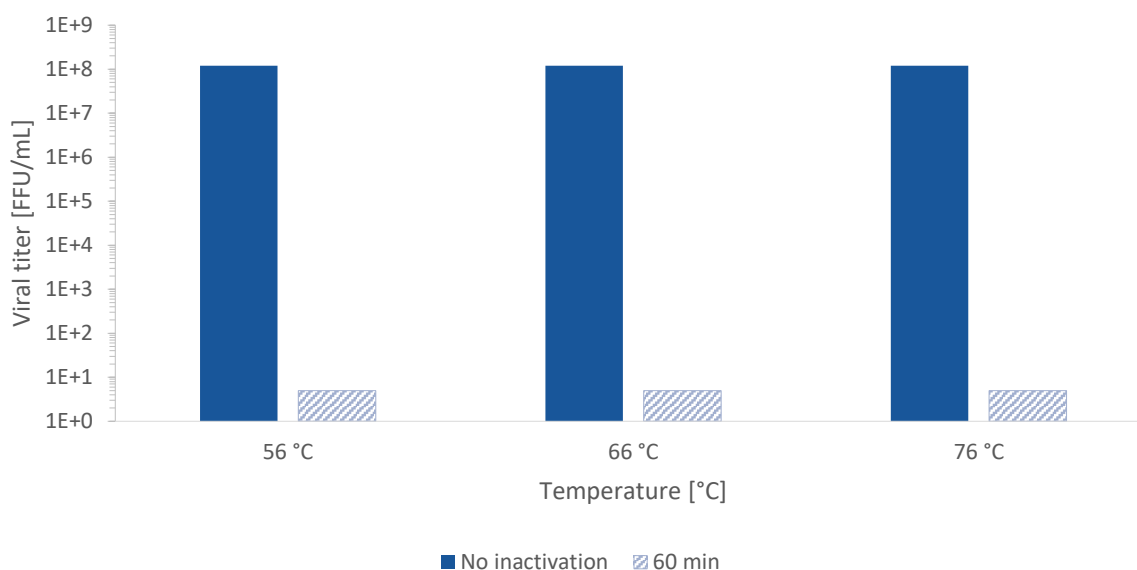


Figure 10: Foci forming units per mL of PF26#278 samples containing LCMV after 60 minutes inactivation at given temperatures (56, 66, and 76 °C). Dashed bars represent samples where the virus titer was below the detection limit of 5 FFU/mL of the FFU-Assay.

With an inactivation time of 60 minutes already at the lowest temperature, 56 °C, no virus particles were detectable in the FFU – assay. At least a 8.1 log clearance of LCMV in PF26#278 cultivation medium was observed, as dashed bars represent a virus titer below the detection limit of 5 FFU/mL.

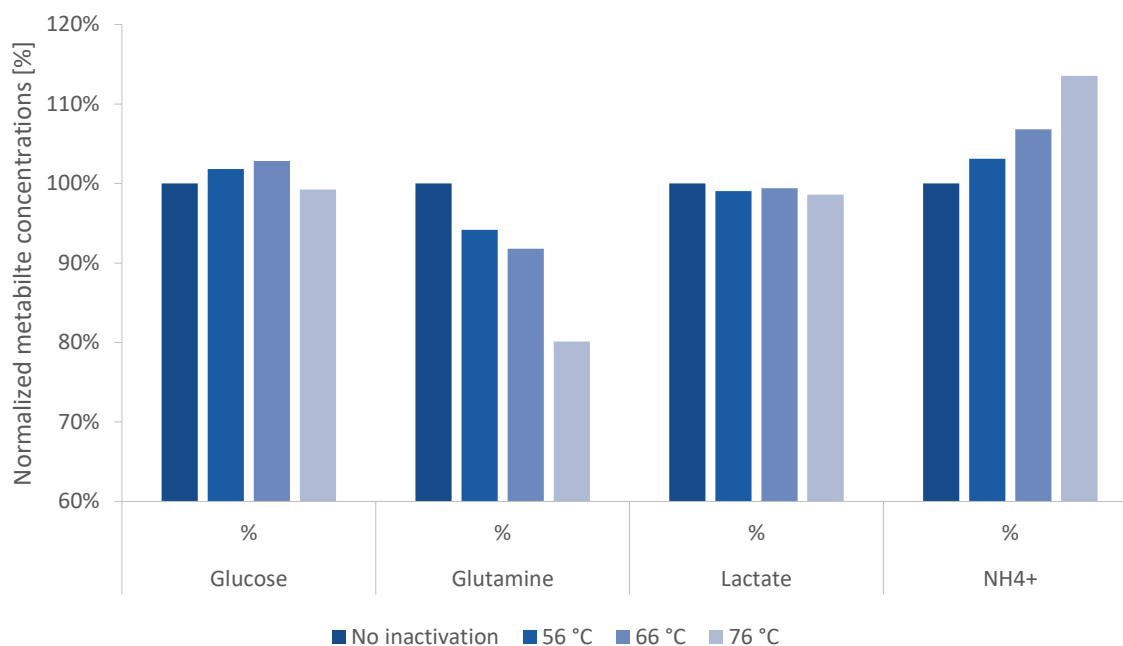


Figure 11: Changes in concentrations of selected metabolites (Glucose, Glutamine, Lactate, and Ammonia) of used PF26#278 cultivation medium after thermal inactivation at 3 different temperature (56, 66, 76 °C) for a duration of 60 minutes. Selected metabolites were analyzed using the Cedex Bio Analyzer. The percentages were calculated from mass concentrations.

Glucose and Lactate levels stayed nearly constant over the whole temperature range (see Figure 11) during the thermal inactivation. In contrast to Glutamine which dropped to 80 % of the untreated control and Ammonia which concentration raised by 14 % at 76 °C.

### 5.3 Alteration of metabolite concentrations of VP-SFM and PF26#280 during thermal inactivation of LCMV for metabolite assays

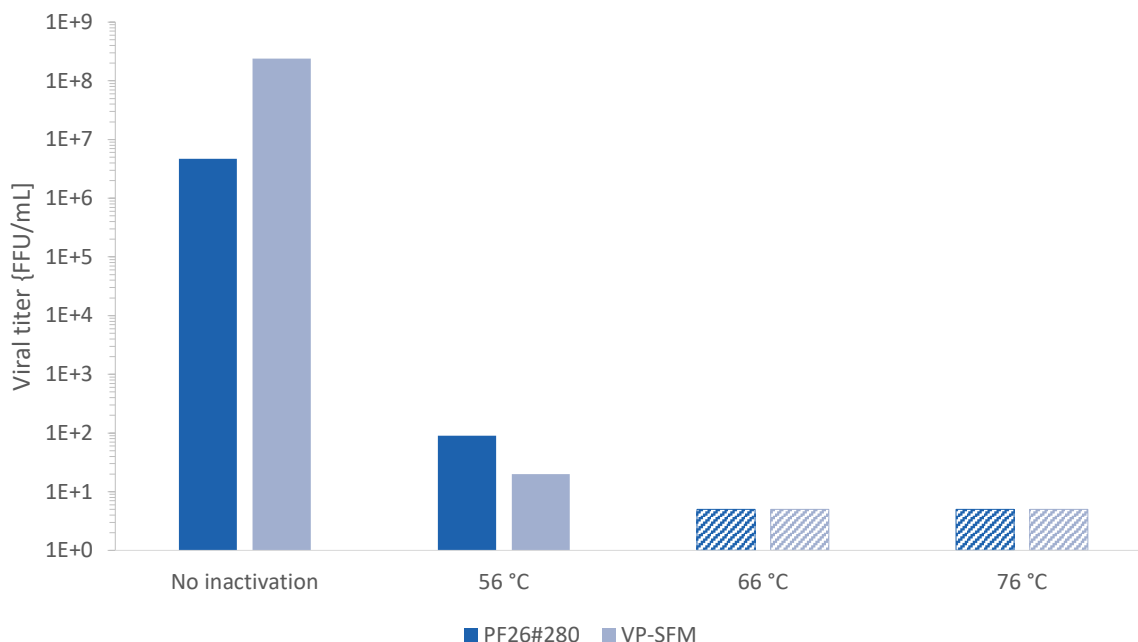


Figure 12: Foci forming units per mL of PF26#280 and VP-SFM samples containing LCMV after 0 and 60 minutes inactivation at given temperatures (56, 66, and 76 °C). Dashed bars represent samples where the virus titer was below the detection limit of 5 FFU/mL of the FFU-Assay.

With an inactivation time of 60 minutes at 66 °C, a full inactivation with an at least 8.4 log clearance of LCMV in VP-SFM, respectively an at least 6.7 log clearance for PF26#280 was observed, as dashed bars represent a virus titer below the detection limit of 5 FFU/mL (see Figure 12).

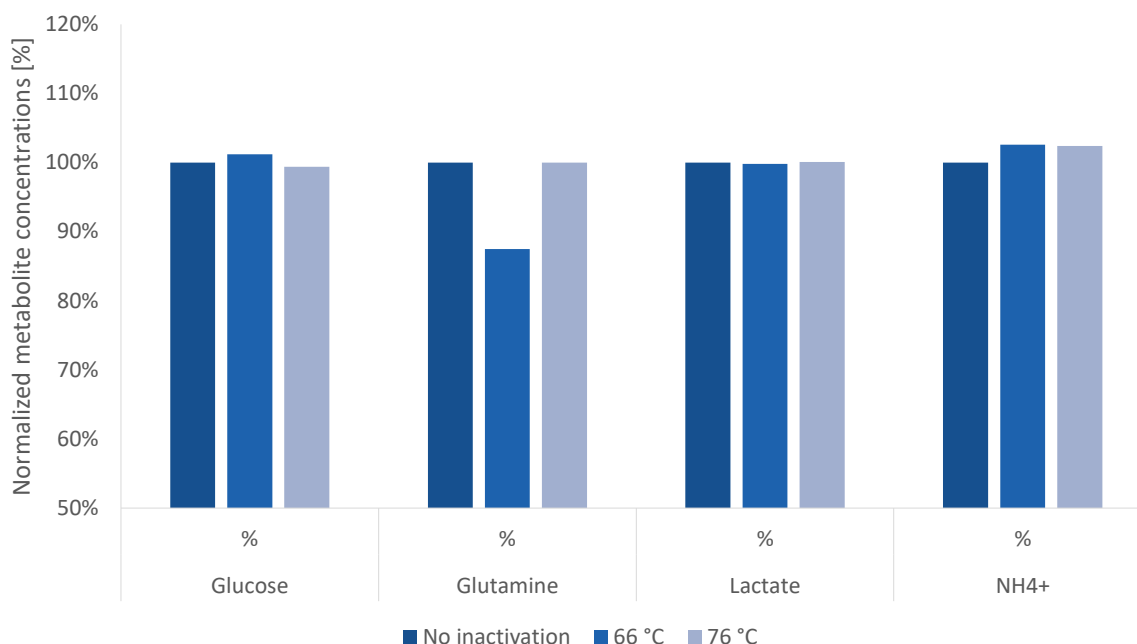


Figure 13: Changes in concentrations of selected metabolites (Glucose, Glutamine, Lactate, and Ammonia) of used PF26#280 cultivation medium after thermal inactivation at 2 different temperature (66, 76 °C) for a duration of 60 minutes. Selected metabolites were analyzed using the Cedex Bio Analyzer. The percentages were calculated from mass concentrations.

The concentrations of Glucose, Glutamine, Lactate, and Ammonia did not change drastically in comparison to the untreated control for 66 and 76 °C during the course of the inactivation for PF26#280 (see Figure 13). An observed drop to 88 % of Glutamine at 66 °C seems to be an outlier, as at 76 °C no change to the untreated control was seen.

For VP-SFM (see Figure 14) Glucose, Glutamine, and Lactate concentrations appeared to be not major influenced by the thermal treatment as concentrations varied by +/- 2 % for Glucose, Glutamine and Lactate at both inactivation temperatures. Ammonia levels however increased with increasing inactivation temperature by 10 % at 66 °C and by 16 % at 77 °C in comparison to the untreated control.

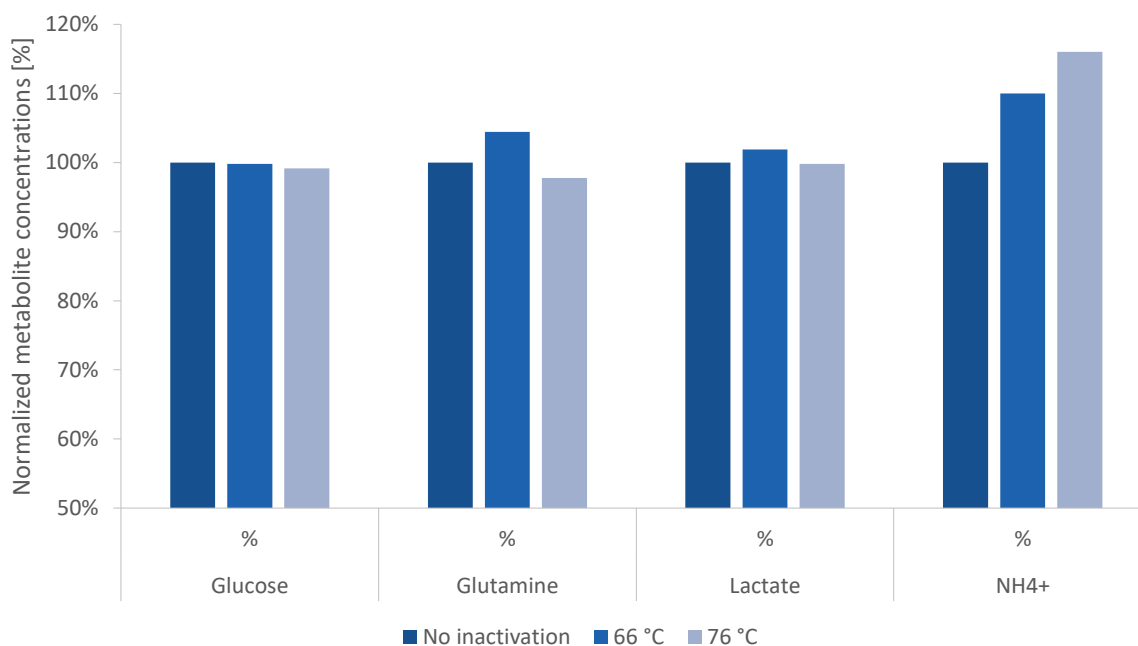
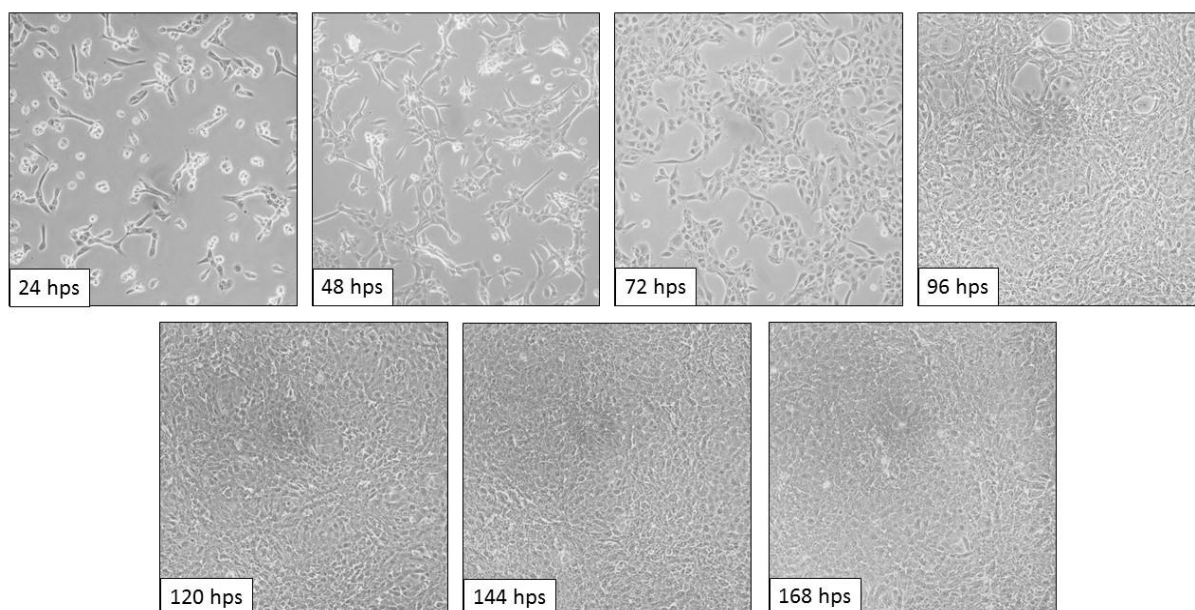


Figure 14: Changes in concentrations of selected metabolites (Glucose, Glutamine, Lactate, and Ammonia) of used VP-SFM cultivation medium after thermal inactivation at 2 different temperature (66, 76 °C) for a duration of 60 minutes. Selected metabolites were analyzed using the Cedex Bio Analyzer. The percentages were calculated from mass concentrations.

## 5.4 Influence of Glutamine and L-alanyl-L-glutamine on Vero cell growth characteristics



Picture 1: Phase contrast images of Vero cells over the course of cultivation.

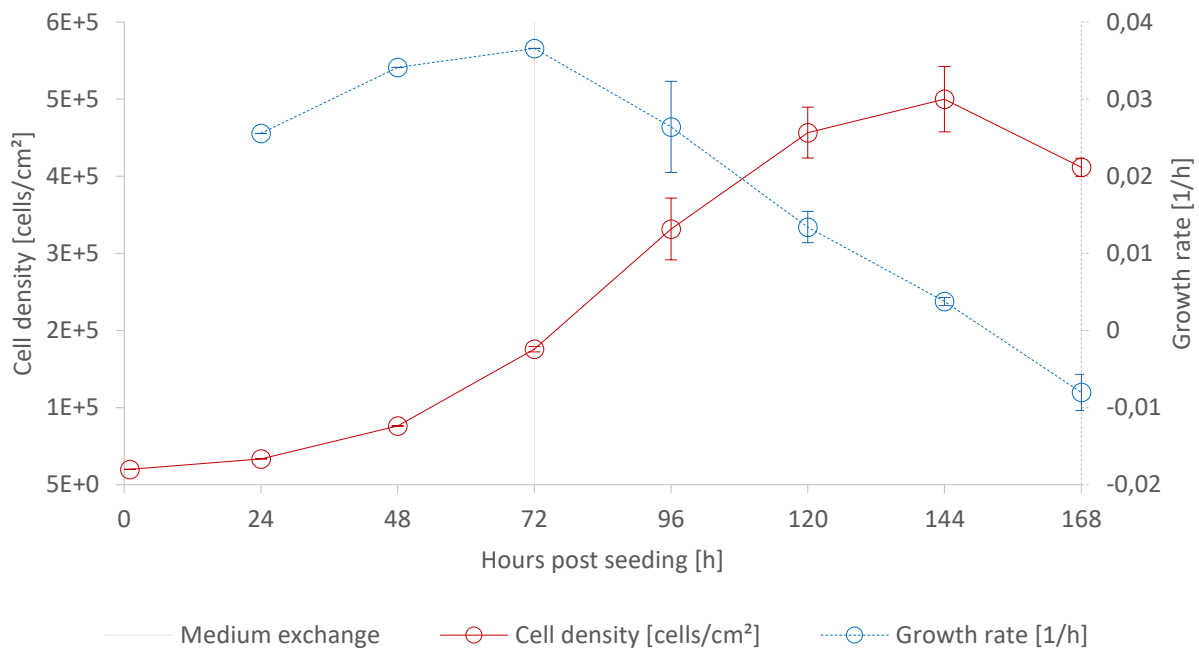


Figure 15: Cell densities [cells/cm<sup>2</sup>] and growth rates [h<sup>-1</sup>] of adherently growing Vero cells over a 168 hour cultivation period. Cells were seeded with  $3 \times 10^4$  cells/cm<sup>2</sup>. A medium exchange was performed 72 hps. Error bars represent the standard deviation of measured duplicates.

The growth behavior of the cells over a duration of 168 hours can be seen in *Figure 15*. For each sampling point the visual appearance was determined microscopically which can be seen in *Picture 1*. After seeding with  $3 \times 10^4$  cells/cm<sup>2</sup> with an initial lag-phase, cells started to expand until 120 hours upon reaching their stationary phase due to limiting surface area. After 144 hps their cell density peaked in  $4.57 \times 10^5$  cells/cm<sup>2</sup>, as cells grew in a full confluent cell layer (see *Picture 1*). A decrease in cell density was observed at the last sampling point. Furthermore the growth rate peaked with a cell density of  $1.78 \times 10^5$  cells/cm<sup>2</sup> 72 hps at 0.037 h<sup>-1</sup> and then steadily declined until 144 hps to 0.0034 h<sup>-1</sup> (*Figure 15*). At the last sampling point, 168 hps, growth rate declined below 0 with -0.008 h<sup>-1</sup>.

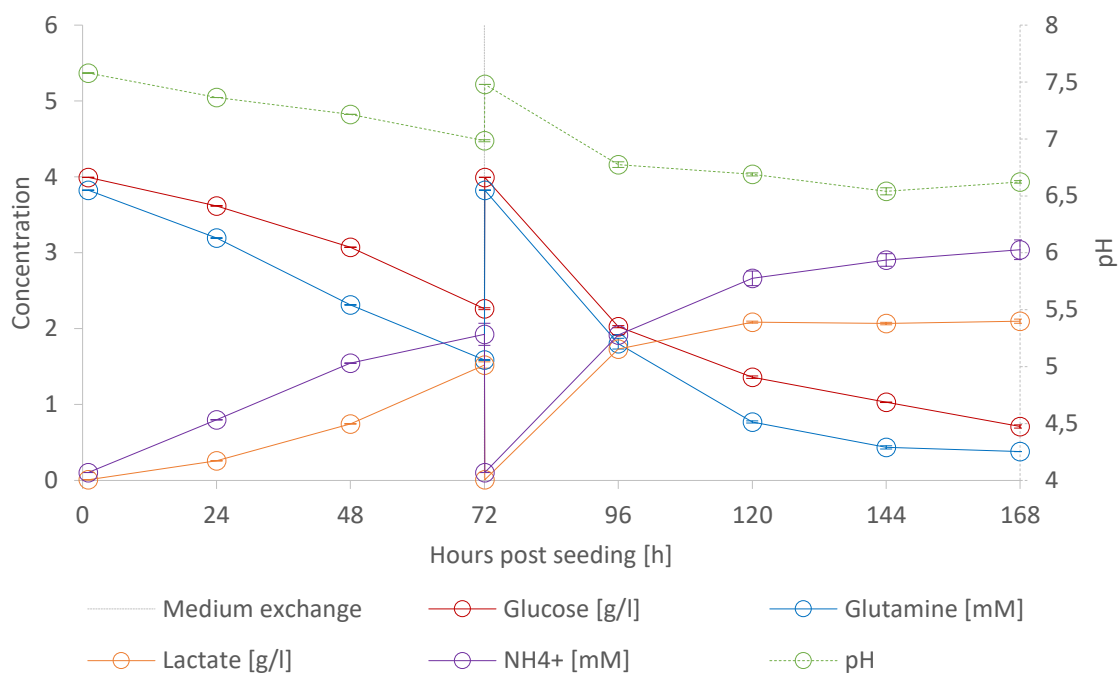


Figure 16: Selected metabolites, Glucose, Glutamine, Lactate and Ammonia on the primary y-axis and pH values on the secondary y-axis of adherently growing Vero cells over a 168 hour cultivation period. A medium exchange was conducted 72 hps. Error bars represent the standard deviation of measured duplicates.

The progression of pH and selected metabolites are depicted in *Figure 16*. Over the duration of 72 hours, until the medium exchange, Glucose levels dropped from 3.99 g/L to 2.26 g/L and Glutamine levels from 3.83 mM to 1.59 mM, whereas Lactate levels raised to 1.52 g/L and Ammonia to 1.93 mM. After a complete medium exchange and further 96 hours of cultivation, Glucose levels finally dropped to 0.71 g/L and Glutamine levels to 0.38 mM. In return, Lactate reached a plateau of approximately 2.1 g/L 120 hps and Ammonia levels peaked with 3.04 mM at the end of the cultivation. The medium acidified from an initial pH of 7.58 by 0.59 pH units until the medium exchange and further 0.96 units to a pH of 6.62 until the end of the cultivation.



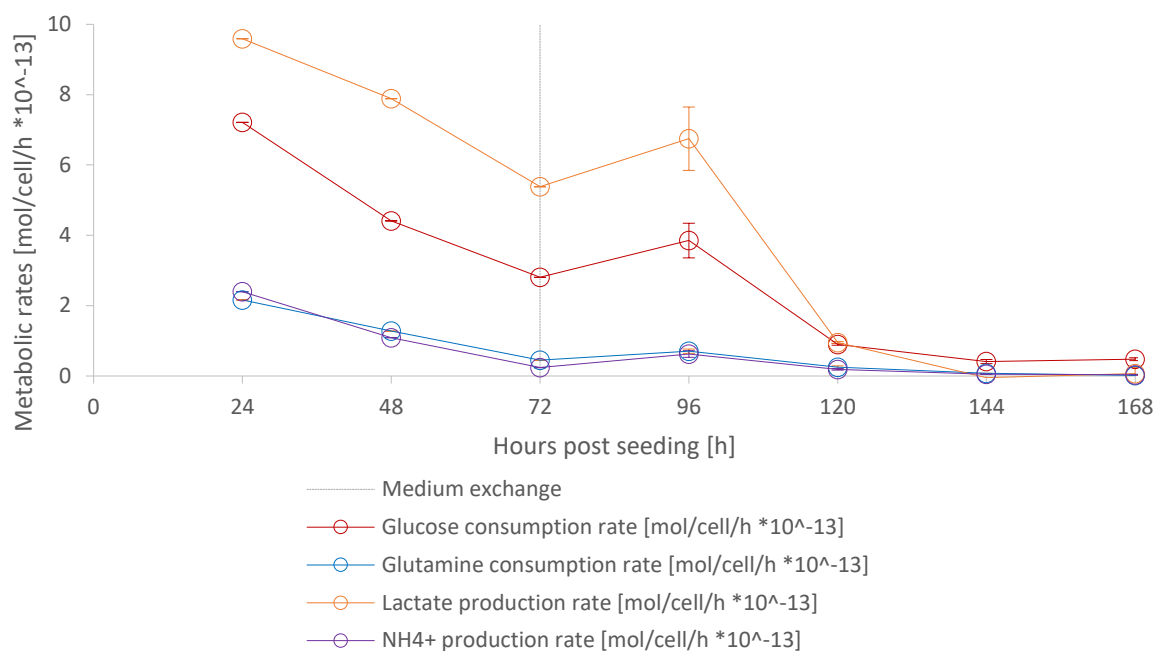


Figure 17: Specific molar metabolite rates [mol/cell/hour \* 10<sup>-13</sup>] of Glucose, Glutamine, Lactate and Ammonia during the course of cultivation. A medium exchange was performed 72 hps. Error bars represent the standard deviation of measured duplicates

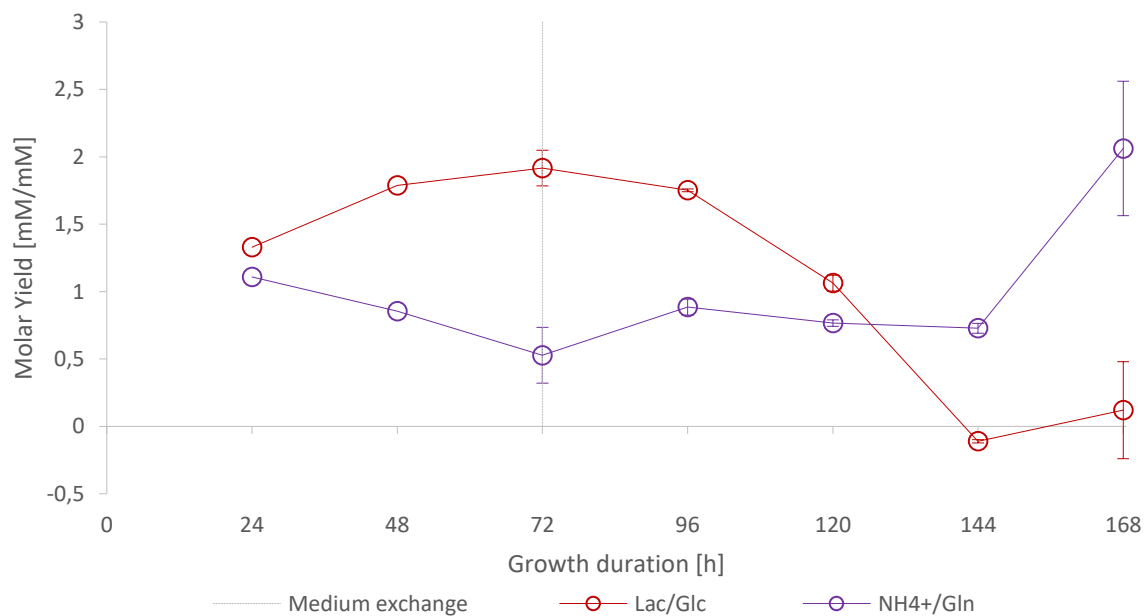


Figure 18: Progress of molar yields during cultivation as mM produced metabolites per mM consumed substrates on primary y- axis. On secondary y-axis in log-scale cells generated per mM substrate are plotted. A total medium exchange was performed 72 hps. Error bars represent the standard deviation of measured duplicates.

*Figure 17* shows the specific molar metabolite rates. The initial rates (Glucose:  $7.21 \times 10^{-13}$ ; Lactate:  $9.59 \times 10^{-13}$ ; Glutamine:  $2.16 \times 10^{-13}$ ; Ammonia:  $2.40 \times 10^{-13}$  mol/cell/hour) declined steadily until the medium exchange (Glucose:  $2.81 \times 10^{-13}$ ; Lactate:  $5.38 \times 10^{-13}$ ; Glutamine:  $0.45 \times 10^{-13}$ ; Ammonia:  $0.24 \times 10^{-13}$  mol/cell/hour). After the exchange, rates temporarily peaked 96 hps (Glucose:  $3.85 \times 10^{-13}$ ; Lactate:  $6.75 \times 10^{-13}$ ; Glutamine:  $0.71 \times 10^{-13}$ ; Ammonia:  $0.63 \times 10^{-13}$  mol/cell/hour) but then rapidly dropped 120 hps ((Glucose:  $0.90 \times 10^{-13}$ ; Lactate:  $0.96 \times 10^{-13}$ ; Glutamine:  $0.25 \times 10^{-13}$ ; Ammonia:  $0.19 \times 10^{-13}$  mol/cell/hour). Until the end of cultivation only a minor decrease was observed (Glucose:  $0.48 \times 10^{-13}$ ; Lactate:  $0.06 \times 10^{-13}$ ; Glutamine:  $0.02 \times 10^{-13}$ ; Ammonia:  $0.04 \times 10^{-13}$  mol/cell/hour). Further, the specific molar Glucose rates were roughly 3 to 6 fold higher than the one of Glutamine over the whole cultivation. The molar Lactate/Glucose yield increased from 1.33 to 1.92 until the medium exchange at 72 hps, where it peaked. Afterwards the yield started to decline to 0.12 until the end of cultivation. The negative shift at 144 hps then reversed the sign of the yield. The molar Ammonia/Glutamine yield decreased by approximately 50 % from 1.11 to 0.53 until the medium exchange and remained mainly constant 0.73 until 144 hps. At the last sampling point a sharp increase to 2.06 was observed.

The three T75 flasks supplemented with the stable dipeptide L-alanyl-L-glutamine instead of Glutamine were compared to the above-described set-up. Cell density, Glucose, Glutamine, Lactate and Ammonia-concentrations were analyzed of one flask 72 hps (see *Figure 19*) and the two other flasks were harvested at the end of the cultivation (see *Figure 20*).

The cell density of Vero cells supplemented with Glutamine after 72 hours cultivation was with  $1.78 \times 10^5$  cells/cm<sup>2</sup> slightly lower than the one with L-alanyl-L-glutamine with  $1.62 \times 10^5$  cells/cm<sup>2</sup>. Glucose and Lactate concentrations showed minor differences supplemented with Glutamine or L-alanyl-L-glutamine (Glucose: 2.26 to 2.12 g/L; Lactate: 1.52 to 1.62 g/L). Glutamine and Ammonia concentrations on the other hand showed a striking difference (Glutamine: 1.59 to 0.01 mM; Ammonia: 1.52 to 0.21 mM)

After 168 hours cell grew to a cell density of  $4.12 \pm 0.12 \times 10^5$  cells/cm<sup>2</sup> with Glutamine and  $4.19 \pm 0.15 \times 10^5$  cells/cm<sup>2</sup> with L-alanyl-L-glutamine. The Glucose concentration of cells supplemented with Glutamine appeared to be slightly lower with 0.71 g/L to 0.91 g/L of cells supplemented with L-alanyl-L-glutamine. Lactate levels did not differ noticeable comparing 2.10 g/L with 2.11 g/L. Glutamine concentrations converged at

## Results

the end of cultivation with 0.38 mM and 0.30 mM. A remarkable difference was observed in Ammonia levels where Glutamine supplemented flasks had a concentration of 3.04 mM whereas flasks supplemented with L-alanyl-L-glutamine showed a concentration of 0.53 mM.

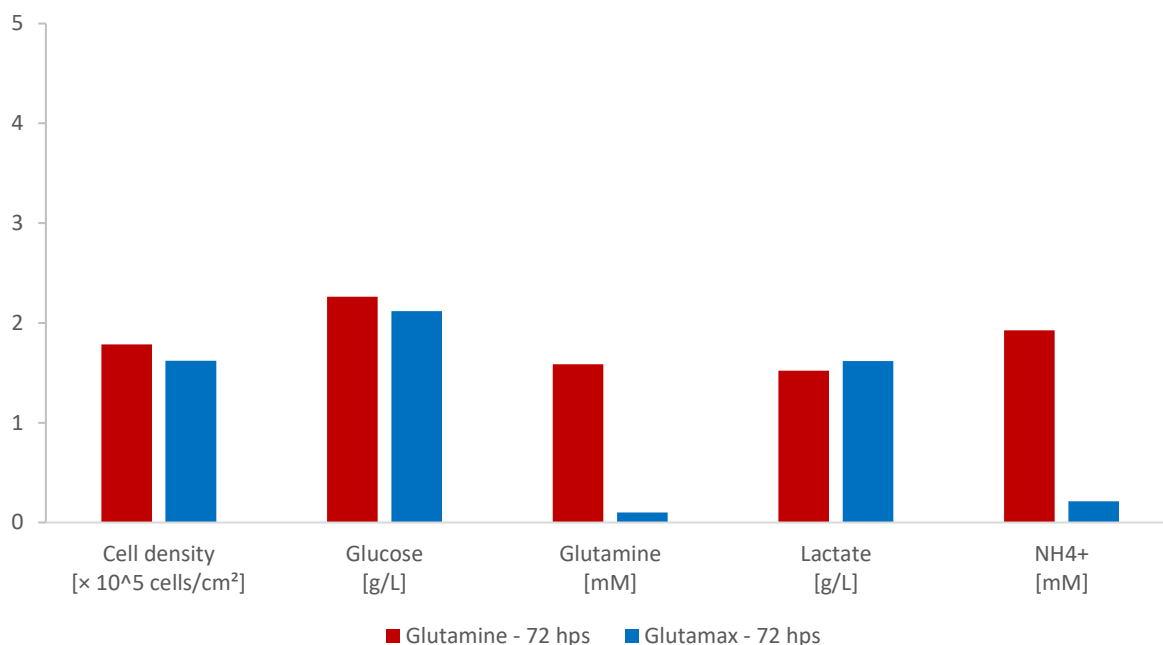


Figure 19: Comparison of Cell density in  $\times 10^5$  cells/cm<sup>2</sup>, Glucose- in g/L, Glutamine- in mM, Lactate- in g/L, and Ammonia-concentrations in mM of Vero cells after 72 hours cultivation supplemented with Glutamine and L-alanyl-L-glutamine, respectively. The units of the different parameters are displayed on the x-axis respectively.

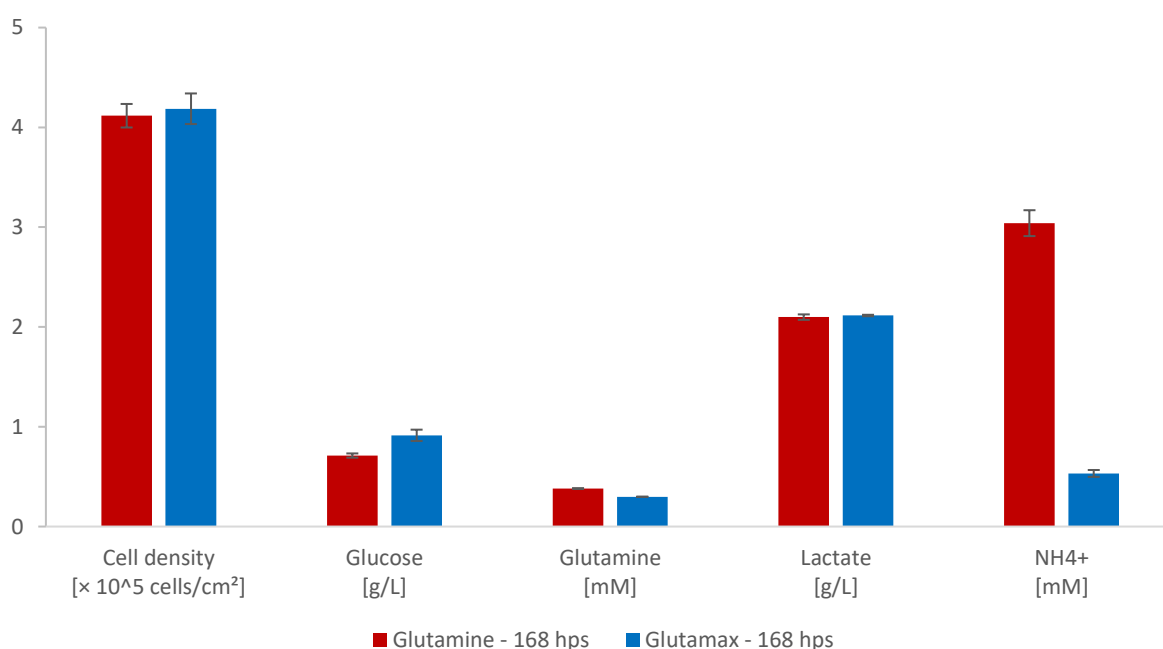


Figure 20: Comparison of Cell density in  $\times 10^5$  cells/cm<sup>2</sup>, Glucose- in g/L, Glutamine- in mM, Lactate- in g/L, and Ammonia-concentrations in mM of Vero cells after 168 hours cultivation supplemented with Glutamine and L-alanyl-L-glutamine, respectively. The units of the different parameters are displayed on the x-axis respectively. Error bars represent the standard deviation of duplicates.

### 5.5 Determination of an optimized MOI and SCD of adherently growing Vero cells

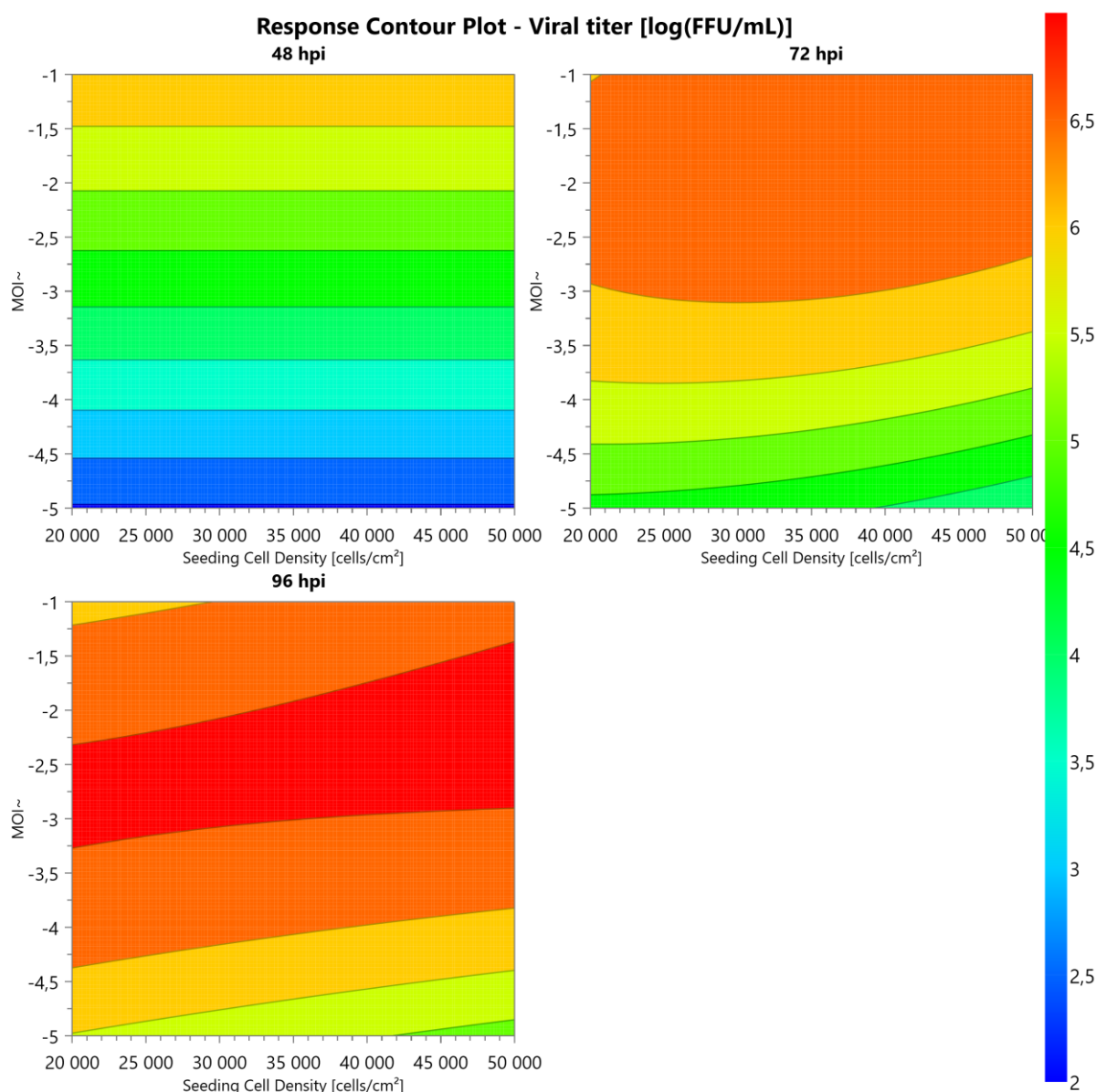
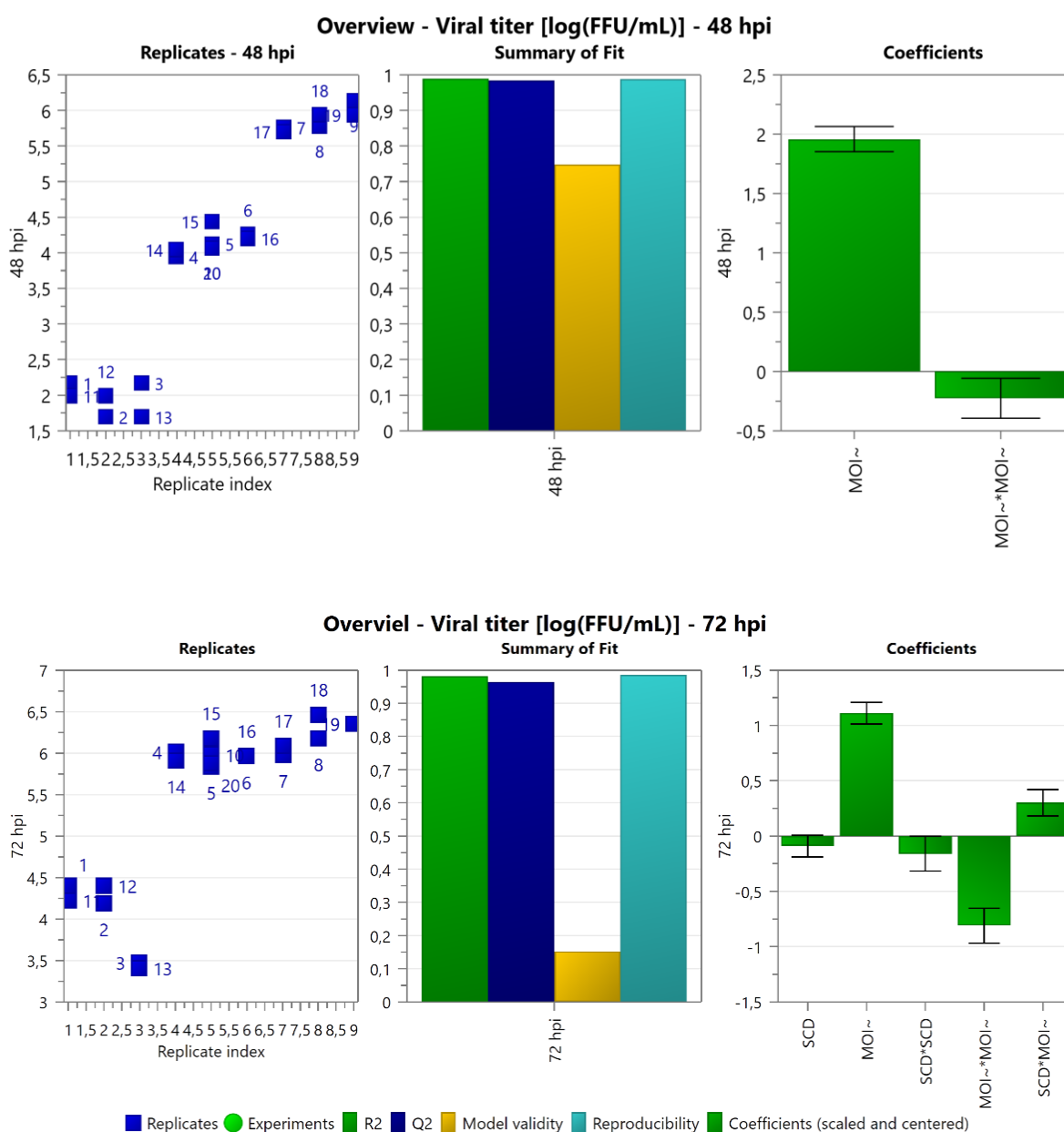


Figure 21: Response Contour Plots for the sampling points 48, 72 and 96 hpi generated with MODDE. The model shows the influence of MOI (y-axis) in log-scale and SCD (x-axis) over the range of  $10^{-5}$  to  $10^{-1}$ , respectively  $2 \times 10^4$  to  $5 \times 10^4$  cells/cm<sup>2</sup> on LCMV titer in [log (FFU/mL)]. Red areas indicate highest responses and blue areas lowest.

In *Figure 21* the virus propagation is modeled at three sampling points, 48, 72, and 96 hour post infection with the seeding cell density on the x-axis and the MOI in log scale on the y-axis. The first increase in LCMV titer was visible at the highest MOI of 0.1 after 48 hours. With increasing infection time also the virus propagation developed and the titer maximum started shifting down. 96 hours post infection the titer peaked with  $6.5 \times 10^6$  FFU/mL. The model indicated the titer maximum for an MOI between  $10^{-2.5}$  and  $10^{-3}$  over the whole investigated cell density range. The generated models showed a good fit and predictability with values over 0.8, only the validity for the 72 hpi-model was lower than 0.25 (see *Figure 22*). The coefficients of the model showed that MOI model terms had the strongest positive influence on each model but decreased with consecutive sampling points.



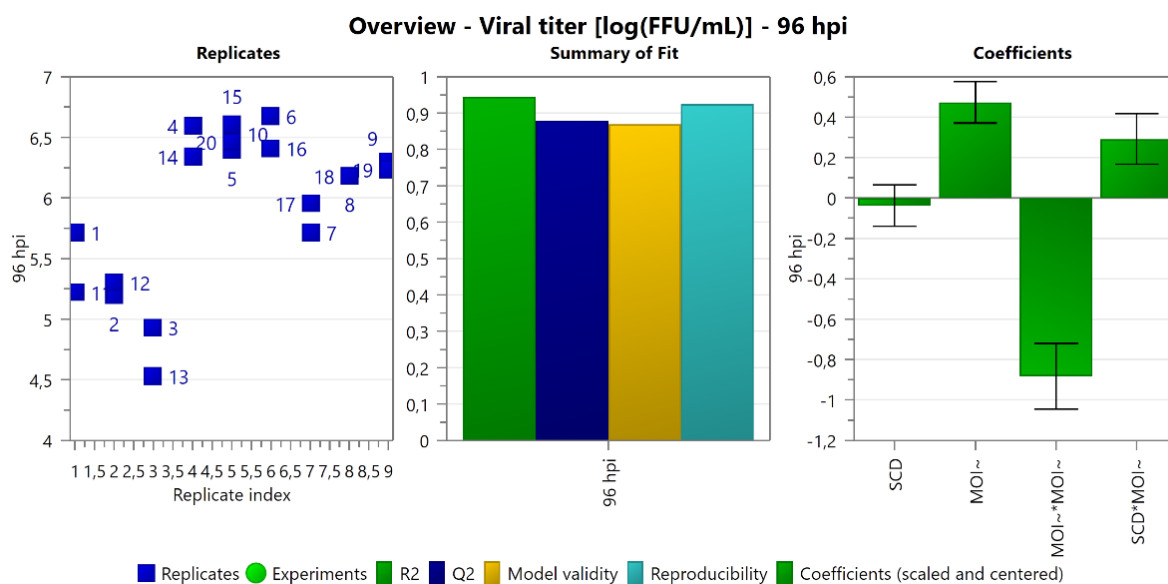
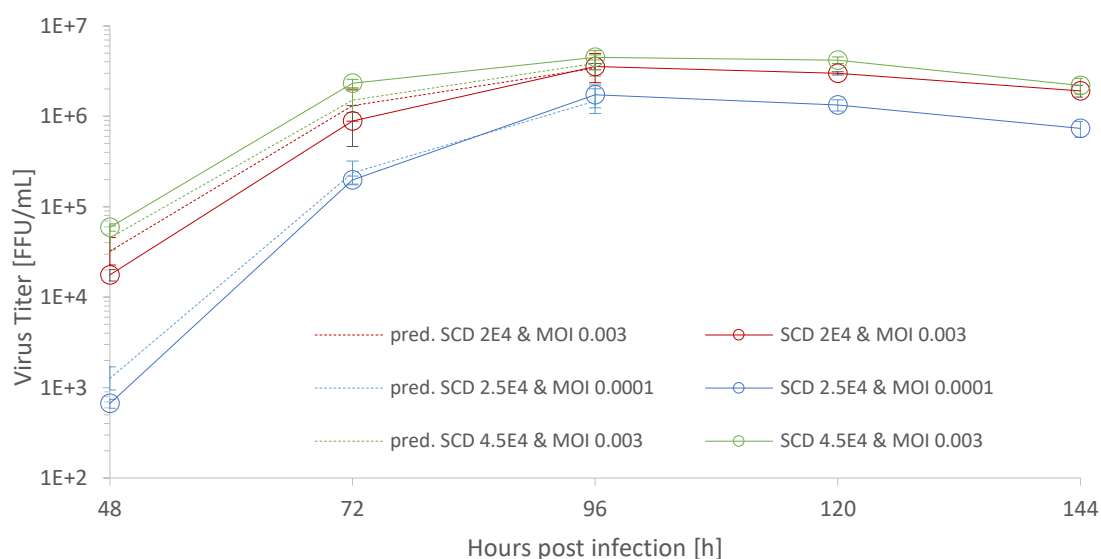


Figure 22: Overview Plots for each Response Contour Plot with the Replicates-, the Summary of Fit-, and Coefficients-Plot. The Replicates-Plot shows individual viral titer results in log (FFU/mL). The Summary of Fit box displays R<sup>2</sup>, which shows how well the data fit the model. Q<sup>2</sup> tells how well the model predicts new data, a value greater than 0.5 shows a good model. A Model validity value less than 0.25 indicates model problems, like present outliers or an incorrect model, but can also be low due to good duplicate values. The reproducibility shows the variation of the replicates to the overall variability and should be greater than 0.5. The Coefficients-Plot displays the coefficients of the linear and quadratic terms of the model. The error bars represent the 95 % confidence interval. Quadratic non-significant model terms, where uncertainty range clearly crossed 0, were removed from the model.

## 5.6 Proof of Concept for infection of adherently growing Vero cells with LCMV



## Results

Figure 23: Virus titers [FFU/mL] in comparison to predicted titers of three investigated set points of the proof of concept. Dashed lines represent predicted values based on the calculated model. Full lines represent values measured in triplicates. Error bars of the predicted values represent lower and upper boundaries. Error bars of measured values represent standard deviation.

Table 4: Lower and upper boundaries for predicted viral titers calculated based on the established model and viral titer results in FFU/mL for each sampling point.

Unit	48 hpi		
	Lower boundary [FFU/mL]	Upper boundary [FFU/mL]	Result [FFU/mL]
SCD 2.0E4 cell/cm <sup>2</sup> & MOI 3E-3 FFU/cell	$2,27 \times 10^4$	$4,57 \times 10^4$	$1,77 \pm 0.26 \times 10^4$
SCD 2.5E4 cell/cm <sup>2</sup> & MOI 1E-4 FFU/cell	$9,42 \times 10^2$	$1,70 \times 10^3$	$6.68 \pm 0.76 \times 10^2$
SCD 4.5E4 cell/cm <sup>2</sup> & MOI 1E-3 FFU/cell	$3,34 \times 10^4$	$6,13 \times 10^4$	$5.92 \pm 0.55 \times 10^4$
Unit	72 hpi		
	Lower - [FFU/mL]	Upper boundary [FFU/mL]	Result [FFU/mL]
SCD 2.0E4 cell/cm <sup>2</sup> & MOI 3E-3 FFU/cell	$8,85 \times 10^5$	$1,96 \times 10^6$	$8.90 \pm 4.26 \times 10^5$
SCD 2.5E4 cell/cm <sup>2</sup> & MOI 1E-4 FFU/cell	$1,75 \times 10^5$	$3,20 \times 10^5$	$1.98 \pm 0.20 \times 10^5$
SCD 4.5E4 cell/cm <sup>2</sup> & MOI 1E-3 FFU/cell	$1,10 \times 10^6$	$2,05 \times 10^6$	$2.32 \pm 0.25 \times 10^6$
Unit	96 hpi		
	Lower - [FFU/mL]	Upper boundary [FFU/mL]	Result [FFU/mL]
SCD 2.0E4 cell/cm <sup>2</sup> & MOI 3E-3 FFU/cell	$2,36 \times 10^6$	$4,96 \times 10^6$	$3.56 \pm 0.29 \times 10^6$
SCD 2.5E4 cell/cm <sup>2</sup> & MOI 1E-4 FFU/cell	$1,08 \times 10^6$	$2,02 \times 10^6$	$1.73 \pm 0.49 \times 10^6$
SCD 4.5E4 cell/cm <sup>2</sup> & MOI 1E-3 FFU/cell	$2,79 \times 10^6$	$5,33 \times 10^6$	$4.49 \pm 0.29 \times 10^6$

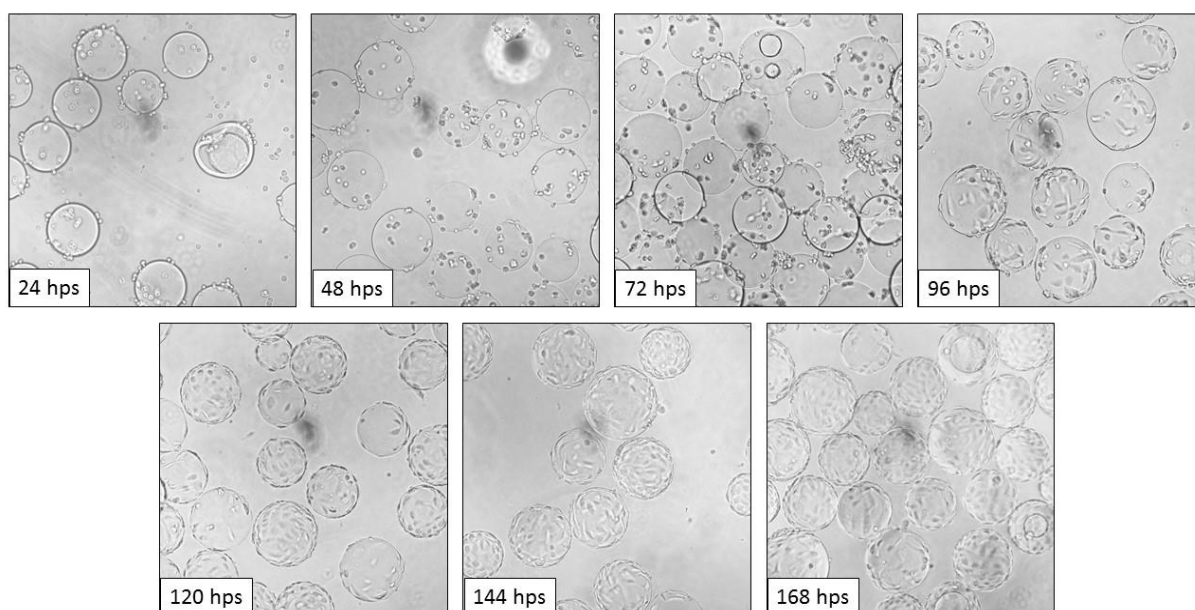
Table 5: Cell density, specific titer and viral yield of Vero cells 96 hpi with LCMV. Cells were seeded with  $2 \times 10^4$  cells/cm<sup>2</sup> and infected with an MOI of 0.003 FFU/cell 72 hps.

Unit	Cell density [cells/cm <sup>2</sup> ]	Specific titer [FFU/cell]	Viral yield
SCD 2.0E4 cell/cm <sup>2</sup> & MOI 3E-3 FFU/cell	$4.16 \pm 0.06 \times 10^5$	$1.23 \pm 0.13$	$409 \pm 44$

As it is stated in Table 4 and Figure 23, at 48 hpi only the set point with the seeding cell density of  $4.5 \times 10^4$  cell/cm<sup>2</sup> and a MOI of 0.003 FFU/cell was within the boundaries. For the other two setpoints the model predicted higher titers than actually measured. In contrast, on the second sampling point, 72 hpi, was the previously mentioned set point outside the upper boundary. The other set points were predicted correctly inside their boundaries. At the last sampling point, 96 hpi, the model

succeeded in the prediction of all 3 investigated set points as, all results were inside their boundaries. The optimal set point showed a specific titer of  $1.23 \pm 0.13$  FFU/cell at the titer peak. This calculates to a  $409 \pm 44$  fold increase in viral titer from the initial virus seed amount. At consecutive sampling points, no further increase in viral titer was observed for all tested set points.

### 5.7 Initial cultivation and infection of Vero cells on microcarriers in shake flasks



*Picture 2: Phase contrast images of Vero cells on Cytodex 1 microcarrier over the course of cultivation.*



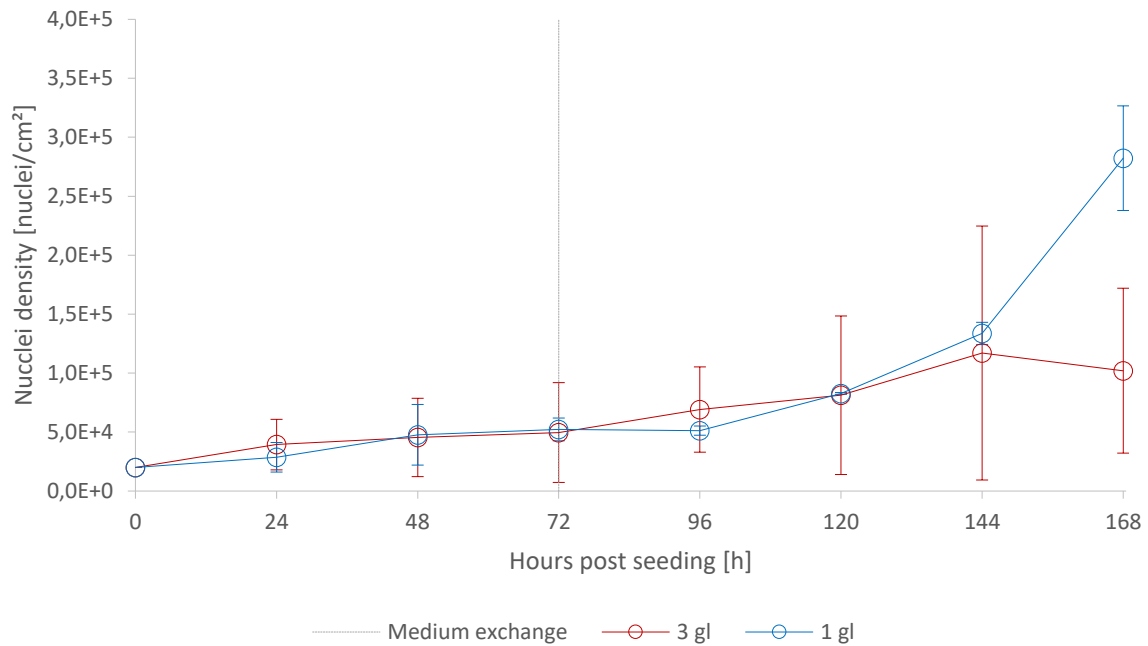


Figure 24: Released nuclei per cm<sup>2</sup> of Vero cells cultivated on Cytodex 1 microcarrier. A medium exchange was performed 72 hps. Error bars represent the standard deviation.

It can be seen in *Picture 2* and in *Figure 24* that although cells showed a successful attachment after the first 24 hours an unknown cell growth-inhibiting factor was interfering. Cell morphology remained spherical and no spreading on the microcarrier surface was observed. Therefore cell density stalled at approximately  $2$  to  $4 \times 10^4$  nuclei/cm<sup>2</sup> until 72-96 hps. After this period, combined with a 60 % medium exchange, some cells seemed to partially overcome this inhibition and started to spread and expanded around the microcarrier until the end of the cultivation period of 168 hours. Other cells (mainly one duplicate unit of the 3 g/L microcarrier flasks) stopped growth completely, which can be seen with the increasing standard deviation over the incubation period.

## 5.8 Evaluation of cell growth inhibiting factors on Vero cells in microcarriers cultivation

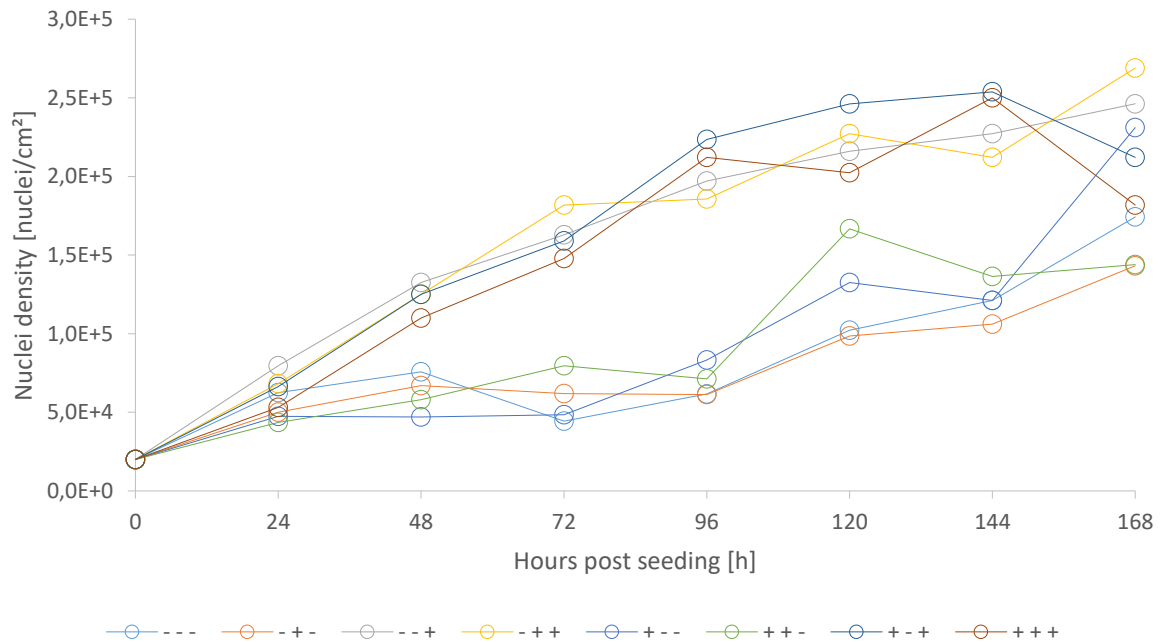
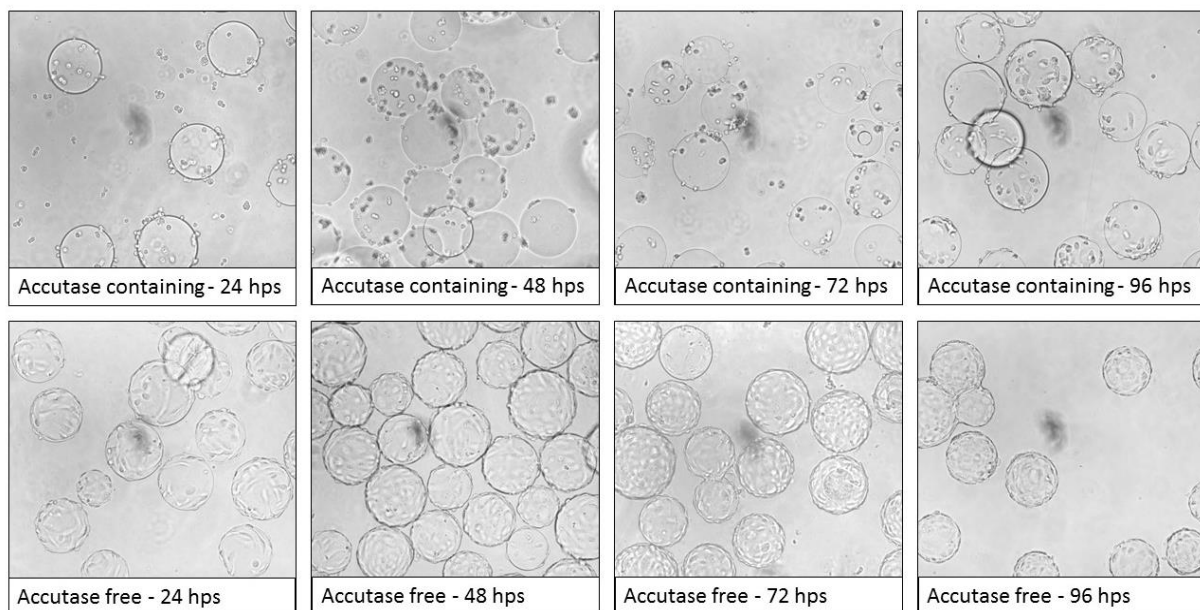
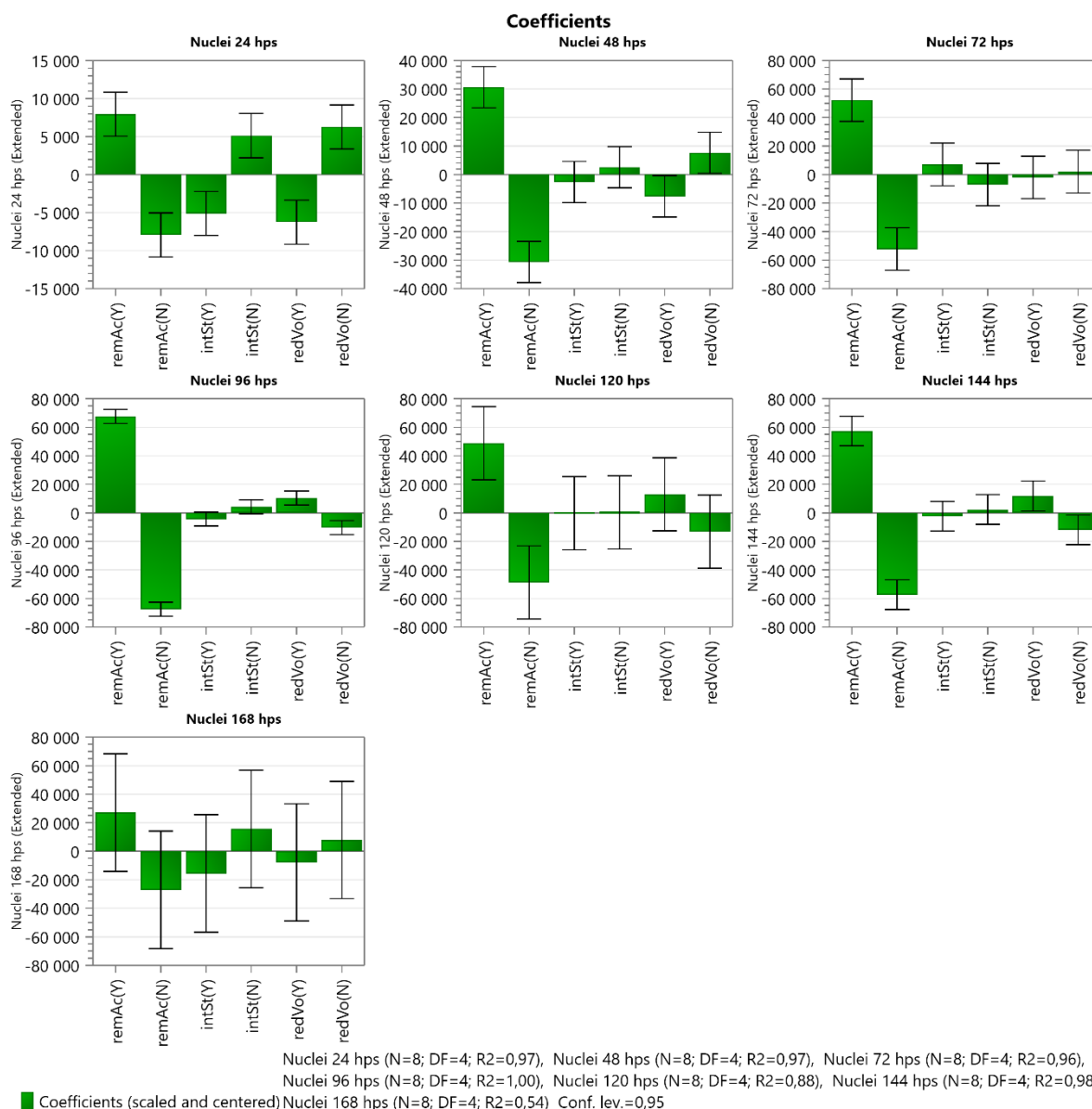


Figure 25: Nuclei per cm<sup>2</sup> of Vero cells on 3g/L microcarrier over the cultivation period. Cells were seeded with  $2 \times 10^4$  cells/cm<sup>2</sup>. A medium exchange, by sedimentation and replacement of 60 % medium was performed 72 hps and cells were infected with LCMV with a MOI of 0.003. In the legend +/- represents the presence or absence of the investigated influence in the order of Reduced volume / Intermittent stirring / Accutase removal.



Picture 3: Phase contrast images of comparison of Vero cells with Accutase remains versus Accutase free medium.

By taking a close look at the cell propagation depicted in *Figure 25* two distinct groups formed. Cells where Accutase was removed prior seeding started earlier to propagate and reached on average a 2 to 3 fold higher cell density over the course of cultivation. At the last sampling points, also the inhibited cells started to propagate. The difference in cell growth is also visible in *Picture 3* where the initial flattening and spreading of the cells around the microcarrier was observed. A clear distinction, as seen for the removed Accutase, could not be confirmed for a reduced volume or intermittent stirring.



*Figure 26: Coefficient Plot of screening model terms of investigated influences on cell growth measured by released nuclei per mL of Vero cells in 3 g/L microcarrier over the cultivation period. remAc represents the removal of Accutase prior seeding. intSt represents intermittent stirring at seeding. redVol represents a reduced volume at seeding. (Y) or (N) stands for “Yes” or “No”. The error bars represent the 95 % confidence interval. Model terms where the uncertainty range crosses Zero can be seen as non-*

## Results

significant. For better discrimination of significant influences, these terms were not removed from the screening model.

An analysis with MODDE of the DoE-setup (see *Figure 26*) showed that in the timeframe between 48 to 144 hps the removal of Accutase showed major positive significant model terms, whereas remaining Accutase showed significant negative model terms for the response VCD. 24 hps the model suggested that all model terms showed a significant influence on the cell density. The expected beneficial effects of a reduced volume and intermittent stirring during seeding could not be seen. At the last cultivation time point the model was not able to distinguish significant influences any more.

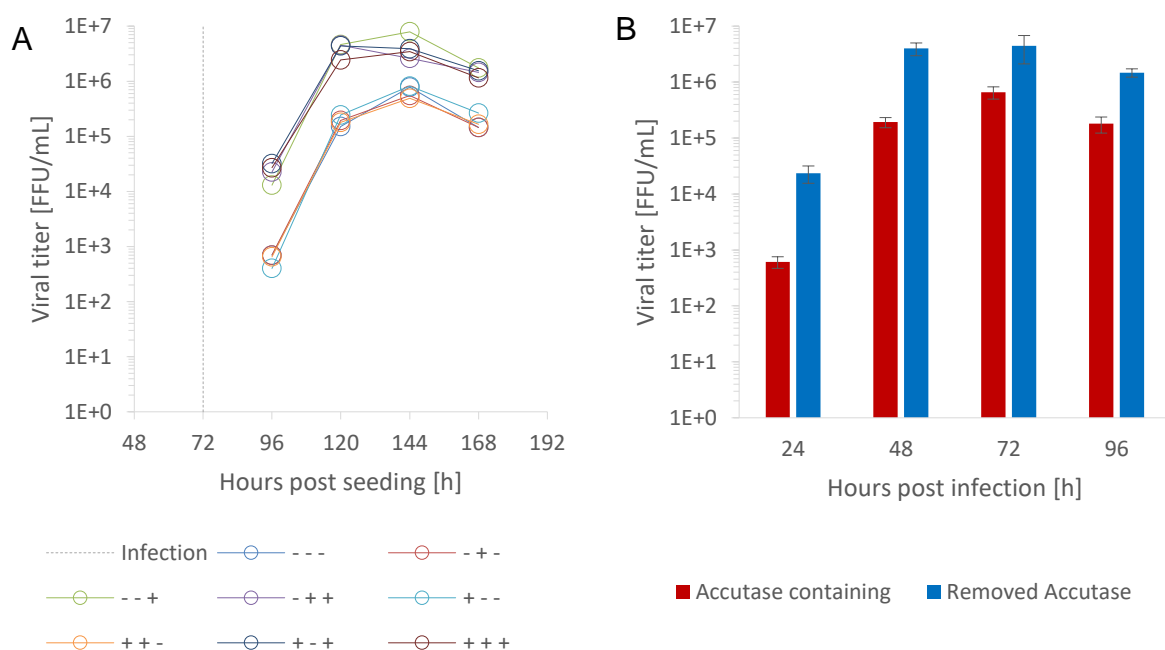


Figure 27: **A:** LCMV titer in FFU per mL in log-scale produced by Vero cells on 3 g/l microcarrier over the cultivation period. Cells were seeded with  $2 \times 10^4$  cells/cm<sup>2</sup>. A medium exchange, by sedimentation and replacement of 60 % medium was performed 72 hps before infection with LCMV with a MOI of 0.003. In the legend +/- represents the presence or absence of the investigated influence in the order of Reduced volume / Intermittent stirring / Accutase removal. **B:** Averaged LCMV titer in FFU/mL in log-scale on y-axis of four units each with or without Accutase over the course of cultivation. Error bars represent the standard deviation.

The effect of the Accutase removal on the viral titer can be seen in *Figure 27*. In *Figure 27B*, averaged from 4 units each with or without Accutase, already after 24 hpi (96 hps) an approximately 40 fold higher viral titer ( $6 \times 10^2$  with Accutase to  $2.4 \times 10^4$  FFU/mL without Accutase) can be observed. At consecutive sampling points as virus

titer started to reach a plateau, the difference declined to approximately 20 fold 48 hpi ( $1.9 \times 10^5$  with Accutase to  $4.0 \times 10^6$  FFU/mL without Accutase), approximately 7 fold 72 hpi ( $6.6 \times 10^5$  with Accutase to  $4.5 \times 10^6$  FFU/mL without Accutase) and approximately 8 fold 96 hpi ( $1.8 \times 10^5$  with Accutase to  $1.5 \times 10^6$  FFU/mL without Accutase). Accutase containing samples showed an average peak 72 hpi, whereas samples with removed Accutase showed their maximum in the timeframe between 48 and 72 hpi.

## 5.9 Cultivation and infection of Vero cells on microcarriers in shake flasks

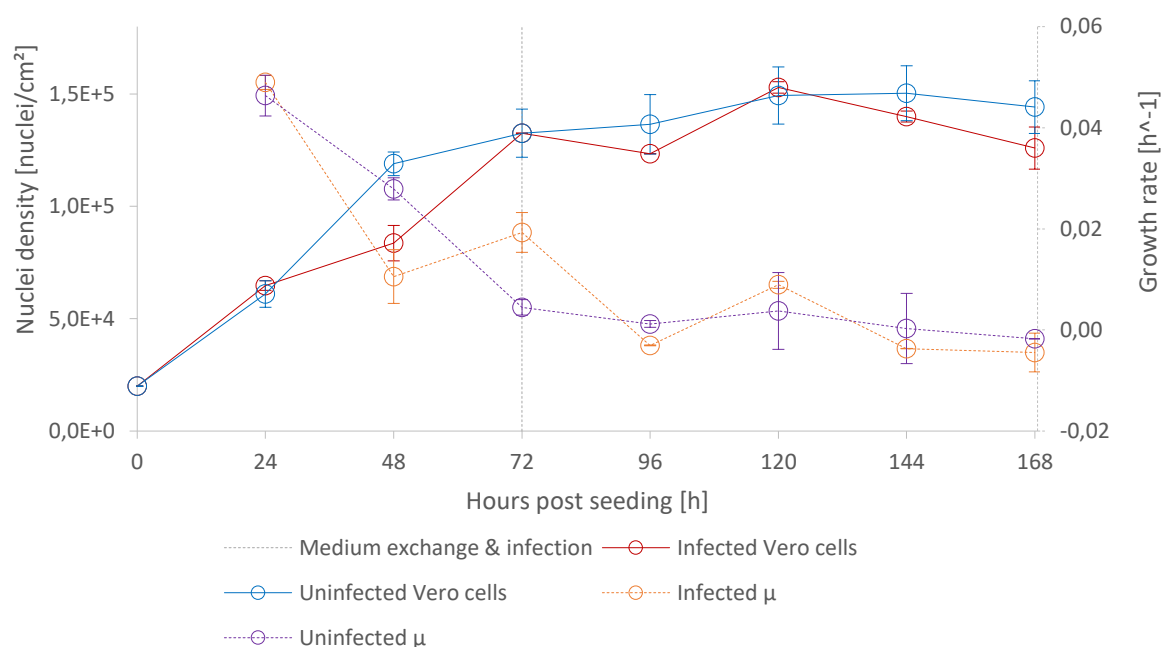
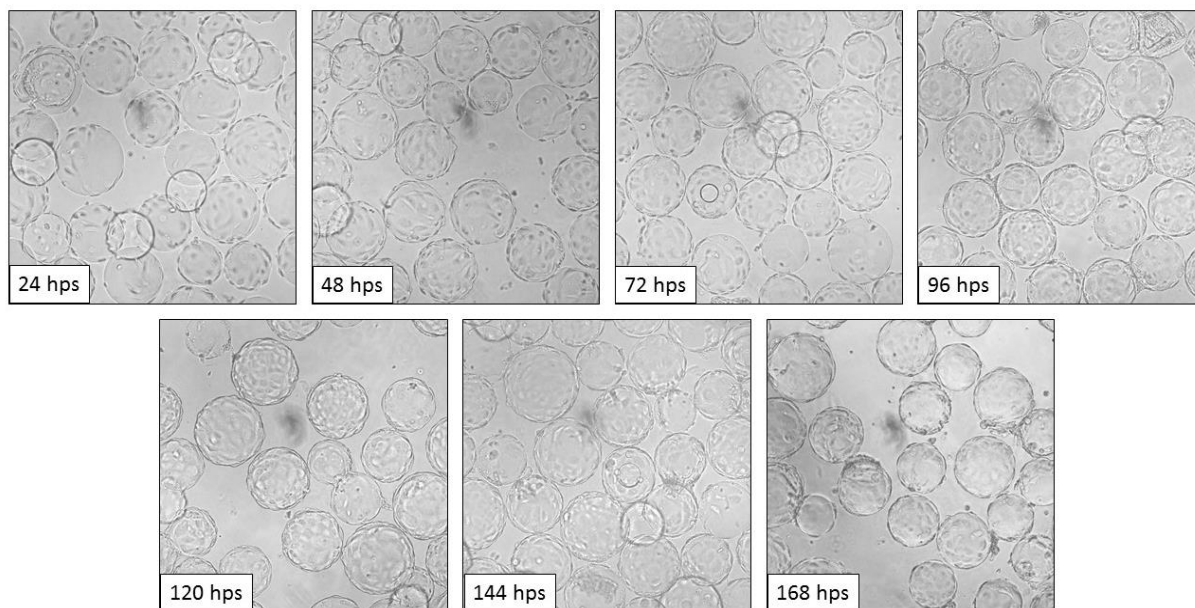


Figure 28: Comparison of the propagation of infected and uninfected Vero cells over the course of cultivation on the primary y-axis. On the secondary y-axis the calculated growth rate in  $h^{-1}$  is displayed for infected and uninfected nuclei. A 60 % medium exchange and infection with LCMV with a MOI of 0.003 FFU/cell occurred 72 hps (dotted line). Error bars represent the standard deviation.



Picture 4: Phase contrast images of propagation of Vero cells on 3 g/L Cytodex 1 microcarrier over the course of cultivation.

In *Figure 28* the comparison of the propagation of infected and uninfected Vero cells on 3 g/L Cytodex 1 microcarrier is plotted. After the seeding of  $2 \times 10^4$  cells/cm<sup>2</sup>, cells attached and started to spread around the microcarrier (see *Picture 2*), increasing to a nuclei density of  $1.33 \times 10^5$  nuclei/cm<sup>2</sup> after 72 hpi. Afterwards a 60 % medium exchange and infection with LCMV with a MOI of 0.003 FFU/nuclei was conducted. In following sampling points, cell propagation stalled reaching its peak at  $1.50 \times 10^5$  nuclei/cm<sup>2</sup> at 144 hps for the uninfected cells, respectively with  $1.53 \times 10^5$  nuclei/cm<sup>2</sup> at 120 hours for the infected cells. At the last two sampling points the cell density of infected cells decreased steadily to  $1.26 \times 10^5$  nuclei/cm<sup>2</sup>. Uninfected cells only showed a minor decrease to  $1.44 \times 10^5$  nuclei/cm<sup>2</sup>. Growth rates declined from initial  $0.049 \text{ h}^{-1}$  and  $0.046 \text{ h}^{-1}$  for at the time uninfected cells to  $0.005 \text{ h}^{-1}$  and  $0.019 \text{ h}^{-1}$  at 72 hps. Uninfected cells then showed a steady decline after the medium exchange to  $-0.002 \text{ h}^{-1}$ . The growth rate of infected cells showed a higher fluctuation between sampling points 72 to 168 hps and settled at  $-0.005 \text{ h}^{-1}$  on the last sampling point.

The replenishment of media, after a 60 % medium exchange, which are reflected in concentration readings of Glucose, Lactate and pH 72 hps, is displayed in *Figure 29*. Glucose concentrations of both uninfected cells declined from 4 g/L to 1.39 and 1.38 g/L respectively. Lactate concentrations increased to 2.27 g/L and 2.29 g/L respectively. 24 hours after the medium exchange Glucose concentration reading dropped from 2.79 g/L to 1.55 g/L for infected cells and from 2.76 g/L to 1.56 g/L for

uninfected cells. Until the end of the cultivations, concentration levels declined to 0.77 g/L for infected cells and to 0.81 g/L for uninfected cells. The Lactate concentration raised from 1.09 g/L to 2.04 g/L for infected cells, and from 1.08 g/L to 2.02 g/L for uninfected cells in the first 24 hours after the medium exchange. A peak in Lactate concentration was reached 120 hps with 2.10 g/L for infected and 2.09 g/L for uninfected cells. Until the end of the experiment, the concentrations dropped slightly to 1.97 g/L and 1.88 g/L for both, infected and uninfected cells. pH values dropped from 7.579 to 6.581 and 6.580 respectively, until the medium exchange. After the exchange, a drop from 7.130 to 6.775 for infected cells and 6.736 for uninfected cells was measured 24 hours later. pH values reached their minimum 144 hps with 6.746 for infected cells and 6.722 for uninfected cells. At the last sampling point a minor increase to 6.764 for infected and 6.790 for uninfected cells was observed.

The uninfected molar Glucose consumption rates, in *Figure 30*, showed a peak 48 hps with  $2.74 \times 10^{-13}$  mol/cell/hour and  $1.90 \times 10^{-13}$  mol/cell/hour. For Lactate both production rates peaked 48 hps with 5.20 and  $3.65 \times 10^{-13}$  mol/cell/hour. Until the medium exchange, molar Glucose consumption rates declined by 0.82 and  $0.83 \times 10^{-13}$  mol/cell/hour. Lactate production rates decreased to 1.17 and  $1.12 \times 10^{-13}$  mol/cell/hour. After the medium exchange a temporally peak in Glucose consumption rate with 1.78 for infected cells and  $1.57 \times 10^{-13}$  mol/cell/hour for uninfected cells and in Lactate production rate with 2.72 for infected cells and  $2.45 \times 10^{-13}$  mol/cell/hour for uninfected cells was observed. Molar Glucose consumption rate then subsequently declined to 0.18 for infected cells and  $0.11 \times 10^{-13}$  mol/cell/hour for uninfected cells 168 hps. The molar Lactate production rate reversed 144 hps and stalled at -0.11 for infected cells and  $-0.24 \times 10^{-13}$  mol/cell/hour 168 hps. The molar yields of Lactate per Glucose showed a peak 48 hpi with 1.90 and 1.92 for infected and uninfected cells. Before the medium exchange, a decrease in molar yields to 1.44 and 1.34 for infected and uninfected cells was observed. After the exchange the yields peaked again with 1.53 (infected) and 1.56 (uninfected) only to decrease steadily at following sampling points to -0.77 (infected) and -1.04 (uninfected). At the last sampling point the yields diverged with -0.62 (infected) to -2.74 (uninfected) due to a possible outlier (standard deviation of  $\pm 2.05$  for the uninfected yield).

The propagation of the virus is shown in *Figure 31*. After the infection with LCMV with a MOI of 0.003 FFU/nuclei, the titer showed an initial strong increase to  $4.05 \times 10^4$  FFU/mL after 24 hours and  $3.48 \times 10^6$  FFU/mL after 48 hpi. After 72 hpi the titer

## Results

reached its plateau with  $5.49 \times 10^6$  FFU/mL. At the following sampling point, 96 hpi, the viral titer started to decrease to  $2.9 \times 10^6$  FFU/mL. The specific titer had its peak also after 72 hpi with 2.71 FFU/cell. This means an increase by 2.97 log units.

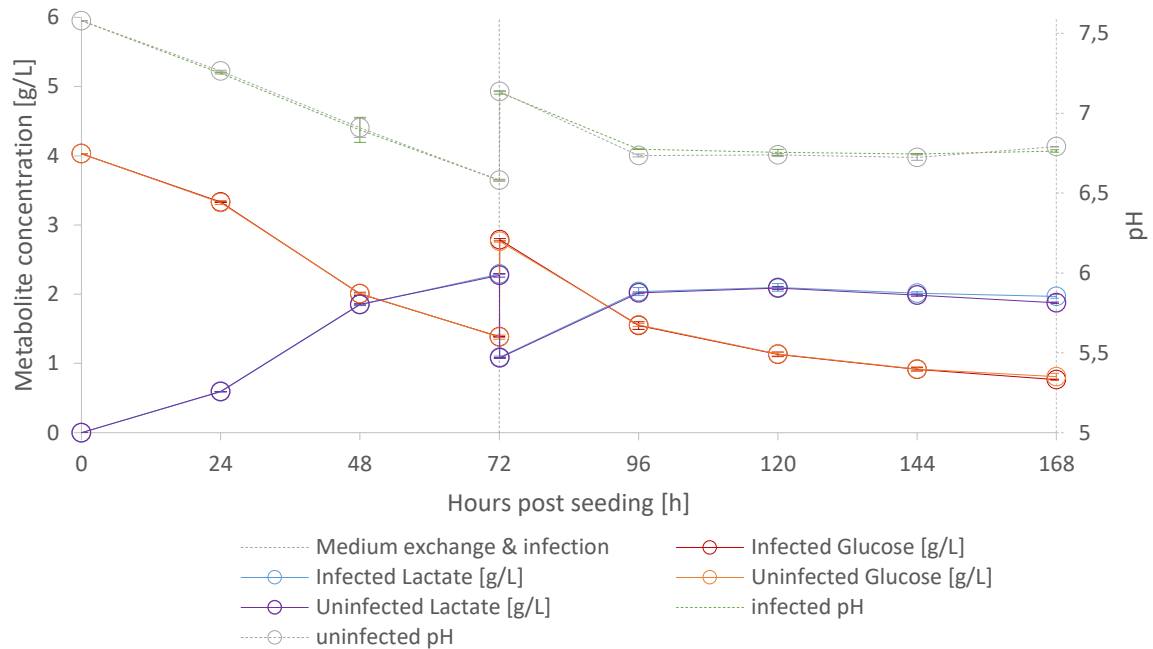


Figure 29: Comparison of Glucose and Lactate concentrations in g/L on the primary y-axis and pH on the secondary y-axis over the cultivation period of infected and uninfected Vero cells. A 60 % medium exchange and infection with LCMV was performed 72 hps (dotted line). Error bars represent the standard deviation



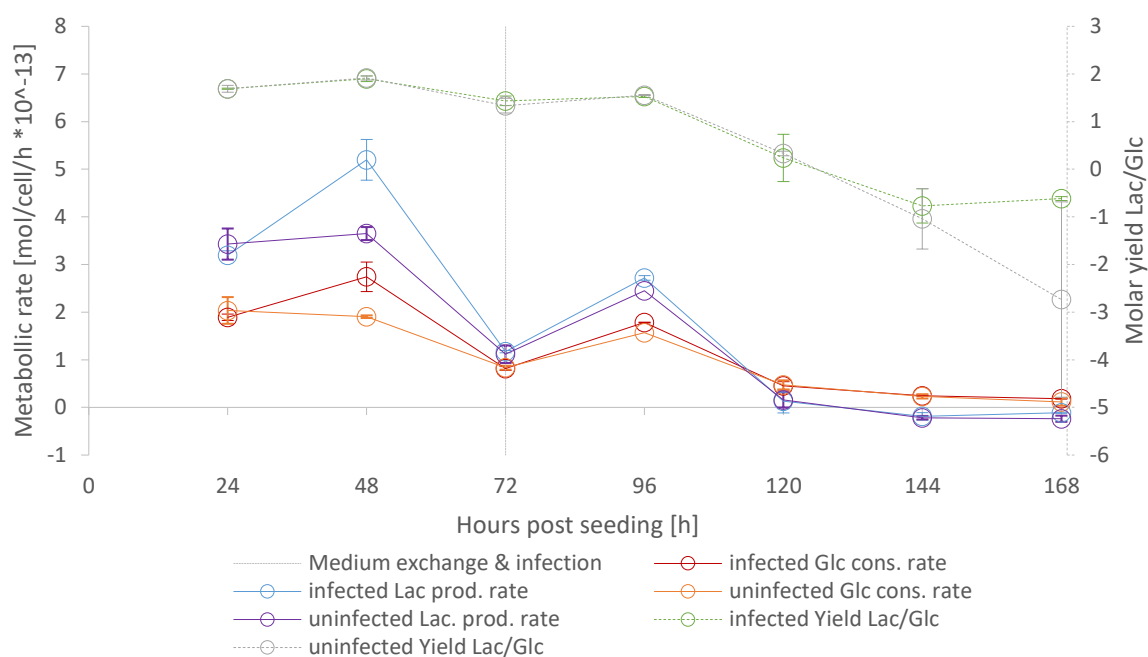


Figure 30: Comparison of Glucose consumption – and Lactate production – rate in  $\text{mol/cell/h}$  on the primary y-axis and the molar Lactate / Glucose-yield on the secondary y-axis over the cultivation period of infected and uninfected Vero cells cultivated on 3 g/L Cytodex 1 microcarrier. A 60 % medium exchange and infection with LCMV was performed 72 hps (dotted line). Error bars represent the standard deviation

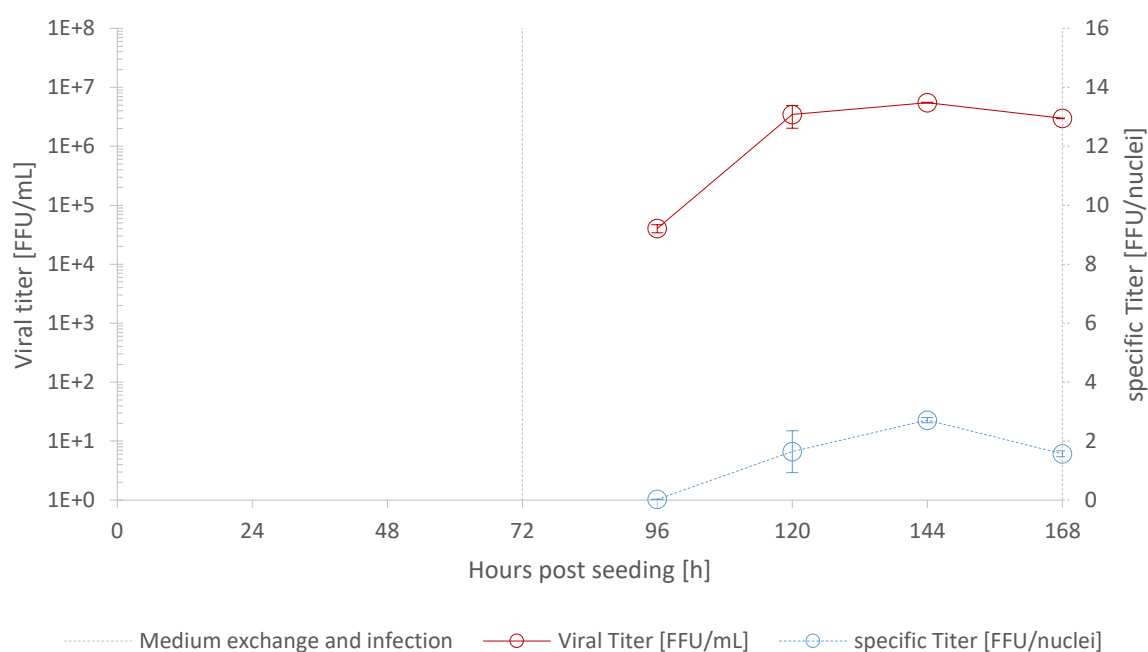


Figure 31: Viral titer of LCMV per mL, produced by Vero cells on 3 g/L Cytodex 1 microcarrier over the cultivation period on the primary y-axis. A 60 % medium exchange and infection with of LCMV with a MOI of 0.003 FFU/nuclei occurred 72 hps (dotted line). On the secondary y-axis the specific Titer in FFU/nuclei is displayed. Error bars represent the standard deviation.

## 5.10 Cultivation and infection of Vero cells on FibraCel discs

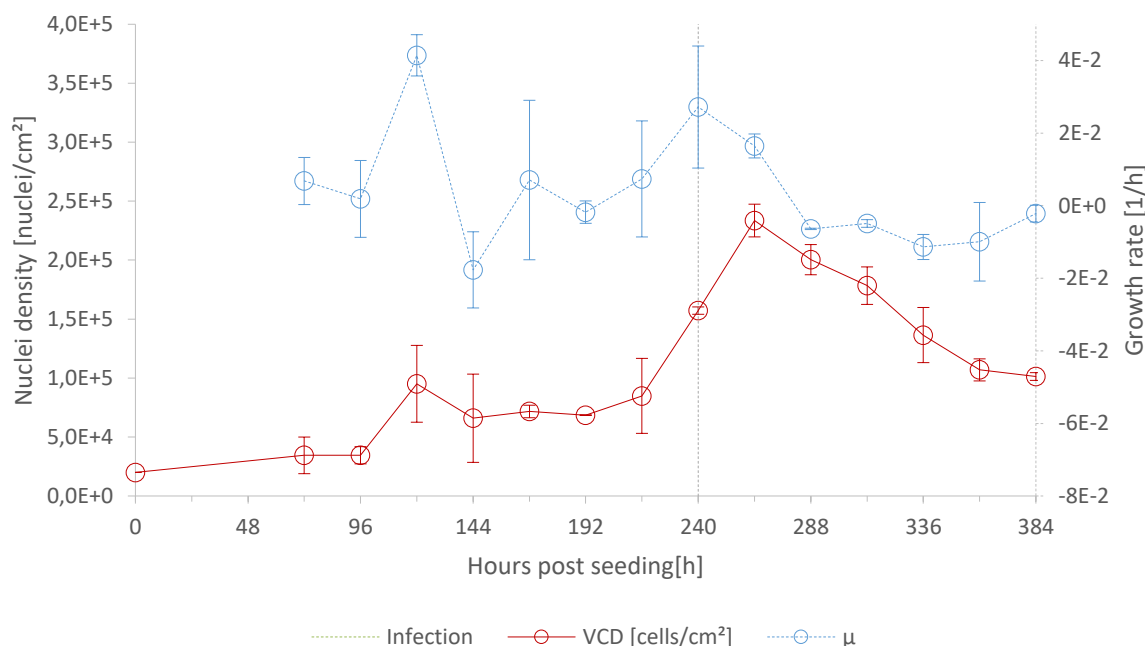


Figure 32: Propagation of infected Vero cells on FibraCel discs over the course of cultivation on the primary y-axis. On the secondary y-axis the calculated growth rate in  $h^{-1}$  is displayed. A total medium exchange was performed 144 and 240 hps. On the last medium exchange infection with LCMV with a MOI of 0.003 FFU/nuclei occurred (dotted line). 24 and 48 hps no sampling occurred. Error bars represent the standard deviation.

In the first 216 hps, in Figure 32, cells showed only minimal growth by increasing in cell density at seeding with  $2 \times 10^4$  to  $8.5 \times 10^4$  cells/cm<sup>2</sup>. The growth rate showed a high fluctuation in this time period ranging from  $-0.018$  to  $0.042 \text{ h}^{-1}$ . After 216 hps cell density started to increase by almost 3 times to  $2.3 \times 10^5$  cells/cm<sup>2</sup> over 48 hours. During this expansion phase, cells were infected after a complete medium exchange at 240 hps with LCMV at an MOI of 0.003 FFU/nuclei. At following sampling points, cell density consecutively decreased from the previously mentioned peak 24 hpi (264 hps) to  $1.0 \times 10^5$  cells/cm<sup>2</sup> at the last sampling point 384 hps.

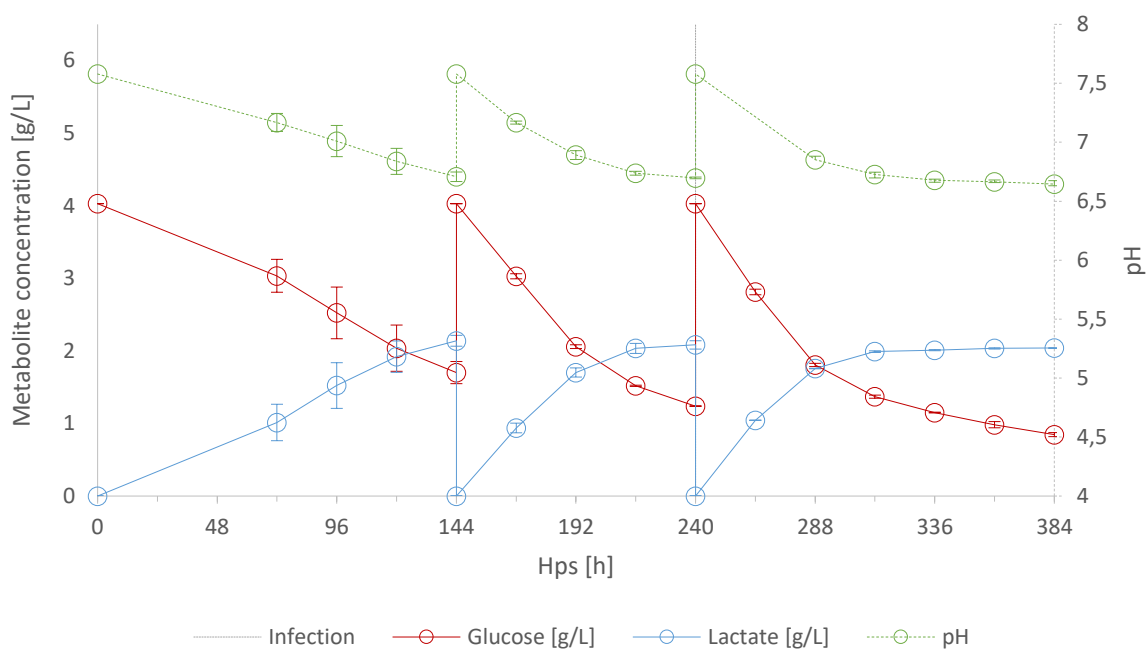


Figure 33: Comparison of Glucose and Lactate concentrations in g/L on the primary y-axis and pH on the secondary y-axis over the cultivation period of infected Vero cells on Fibracel discs. A total medium exchange was performed 144 and 240 hps. On the last medium exchange infection with LCMV with a MOI of 0.003 FFU/nuclei occurred (dotted line). 24 and 48 hps no sampling occurred. 264 hps no pH was measured. Error bars represent the standard deviation.

During the cultivation the medium was replenished 3 times. The first one was 24 hps as cells on discs were transferred from a 125 mL shaker flask into a 500 mL one and the working volume was increased from 25 mL to 200 mL. No sampling occurred during this period hence the exchange is not visible in *Figure 33*. After 144 hps as pH dropped from initial 7.579 to 6.708 and Glucose concentration from 4.03 g/L to 1.7 g/L and Lactate concentration increased to 2.14 g/L a first complete medium exchange was performed. The third medium exchange was conducted prior to the infection 240 hps as pH reached 6.698, Glucose concentration 1.24 g/L and Lactate concentration 2.08 g/L. After the infection, pH approached approximately 6.7, Glucose concentration approximately 1 g/L and Lactate concentration approximately 2 g/L after 72 hpi. In the consecutive 3 sampling points until the end of cultivation 384 hps the readings changed slightly to final values of pH 6.646, Glucose concentration of 0.85 g/L and Lactate concentration stalled at 2.04 g/L.

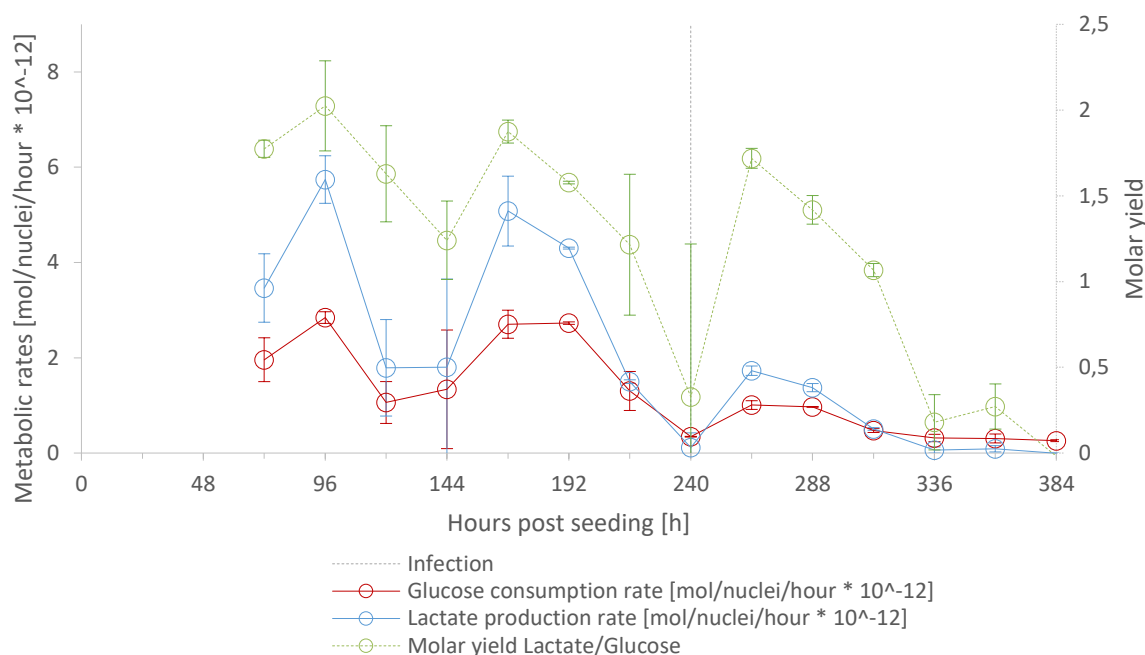


Figure 34: Comparison of Glucose consumption – and Lactate production – rate in mol/cell/h on the primary y-axis and the molar Lactate / Glucose-yield on the secondary y-axis over the cultivation period of infected Vero cells on FibraCel discs. A total medium exchange was performed 144 and 240 hps. On the last medium exchange infection with LCMV with a MOI of 0.003 FFU/nuclei occurred (dotted line). 24 and 48 hps no sampling occurred. Error bars represent the standard deviation.

Metabolic rates, plotted in Figure 34, for Glucose and Lactate showed an initial increase after the first 96 hours (Glucose: from  $1.96$  to  $2.86 \times 10^{-12}$  mol/cell/hour; Lactate: from  $3.46$  to  $5.74 \times 10^{-12}$  mol/cell/hour) followed by a decline (Glucose:  $1.34 \times 10^{-12}$  and Lactate:  $1.80 \times 10^{-12}$  mol/cell/hour) until the second exchange 144 hps. Afterwards both rates temporarily peaked (Glucose:  $2.73 \times 10^{-12}$  and Lactate:  $5.08 \times 10^{-12}$  mol/cell/hour) and again declined with consecutive sampling points. After the third medium exchange and infection 240 hps rates showed a lower peak (Glucose:  $1.01 \times 10^{-12}$  and Lactate:  $1.73 \times 10^{-12}$  mol/cell/hour) and then finally declined at the end of the cultivation (Glucose:  $0.26 \times 10^{-12}$  and Lactate:  $0.09 \times 10^{-12}$  mol/cell/hour). The molar yield of Lactate produced per Glucose consumed peaked with 1.71 to 1.87 for the sampling point after the medium exchange and declined with consecutive sampling points with a final minimum close to zero ( $-0.019$ ) at the end of the experiment.

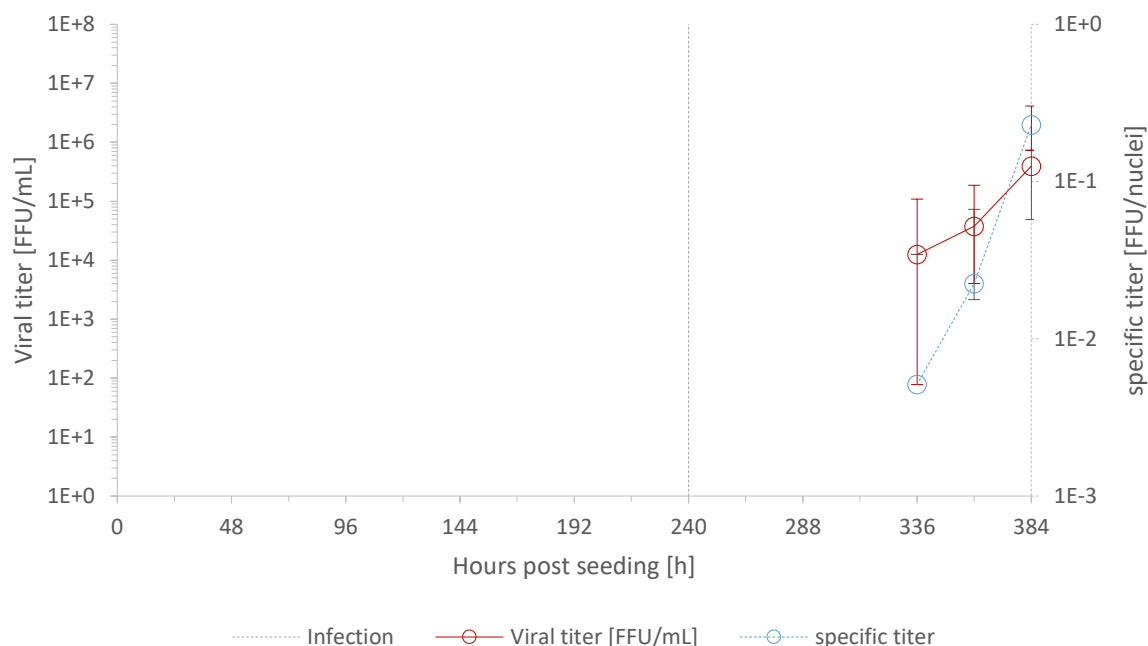


Figure 35: Viral titer of LCMV per mL, produced by Vero cells on FibraGel discs over the cultivation period on the primary y-axis in log scale. Cells were infected with LCMV with a MOI of 0.003 FFU/nuclei 240 hps (dotted line). On the secondary y-axis the specific Titer in FFU/nuclei in log scale is displayed. Missing titer values after the infection were lower than the detection limit of the chosen dilution of the assay. Viral titer values were multiplied by a factor of 2.5 for better comparability with titer values of experiments with 80 mL working volume due to the increased working volume of 200 mL. Error bars represent the standard deviation.

The viral titer, in Figure 35, showed a slow growth, reaching  $1.25 \times 10^4$  FFU/mL after 96 hours increasing to  $3.75 \times 10^4$  FFU/mL 24 hours later and  $3.94 \times 10^5$  FFU/mL at the end of cultivation. The peak found in previous experiments could not be reproduced in this set-up. The specific titer ranged from  $5.12 \times 10^{-3}$ , over  $2.25 \times 10^{-2}$  to  $2.30 \times 10^{-1}$  FFU/nuclei at the same sampling points.

## 5.11 Suspension infection process using HEK-293 cells

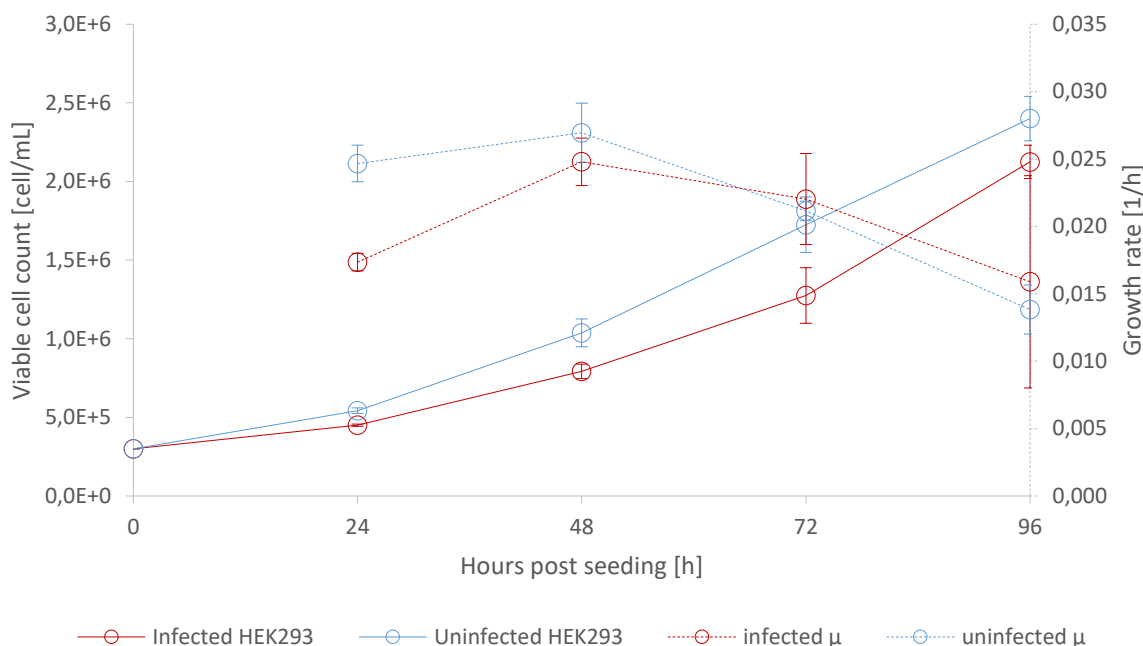


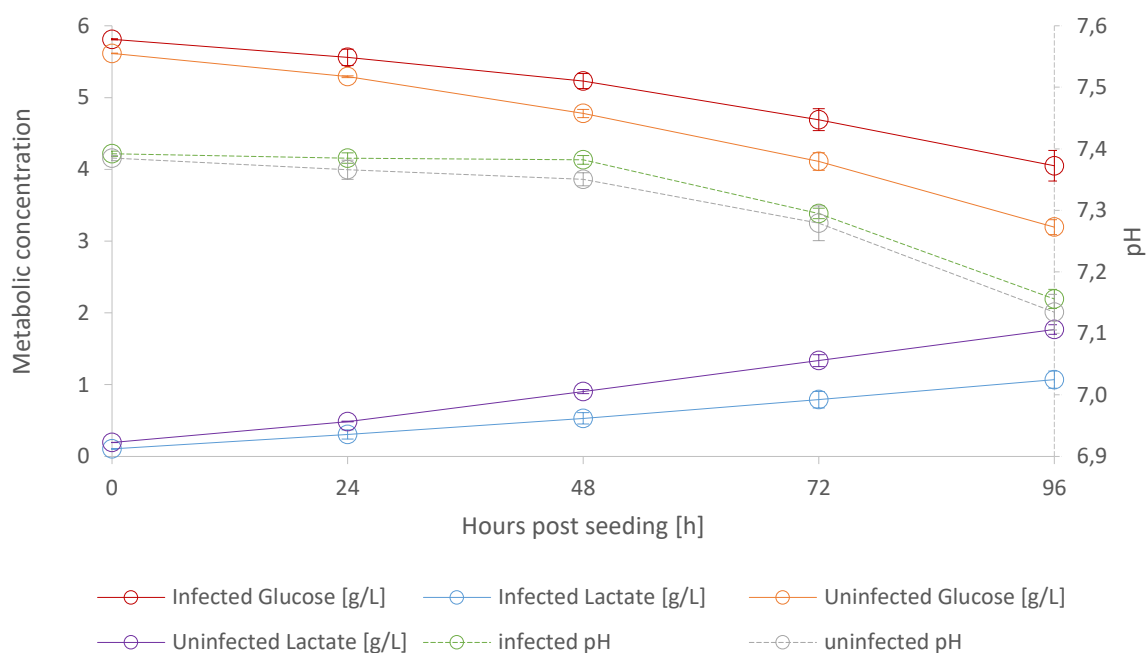
Figure 36: Comparison of the propagation of infected and uninfected suspension HEK-293 cells in cells/mL over the course of cultivation on the primary y-axis. On the secondary y-axis the calculated growth rate in  $h^{-1}$  is displayed for infected and uninfected cells. Cells were infected at seeding of  $3 \times 10^5$  cells/mL with LCMV with a MOI of  $10^{-5}$  FFU/cell. Error bars represent the standard deviation.

Figure 36 showed uninfected cells with a higher cell density than the infected ones over the whole cultivation. At the end of cultivation, uninfected reached a cell density of  $2.4 \times 10^6$  cells/mL, whereas infected cells grew to  $2.13 \times 10^6$  cells/mL. This is also recognizable at the growth rate of the uninfected cells which was at 24 hps with  $0.0247 h^{-1}$  higher than afterwards the growth rate of infected cells with  $0.0169$ . During the further cultivation growth rates aligned and started to decrease, whereas it appeared that infected cells showed a slightly higher growth rate during the last two sampling points, 72 and 96 hps/infection.

In Figure 37 the pH dropped from approximately 7.4 to 7.15 after 96 hours. The pH of the medium with uninfected cells was here slightly lower than the one with infected cells (7.135 to 7.156 after 96 hours). This is also reflected in the concentrations of Glucose and Lactate. On the one hand, infected cells showed higher Glucose readings; on the other hand, lower Lactate readings of the medium. The calculated metabolic rates, in Figure 38, show that the Glucose consumption rate and the Lactate production rate of infected HEK-293 cells was lower than of uninfected ones. With increasing cultivation duration the rates for Glucose and Lactate declined. Infected

cells showed furthermore a lower Lactate/Glucose yield. In addition, both yields decreased with increasing cultivation duration from 1.80 to 0.95 for uninfected cells, and from 1.67 to 0.87 for the infected cells.

After the infection, plotted in *Figure 39*, with the titer climbed to  $1.40 \times 10^2$  FFU/mL after 24 hours and  $1.43 \times 10^5$  FFU/mL after 48 hpi. 72 hpi the titer reached its peak with  $1.63 \times 10^7$  FFU/mL. At the following sampling point, 96 hpi, the viral titer started to decrease to  $1.10 \times 10^7$  FFU/mL. The specific titer had its peak also after 72 hpi with 12.89 FFU/cell. This means an increase by 6.11 log units.



*Figure 37: Comparison of Glucose and Lactate concentrations in g/L of infected and uninfected suspension HEK-293 cells over the course of cultivation on the primary y-axis. On the secondary y-axis the pH is displayed for infected and uninfected cells. Cells were infected at seeding of  $3 \times 10^5$  cells/mL with LCMV with a MOI of  $10^{-5}$  FFU/cell. Error bars represent the standard deviation.*

## Results

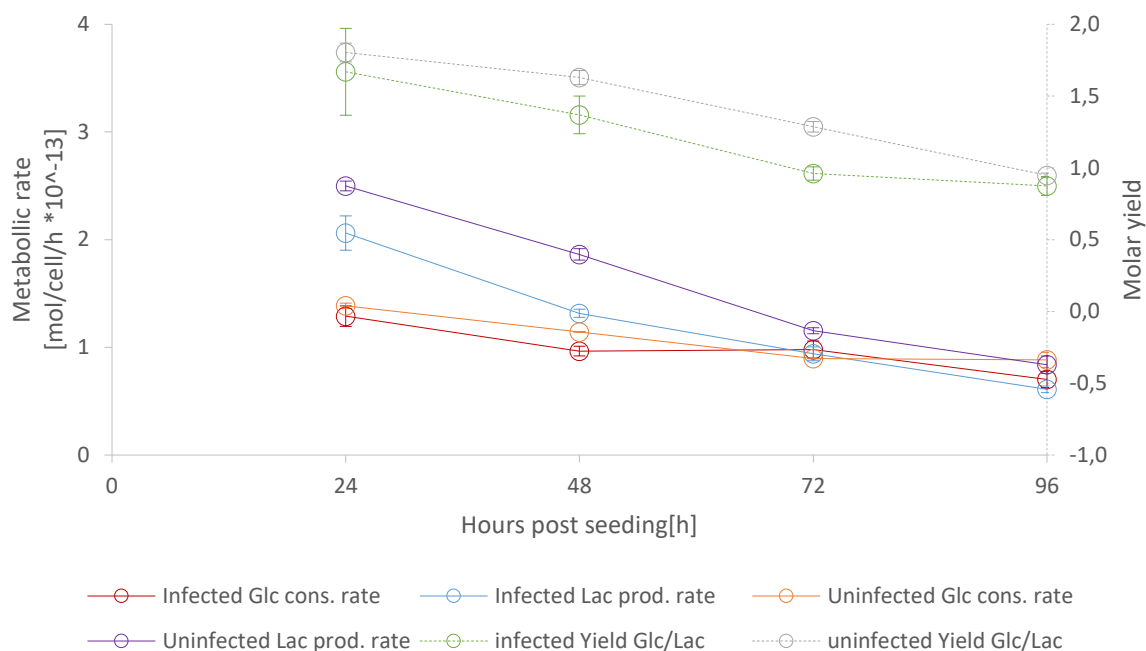


Figure 38: Comparison of Glucose consumption and Lactate production rate in mol/cell/hour of infected and uninfected HEK293 cells on the primary y-axis against the cultivation period. On the secondary y-axis the molar Lactate/Glucose yield is plotted. The error bars represent the standard deviation.

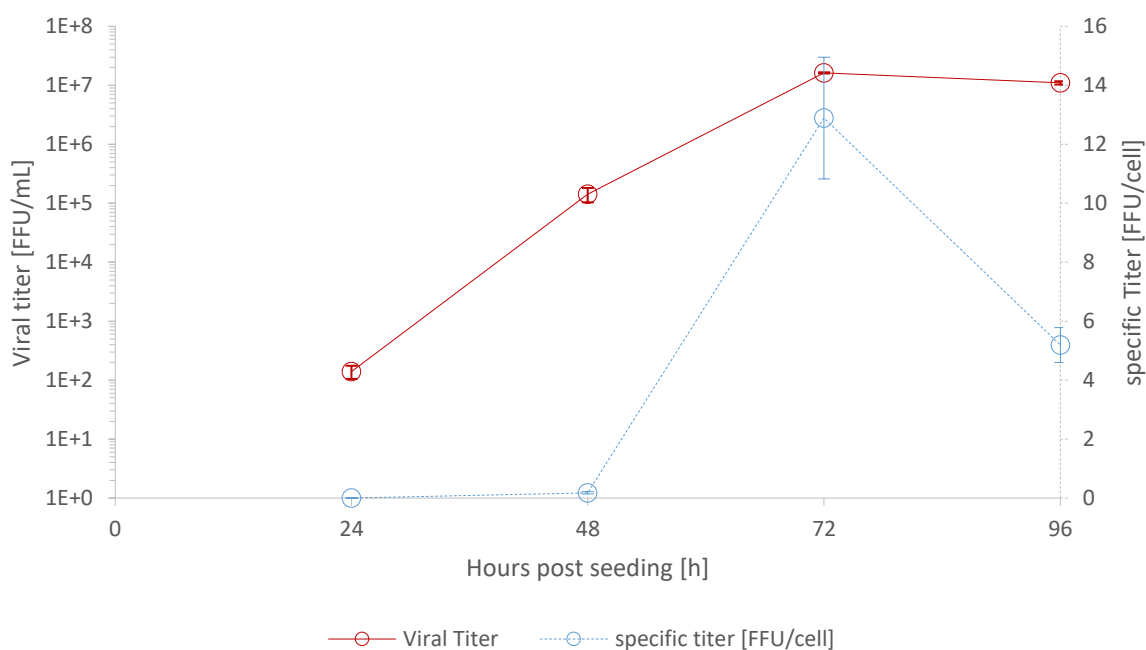


Figure 39: Viral titer of LCMV per mL, produced by HEK-293 suspension cells over the cultivation period plotted on the primary y-axis. Infection with LCMV with a MOI of  $10^{-5}$  FFU/cell occurred at seeding. On the secondary y-axis the viral titer per cell in FFU/cell is displayed. Error bars represent the standard deviation.



## 6 Discussion

### 6.1 Alteration of metabolite concentrations of PF26#278 during thermal inactivation of LCMV for metabolite assays I

The inactivation of virus-containing samples was needed for measurement of metabolites (Glucose, Lactate, Glutamine and Ammonium). Inactivation time and temperature where the virus titer read-out was lower than the detection limit of the most sensitive assay at Hookipa Biotech AG, the FFU-Assay, with 5 FFU/mL needed to be determined. The set points, where no manipulation of metabolite concentration by thermal degradation was observed, will be used for the inactivation procedure. Starting material had a virus concentration of  $1.2 \times 10^8$  FFU/mL. Originally Armstrong reported that at a temperature of 55 to 56 °C for 20 minutes the infectivity of the virus was destroyed (Armstrong and Lillie, 1934), unfortunately no information on the virus concentration at the time point of inactivation was documented. Reports on another enveloped RNA virus, influenza, documented by Chen et al in 2011, stated an inactivation time of 30 minutes at 60°C for virus concentrations in the range of  $1.0 \times 10^8$  TCID<sub>50</sub>/mL. It appeared in *Figure 8* that the model predicted a complete inactivation of LCMV in PF26#278 medium around the highest set point, 56 °C for 45 minutes. That this does not hold true can be verified by taking a closer look at the actual measured titer values, where still 100 FFU/mL were detectable. For this particular model a linear and not a logarithmic transformation was chosen, as this transformation resulted in a model which proposed the titer maximum against all logic not at the mildest inactivation conditions (see *Appendix Figure 41*). This investigated set points resulted in detectable virus particles which led into the follow-up experiment 6.2. In the case of an unsuccessful thermal inactivation the virus reduction by UV radiation or by pH shift remains as an alternative which needs evaluation.

### 6.2 Alteration of metabolite concentrations of PF26#278 during thermal inactivation of LCMV for metabolite assays II

In this follow-up experiment (see 5.2), with temperatures of 56, 66, 76 °C, and a fixed inactivation time of 60 minutes, already at the lowest set point no viral particles were detectable with the FFU assay and a 8.1 log viral clearance was observed. Glutamine showed to be instable at elevated temperatures during the inactivation. This led to a

decrease in Glutamine- and increase in Ammonia levels. For PF26#278 only Glucose and Lactate levels were stable and allowed a reliable determination with metabolite assays.

### 6.3 Alteration of metabolite concentrations of VPSFM and PF26#278 during thermal inactivation of LCMV for metabolite assays

As other media were also used for virus production, the set-up of the follow up experiment was repeated with the production media VP-SFM and PF26#280 (see 5.3). For both media no virus particles were detectable with the FFU – assay at 66 °C after 60 minutes with an at least 8.4 log, respectively a 6.7 log clearance. It can be seen that also the media composition affects the stability of the virus. Of the analyzed metabolites a subset was not stable during the thermal inactivation. Only the metabolites which showed no alteration in concentration during the inactivation were used in upcoming metabolite assays. For PF26#278 these were Glucose and Lactate, for VP-SFM Glucose, L-Glutamine, and Lactate were chosen to be determined. The analyzed metabolite concentrations determined in PF26#280 seemed not to be drastically affected by the temperature during the inactivation procedure. It has to be kept in mind that due to the inactivation procedure a variation in concentration results is still possible.

For metabolite assays, a uniform thermal inactivation of LCMV in the media PF26#278, PF26#280, and VP-SFM was chosen to be performed at 66 °C for 60 minutes.

### 6.4 Influence of Glutamine and L-alanyl-L-glutamine on Vero cell growth characteristics

This experiment was conducted by harvesting for each sampling point a separate flask, due to the restrains of the cell count determination of adherent cells as discussed in 4.2.9.2. This possibly result in a higher variation between units.

In *Figure 15*, cells showed a short lag phase after the attachment with less cell growth, where spreading out was observed. Afterwards, the growth phase was observed 48 to 96 hps where also specific cell growth rate peaked. Cells reached a confluent state around 96 hps. Illustrated in the photographs in *Picture 1* a confluent cell monolayer

developed. In following sampling points growth rate declined and cell density increased in smaller increments. It appeared in the photographs as cells started to shrink, in order to grow to higher cell densities. At the end of the cultivation, the beginning of the death phase was observed, noticeable by a decline in cell density. This can be the result of the observed decline in substrates and the acidification of the medium by the production of Lactate and Ammonia.

For future infection protocols using Vero cells as hosts, the time of infection was set to 72 hps. At this time point the cell layer was still sub confluent and the growth rate peaked. The most active cell state was utilized for the infection. To further aid this state prior to the infection a medium exchange was performed.

It has to be mentioned that glutamine decomposes spontaneously, which results in Ammonia and pyrrolidine carboxic acid formation, and can inhibit cell growth (Tritsch and Moore, 1962). Ammonia has an inhibiting effect on virus release from endosomes to cytoplasm because it shifts the acidification of the endosomal pH (Cruz et al., 2000; Ferreira et al., 2007).

In *Figure 19* the low reading of Glutamine after 72 hours was expected, as most of the Glutamine was present in its stable dipeptide form, which could not be determined with the available test kits, or already has been metabolized by the cells. The attention was drawn by the striking difference in Ammonia levels at both time points (*Figure 19* & *Figure 20*), where after 72 hours a nearly 10 fold and after 168 hours a 6 fold decrease in Ammonia concentrations in flasks containing L-alanyl-L-glutamine was observed.

For future experiments the stable dipeptide alternative, L-alanyl-L-glutamine was used. Although no major detrimental effects on cell growth were observed by using Glutamine as supplement, the usage of the stable L-alanyl-L-glutamine showed advantages regarding in an indirect more stable Glutamine concentration and resulting in a less excessive amount of free Ammonia. It shall be mentioned that the compared process with suspension HEK-293 cells also used L-alanyl-L-glutamine as supplement. In terms of a better comparability, the usage of L-alanyl-L-glutamine was therefore beneficial.

## 6.5 Determination of an optimized MOI and SCD of adherently growing Vero cells

The intention of this experiment, which results are outlined in 5.5, was to achieve the highest viral titer with optimal SCD and MOI. The first 24 to 48 hours after the infection the highest increase in viral titer could be observed. As the virus titer production started to decrease in the following sampling points the beginning of a plateau formation at approximately  $3.5 \times 10^6$  FFU/mL was observed. This indicated that the virus propagation was near its peak. The MOI had a major influence on the viral titer. This can either be recognized by the higher amount of increments along the MOI (y) – axis, as to the SCD (x) - axis in *Figure 5*, or the linear and quadratic MOI coefficient terms in *Figure 22*. As the influence of the seeding cell density was negligible, the lowest possible point of the design space was chosen with  $2 \times 10^4$  cells/cm<sup>2</sup>. The MOI of 0.003 FFU/cell, in *Figure 5*, marked the center of the red area, which indicated the titer maximum at 96 hpi at the chosen seeding density.

## 6.6 Proof of Concept for infection of adherently growing Vero cells with LCMV

The PoC was conducted in order to confirm the, in 5.5, generated models. Viral titer values for three chosen setpoints in the design space (see 5.5) were predicted by the models for three sampling points (see 4.2.7.6).

*Table 4* shows that the model was not able to predict the values at the first and second sampling points as 2 out of 3 setpoints were outside their boundaries. After 96 hpi all values were between their predicted boundaries, which confirms the model for 96 hpi.

The viral peaks, in *Figure 23*, for all set points were reached 96 hpi. At consecutive sampling points a stalling and decrease in viral titer was observed. With the acquired data, it can be stated the main production period would last between 72 to 120 hpi. It has to be mentioned, that this timespan needs an additional screening with tighter sampling points to determine the exact peak time point.

The time point of the viral titer in the DoE- and the PoC-plot (*Figure 21* & *Figure 23*) both were dependent on the MOI. While a higher MOI peaked earlier, the lower MOI showed a slower growth and peaked later.

After the PoC, the future cultivation parameters for Vero cells were set to a seeding density of  $2 \times 10^4$  cells/cm<sup>2</sup>, followed by a 72 hps medium exchange with a consecutive infection with LCMV with a MOI of 0.003 which then showed a peak titer 96 hpi.

For the discussion of the viral titers see the discussion sub-chapter “*Viral titers of different cultivation modes*” below.

### 6.7 Initial cultivation and infection of Vero cells on microcarriers in shake flasks

Vero cells, cultivated on Cytodex 1 microcarriers, showed an altered growth behavior, in contrast to Vero cells grown in T-Flasks. Illustrated in *Picture 2*, cells remained spherical on the carriers and no spreading out was observed. Also in *Figure 25*, no cell proliferation was observed until approximately 120 hps and afterwards also only for a subset of cells. Such a process cannot be used for an infection protocol. Therefore no infection with LCMV was carried out in this experiment.

The selection of correct starting conditions for microcarrier culture is vital for high cell yields (Clark and Hirtenstein, 1981). It is stated that a seeding volume reduced to 30 % and intermittent stirring can be crucial for successfully initiating a microcarrier cell culture. Detrimental shear stress caused by agitation was ruled out, as stirring speed was set in a manner, that microcarrier were kept nearly in suspension. This reduced the shear rates to a possible minimum. One additional suspicion was drawn to remaining inactivated cell detachment reagent from cell preparation in the seeding volume. The possible cause of the inhibition had to be determined in a follow up experiment.

### 6.8 Evaluation of cell growth inhibiting factors on Vero cells in microcarriers cultivation

The results from the 2<sup>3</sup>-full factorial screening design of inhibiting factors, outlined in 5.8, showed a clear negative influence of the residual cell detachment reagent Accutase on the cell propagation. As a consequence, the viral titer showed an 8-fold difference. The coefficient plot of model terms in *Figure 26* did not show positive influences of a decreased seeding volume and intermittent stirring, with respect to the results reported by Clark et al. Although, successful cultivations were not able to reach

the peak cell densities as observed in T-Flask studies. Experiments performed in T-Flasks, as routine cell culture, which contained residual deactivated cell detachment reagent, did not show this behavior in static cultivation conditions. It is therefore suspected that not only the inactivated residual cell detachment reagent inhibited growth, but a combination or superposition of other unknown influences. By time demands this couldn't be observed in this experimental set-up and in this masterthesis.

In *Figure 27B* it appeared as the infection peak shifts to an earlier timeframe between 48 and 72 hpi for units where cell detachment reagent was removed. A well-founded claim cannot be stated in this experiment, as a tighter sampling would be needed. Additionally possible influences, of the two other treatments, cannot be completely ruled out.

It could be shown that the removal of residual inactivated cell detachment reagent is from highest importance for a successful cultivation of Vero cells in microcarrier cultivation. The future cell preparation protocols were adapted and expanded by a cell detachment removal step by means of centrifugation and resuspension of cells in fresh medium.

## 6.9 Cultivation and infection of Vero cells on microcarriers in shake flasks

With the adapted cell preparation procedure, described in 6.8, the cultivation of Vero cells on Cytodex 1 microcarrier has been shown to be successful. Cells attached to the carriers, started to spread and proliferate, as displayed in *Picture 4* and *Figure 28*. In contradiction to static cultivation results in T-Flasks, in 5.4, similar cell densities were not observed. The growth rate profile showed an initial higher and faster decreasing growth rate, as in static cultivation. Infected cells in *Figure 28* appeared to be slightly more inhibited in cell growth than uninfected cells, which was reflected by a lower nuclei density and growth rate. For infected and uninfected cells no striking difference in metabolite concentrations, stated in *Figure 29*, were observed. As in T-Flasks, a slightly decrease in Lactate concentration was observed in very late stages of microcarrier cultivation. Both determined metabolic rates in *Figure 30* showed to be boosted by media replenishment but decreased as cells grew confluent and decreased their growth rates. A shift in metabolic rates between infected and uninfected cells could not be observed. The peak for both rates of uninfected cells at 48 hps can be

caused by an imprecisely determined cell count due to an inhomogeneous microcarrier distribution at sampling. With increasing cultivation duration and decreasing substrate concentration less Lactate per Glucose was produced by infected as well as non-infected cells.

For the discussion of the viral titers see the discussion sub-chapter “*Viral titers of different cultivation modes*” below.

### 6.10 Cultivation and infection of Vero cells on Fibracel discs in shake flasks

After seeding Vero cells on Fibracel discs little to no increase in cell density was observed in *Figure 32*. A noticeable cell expansion occurred after 9 days of cultivation. After the infection with LCMV 10 days post seeding a 50% decrease in cell density was measured, because cells detached from the discs. Metabolic rates and the molar Lactate per Glucose yield, in *Figure 34*, decreased with decreasing substrate concentrations. After a medium exchange, rates and yield increased at the consecutive sampling point. In comparison to static (*Figure 17*) and microcarrier cultivation (*Figure 30*) metabolic rates were observed to be approximately 5 to 10 fold higher. This leads to the assumption that the cell density was underestimated, due to an inhomogeneous cell distribution on the discs. Another drawback, other than the long cultivation period of 16 days, was that the medium had to be exchanged three times during this cultivation. This resulted in a way higher expenditure of medium as with the other cultivation modes.

For the discussion of the viral titers, see the discussion sub-chapter “*Viral titers of different cultivation modes*” below.

### 6.11 Suspension infection process using HEK-293 cells

The standard process using suspension HEK-293 cells, in *5.11*, was shorter than the other observed processes using adherent Vero cells. Further did HEK-293 require a different medium than the one used for Vero cells. With a 50 % higher initial Glucose concentration, no medium exchange was necessary.

In contrast to adherent cell cultivation, no expansion phase was needed and cells were infected directly at seeding. Infected cells, in *Figure 36*, showed inhibited growth and reached a lower cell density and growth rate than uninfected cells. In *Figure 37*

infected cells showed a reduced medium consumption until the end of the cultivation. As infected cells generated lower amounts of Lactate, also the pH of the medium was higher than the one of uninfected cells. The observed metabolic rates and the molar Lactate/Glucose yield, in *Figure 38*, decreased until the end of the cultivation and showed to be lower for infected than uninfected ones. This led to the assumption that infected cells required more Glucose for virus production.

For the discussion of the viral titers see the discussion sub-chapter “*Viral titers of different cultivation modes*” below.

### 6.12 Viral titers of different cultivation modes

The produced viral titers by the different production modes were the most anticipated results of this master thesis as they mainly contributed to the decision which process performed best for the production of viral vectors and could be used for further evaluation and finally in future production runs. For a better comparability, the discussion of the viral titer results was condensed in this subchapter with a supportive figure using key results of the different cultivation modes at their peak performance.

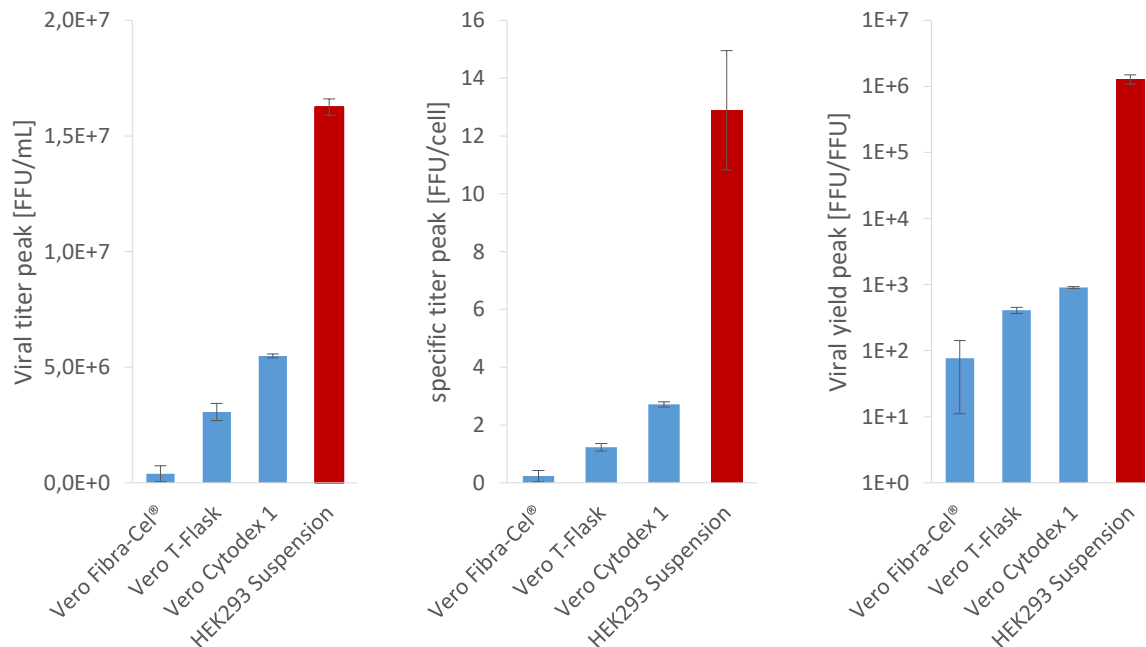


*Figure 40: Supportive graph for comparison of viral titer of different cultivation modes by viral titer [FFU/mL], specific titer [FFU/cell] and viral yield [FFU/FFU] at titer peak. Error bars represent the standard deviation.*

The established suspension cultivation process with HEK-293 cells showed to be superior to the other investigated cultivations using adherently growing Vero cells. The



peak of the viral titer concentration highlights that with an equal working volume the virus concentration of the suspension process is about three fold higher than the second best, the microcarrier approach. As the virus concentration alone can be misleading for comparison of process performance of adherent and suspension processes (e.g. by different working volumes and different amount of cells producing virus), the specific virus titer peak for each cell was calculated. It is therefore possible to compare regardless of different used volumes or total amount of cells. With a nearly 5 fold increase against the microcarrier process the suspension process here also showed to be superior. This means that with the same amount of cells a higher amount of virus will be produced by the suspension process. The right graph displays the viral yield peak, which is the quotient of virus harvested and virus used for infection. The higher the value the higher the amount of virus produced per spent virus, which translates to a higher amount of vaccine doses per production run if the same amount of virus is used for infection. Also here the suspension process showed an approximately 1000 fold increase to the microcarrier process. With such an obvious outcome it should be clear that the use of a HEK-293 cell suspension cultivation is highly favorable for future production runs. For the further discussion of the support growth matrix process itself see the sub-chapter 6.14.4.

## 6.13 General considerations regarding the production process

### 6.13.1 Timeframes for production

Vero cells required a growth phase until they reached a sufficient cell density for infection. A microcarrier based process approach, in 5.9, needed 168 hours for completion, whereas the suspension process, in 5.11, where no growth phase was necessary and infection occurred directly at seeding, was finished after 96 hours and produced a higher viral titer. Virus production period was for both processes between 72 to 96 hours. The, in 5.10, observed Fibracel discs approach, showed after 384 hours of cultivation no viral titer peak and should not be considered in the current state. By taking preparation work into account this gap increases even more. As stated in 4.2.2.2, required the pretreatment of microcarriers about 3 additional days. Suspension cells didn't require a pretreatment and could be infected directly at seeding. The exact peak time points may still slightly vary as sampling intervals were set to 24 hours, but as the processes durations showed so distinct differences this should only have a minor effect on overall productivity. As a vast number of combinations of production

methods for diverse viral vectors with different cell substrates exists, a brief overview of a subset of successful cultivations is presented here. Josefsberg and Buckland reported in 2012 the use of adherent PER.C6 cells, an immortalized human cell line derived from retinoblasts, for production of Adenovirus vectors by Merck. Adherent cells were grown in cell factories with a production level of  $> 5 \times 10^6$  virus particles per tray. Suspension Per.C6 cells were scaled up to 250 L in a stirred tank reactor, but no information on virus concentration was given, Genzel and Reichl summarized in *Continuous cell lines as production system for influenza vaccines* in 2009 different processes for the production of influenza virus strains. The most successful processes by scale are condensed in *Table 1* below.

*Table 6: Excerpt of an overview of data on influenza virus production (Genzel and Reichl, 2009).*

Vaccine	Cell line	Scale (L)	Vessel	Medium	Company
Optaflu	MDCK 33016 (Suspension)	> 1000	STR	-	Novartis
FluMist	MDCK CCL 34 (Adherent)	< 2500	STR	Taub's+MediVS F103(SFM)	Medimmune Vaccine
Influject	Vero CCL 81 (Adherent)	6000	STR	DMEM/ Ham's F12	Shire

### 6.13.2 Required amount of cell substrate

For comparing the amount cells needed for adherent and suspension production processes at first the different units have to be converted. During the peak of virus concentration Vero cells on microcarrier reached a cell density of approximately  $1.5 \times 10^5$  cells/cm<sup>2</sup>, with a microcarrier concentration of 3 mg/mL (both see 5.9) and a surface area of 4.4 cm<sup>2</sup>/mg (see 4.2.2.2), this calculates to a cell density of roughly  $2.0 \times 10^6$  cells/mL after 120 to 144 hours post seeding. The observed cell densities were similar to reported values in literature by Barret et al., 2009. It appears only slightly higher than the cell density of HEK-293 suspension cells, which grew to a density of approximately  $1.7 \times 10^6$  cells/mL (see 5.11) at virus peak concentration. As also stated below in 6.15 *Future prospective* the microcarrier concentration still can be optimized and therefor the required amount of cell substrate for virus production using Vero cells can be subject to notably change. Generally, a lower amount of cells is more

suitable, as medium exchanges are fewer or even not at all necessary and process steps like cell separation, e.g. filtration, are more easily achievable. Microcarriers show an advantage in cell retention due to their higher density and faster sedimentation velocity, which simplifies medium exchanges if necessary. Finally the effort for purification has to be taken into account, where a higher cell density also leads to a higher amount of impurities, e.g. residual host cell protein and DNA, which need to be removed. These unit operations also can have a significant impact on final virus quantity.

### 6.13.3 Product quality & Safety aspects

The adaption from adherent to suspension cell growth introduces changes to the cell and can therefor also affect the produced viruses. A study performed by Donis et al. in 2014 evaluated the influence of adherent and suspension cultivation of MDCK cells on the genetic stability of influenza by comparing the cumulative number of mutations of the isolated virus. The differences were small and lacked statistical significance. This suggests that virus propagation in the investigated cell lines did not lead to major changes in the amino acid sequence (Donis et al., 2014). If a production process using Vero cells is established also the genetic stability of the virus needs to be assessed before. To further ensure product quality and safety for each batch of the produced vaccine, the identity, sterility, stability and potency needs determination. For stability the maintenance of potency should be demonstrated during the period of validity. The potency reflects the infectivity of the vector and expression of the heterologous antigen, e.g. in the form of the infectivity titer in vitro, or/and the immunogenicity in vivo. Each single harvest should be tested for residual host cell protein and residual host cell DNA and extraneous agents. A comprehensive list of requirements is provided by the European Medicines Agency (EMA) in their *Guideline on quality, non-clinical and clinical aspects of recombinant viral vectored vaccines* (2010).

### 6.13.4 Amount of process steps

The amount of process steps differed drastically between adherent and suspension routine cell cultures, as in preparation, and production processes itself. Handling steps, described in 4.2.3 *Cell culture methods*, resulted not only in a higher time and material consumption for the expansion of adherently growing cells, also the risk for a contamination or failure increased with each step. The same applies for preparation of microcarrier processes which need a pretreatment for a successful cultivation, thus

increasing the overall process time and also the complexity of such a process in comparison to the described suspension cultivation. If such a complex process is transferred to a Contract Manufacturing Organization (CMO) more time, costs, goods and knowledge are required to transfer. Besides that, the purification feasibility of a Vero cell harvest has to be determined by the downstream department, as cells, generated byproducts and different media components might affect purification.

## 6.14 General considerations regarding experimental set-ups

### 6.14.1 Choice of medium

Chen et al (2011) evaluated different media, namely OptiPro SFM (Invitrogen), VP-SFM (Invitrogen), EX-CELL Vero SFM (SAFC Bioscience), Provero-1 (Lonza) and HyQ SFM4MegaVir (HyClone) for Vero cell cultivation. It was shown that viable cell density and viral titer is dependent on the used media. VP-SFM promised one of the highest yields with Vero cells on Cytodex 1 microcarriers for influenza virus. As influenza virus and LCMV are both enveloped RNA viruses, the animal-component free, serum-free medium and, at the time, commercially available VP-SFM was used for this master thesis. If the medium composition is altered or the medium is completely switched, the design space, the infection kinetics as specific titers and viral yields need to be reevaluated.

### 6.14.2 Process changes which may affect the design space

During the execution of this master thesis an unknown inhibition of cell growth, after the attachment of Vero cells to Cytodex 1 microcarrier, showed to be a tremendous problem. By identifying the cell detachment reagent Accutase as one inhibiting factor for Vero cells grown on Cytodex 1 microcarrier beads, a change to the initial infection protocol was introduced. This may affect the infection kinetic and could possible shift the optimized MOI. Same goes for the cultivation and infection of Vero cells on Cytodex 1 microcarrier. With the increased control possibilities bioreactors offer, a scale-up also requires an additional design space, as general conditions would again have changed. This uncertainties weren't resolved in the scope and timeframe of this master thesis.

### 6.14.3 Comparison between cell counting methods

For Vero cells grown on microcarriers and Fibracel discs the nuclei density instead of cell density was determined. The evaluation of the results was conducted under the assumption, that every nuclei represented one cell. This has to be taken into account by comparing cell counts, specific rates and specific titers of adherently and in suspension growing cells.

### 6.14.4 Performance of Fibracel discs

The performance of Vero cells on Fibracel discs for LCMV production was not ideal. After 384 hours of cultivation, in *Figure 35*, no plateau phase or virus peak was reached in this experimental set-up. This leads to the assumption that the infection kinetic was slowed down. As mentioned in 6.10, it could be possible that the cell density was underestimated or not determined correctly, due to inhomogeneous distribution of the cells on the Fibracel discs, which led to an actual lower MOI and as a consequence to a slower infection. Discs were kept in suspension in shake flasks in this experimental set-up. The possibility of inhomogeneity of cell attachment on the Fibracel also can appear in a packed bed perfusion reactor set-up. The correct determination of the cell density is of utmost importance at the time point of infection, as MOI and therefor the infection kinetic depend on it. For a possible future use of this cultivation mode, evaluation of indirect cell count determination methods, as mentioned by Mirro (2011), and optimization should be performed, taking aforementioned problems into account.

## 6.15 Future prospective

Although the specific titers of LCMV for Vero cells were lower than the ones observed when using HEK-293 cells, the overall titer of a microcarrier based cultivations could still be boosted, by optimizing the microcarrier concentrations. With an increase in microcarrier concentration also a higher amount of cells for seeding, with preceding expansion effort, as a more often necessary media exchange, and an increased amount of impurities in the supernatant need to be taken into account. All these contribute to increased material costs and handling steps. Further a higher degree of purification might be necessary, whereas the virus concentration can be prone to significant decreases and led to a decrease of overall process performance.

In this master thesis the evaluation of virus production was done in shaker flasks. At this scale, process parameters, like pH and dissolved oxygen concentration could not

be controlled. If the culture system is scaled up to a stirred tank reactor, the initial determined design space needs to be reevaluated. The increased control, a reactor system offers, also requires further optimization. All this can alter, positively as negatively, the determined performance, which was observed in the shaker flask scale. If further steps towards a microcarrier based Vero cell approach are taken, this needs consideration.

## 6.16 Conclusio

In this master thesis the robustness of the metabolites Glucose, Lactate, Glutamine, and Ammonia was assessed for the thermal inactivation of replication competent virus particles in three different cultivation media. In all media Glucose and Lactate concentrations showed no alteration during the inactivation. Their reliable determination will ensure the knowledge gain for further BSL 2 processes.

The comparison of three different cultivation modes for adherently growing Vero cells and in suspension growing HEK-293 cells led into a significant result. Suspension HEK-293 cells showed by far the highest viral titer, specific titer and viral yield, with simultaneously the shortest cultivation duration. In the middle of the field the LCMV production with Vero cells in T-Flasks and Cytodex 1 microcarrier was found. A cultivation with microcarrier beads further required the highest amount of handling steps, consisting of microcarrier preparation, cell expansion and medium exchanges. LCMV production using Vero cells on FibraCel discs, performed far behind other investigated cultivations. Besides the generation of only a fraction of viral titer, showed this method by far the longest cultivation duration, with highest medium expenditure.

As mentioned Vero cells have the advantage of being the most widely accepted cell substrate by regulatory authorities for vaccine development. The use of microcarriers offers advantages in the scale-up of adherently growing cells and certain process steps, e.g. harvest and retention of cells. Nevertheless cultivations with adherently growing Vero cells were more complex than the suspension process with HEK-293 cells. With increasing complexity also the possibility for problems increased. Observed growth inhibition of Vero cells on Cytodex 1 microcarrier beads, during the evaluation for LCMV production was connected to a residual cell detachment reagent, which prevented cell spreading after cell attachment. Attributed to the different cultivation surfaces, this effect was not observed in static cultivation, where cell proliferation seemed not to be as tremendously effected, as in a microcarrier based approach.

Further processability and recovery of LCMV, generated by using Vero cells was not assessed by the downstream department. Purification processes for LCMV generated by HEK-293 were already evaluated and showed good performance.

---

The use of a suspension cultivation process with  
HEK-293 cells for production of Lymphocytic  
Choriomeningitis virus is therefore highly favorable.

---



## 7 References

### 7.1 List of Figures

Figure 1: Phylogenetic tree of arenavirus Z protein (from Urata and Yasuda, 2012)..	6
Figure 2: Left: Schematic graphic of LCMV; Right: RNA genome of LCMV (graphic by Klaus Orlinger, PhD, Hookipa Biotech AG).....	7
Figure 3: Flowchart of performed experiments .....	21
Figure 4: The 3 <sup>2</sup> -full factorial central composite face design of experimental set-up with inactivation time (5, 25, and 45 minutes) and temperature (36, 46, and 56 °C) as factors for the thermal inactivation of LCMV in PF26#278 for metabolite assays with foci forming units per mL as response. The design was conducted in singelsts. ....	23
Figure 5: DoE set-up for determination of an optimized MOI of adherently growing Vero cells .....	26
Figure 6: Design space of the SCD and MOI optimization experiment. Black dots show the initial determined setpoints. Colored dots show the investigated setpoints for the proof of concept.....	27
Figure 7: DoE set-up for evaluation of cell growth inhibiting factors on Vero cells in microcarrier cultivation.....	28
Figure 8: Response Contour Plot of foci forming units per mL for thermal inactivation of LCMV in PF26#278, generated with a 3 <sup>2</sup> -full factorial design of experimental set-up with temperature (36 to 56 °C) on the x-axis and inactivation time (5 to 45 minutes) on the y-axis as factors. Red areas indicate highest responses and blue areas lowest. R <sup>2</sup> : 0.94825; Q <sup>2</sup> : 0.795.....	39
Figure 9: Foci forming units per mL of PF26#278 samples containing LCMV samples after 5, 25, and 45 minutes and 36, 46, and 56 °C thermal inactivation following a full factorial design of experimental set-up. ....	40
Figure 10: Foci forming units per mL of PF26#278 samples containing LCMV after 60 minutes inactivation at given temperatures (56, 66, and 76°C). Dashed bars represent samples where the virus titer was below the detection limit of 5 FFU/mL of the FFU-Assay.....	41
Figure 11: Changes in concentrations of selected metabolites (Glucose, Glutamine, Lactate, and Ammonia) of used PF26#278 cultivation medium after thermal inactivation at 3 different temperature (56, 66, 76 °C) for a duration of 60 minutes.	

Selected metabolites were analyzed using the Cedex Bio Analyzer. The percentages were calculated from mass concentrations.....	42
Figure 12: Foci forming units per mL of PF26#280 and VP-SFM samples containing LCMV after 0 and 60 minutes inactivation at given temperatures (56, 66, and 76 °C). Dashed bars represent samples where the virus titer was below the detection limit of 5 FFU/mL of the FFU-Assay.....	43
Figure 13: Changes in concentrations of selected metabolites (Glucose, Glutamine, Lactate, and Ammonia) of used PF26#280 cultivation medium after thermal inactivation at 2 different temperature (66, 76 °C) for a duration of 60 minutes. Selected metabolites were analyzed using the Cedex Bio Analyzer. The percentages were calculated from mass concentrations. ....	44
Figure 14: Changes in concentrations of selected metabolites (Glucose, Glutamine, Lactate, and Ammonia) of used VP-SFM cultivation medium after thermal inactivation at 2 different temperature (66, 76 °C) for a duration of 60 minutes. Selected metabolites were analyzed using the Cedex Bio Analyzer. The percentages were calculated from mass concentrations.....	45
Figure 15: Cell densities [cells/cm <sup>2</sup> ] and growth rates [h <sup>-1</sup> ] of adherently growing Vero cells over a 168 hour cultivation period. Cells were seeded with 3 × 10 <sup>4</sup> cells/cm <sup>2</sup> . A medium exchange was performed 72 hps. Error bars represent the standard deviation of measured duplicates.....	46
Figure 16: Selected metabolites, Glucose, Glutamine, Lactate and Ammonia on the primary y-axis and pH values on the secondary y-axis of adherently growing Vero cells over a 168 hour cultivation period. A medium exchange was conducted 72 hps. Error bars represent the standard deviation of measured duplicates. ....	47
Figure 17: Specific molar metabolite rates [mol/cell/hour *10 <sup>-13</sup> ] of Glucose, Glutamine, Lactate and Ammonia during the course of cultivation. A medium exchange was performed 72 hps. Error bars represent the standard deviation of measured duplicates .....	48
Figure 18: Progress of molar yields during cultivation as mM produced metabolites per mM consumed substrates on primary y- axis. On secondary y-axis in log-scale cells generated per mM substrate are plotted. A total medium exchange was performed 72 hps. Error bars represent the standard deviation of measured duplicates.....	48
Figure 19: Comparison of Cell density in × 10 <sup>5</sup> cells/cm <sup>2</sup> , Glucose- in g/L, Glutamine- in mM, Lactate- in g/L, and Ammonia-concentrations in mM of Vero cells after 72 hours	

cultivation supplemented with Glutamine and L-alanyl-L-glutamine, respectively. The units of the different parameters are displayed on the x-axis respectively.....	50
Figure 20: Comparison of Cell density in $\times 10^5$ cells/cm <sup>2</sup> , Glucose- in g/L, Glutamine- in mM, Lactate- in g/L, and Ammonia-concentrations in mM of Vero cells after 168 hours cultivation supplemented with Glutamine and L-alanyl-L-glutamine, respectively. The units of the different parameters are displayed on the x-axis respectively. Error bars represent the standard deviation of duplicates. ....	51
Figure 21: Response Contour Plots for the sampling points 48, 72 and 96 hpi generated with MODDE. The model shows the influence of MOI (y-axis) in log-scale and SCD (x-axis) over the range of $10^{-5}$ to $10^{-1}$ , respectively $2 \times 10^4$ to $5 \times 10^4$ cells/cm <sup>2</sup> on LCMV titer in [log (FFU/mL)]. Red areas indicate highest responses and blue areas lowest. ....	51
Figure 22: Overview Plots for each Response Contour Plot with the Replicates-, the Summary of Fit-, and Coefficients-Plot. The Replicates-Plot shows individual viral titer results in log (FFU/mL). The Summary of Fit box displays R <sup>2</sup> , which shows how well the data fit the model. Q <sup>2</sup> tells how well the model predicts new data, a value greater than 0.5 shows a good model. A Model validity value less than 0.25 indicates model problems, like present outliers or an incorrect model, but can also be low due to good duplicate values. The reproducibility shows the variation of the replicates to the overall variability and should be greater than 0.5. The Coefficients-Plot displays the coefficients of the linear and quadratic terms of the model. The error bars represent the 95 % confidence interval. Quadratic non-significant model terms, where uncertainty range clearly crossed 0, were removed from the model. ....	53
Figure 23: Virus titers [FFU/mL] in comparison to predicted titers of three investigated set points of the proof of concept. Dashed lines represent predicted values based on the calculated model. Full lines represent values measured in triplicates. Error bars of the predicted values represent lower and upper boundaries. Error bars of measured values represent standard deviation.....	54
Figure 24: Released nuclei per cm <sup>2</sup> of Vero cells cultivated on Cytodex 1 microcarrier. A medium exchange was performed 72 hps. Error bars represent the standard deviation. ....	56
Figure 25: Nuclei per cm <sup>2</sup> of Vero cells on 3g/L microcarrier over the cultivation period. Cells were seeded with $2 \times 10^4$ cells/cm <sup>2</sup> . A medium exchange, by sedimentation and replacement of 60 % medium was performed 72 hps and cells were infected with	

LCMV with a MOI of 0.003. In the legend +/- represents the presence or absence of the investigated influence in the order of Reduced volume / Intermittent stirring / Accutase removal. ....	57
Figure 26: Coefficient Plot of screening model terms of investigated influences on cell growth measured by released nuclei per mL of Vero cells in 3 g/L microcarrier over the cultivation period. remAc represents the removal of Accutase prior seeding. intSt represents intermittent stirring at seeding. redVol represents a reduced volume at seeding. (Y) or (N) stands for “Yes” or “No”. The error bars represent the 95 % confidence interval. Model terms where the uncertainty range crosses Zero can be seen as non-significant. For better discrimination of significant influences, these terms were not removed from the screening model.....	58
Figure 27: <b>A:</b> LCMV titer in FFU per mL in log-scale produced by Vero cells on 3 g/l microcarrier over the cultivation period. Cells were seeded with $2 \times 10^4$ cells/cm <sup>2</sup> . A medium exchange, by sedimentation and replacement of 60 % medium was performed 72 hps before infection with LCMV with a MOI of 0.003. In the legend +/- represents the presence or absence of the investigated influence in the order of Reduced volume / Intermittent stirring / Accutase removal. <b>B:</b> Averaged LCMV titer in FFU/mL in log-scale on y-axis of four units each with or without Accutase over the course of cultivation. Error bars represent the standard deviation. ....	59
Figure 28: Comparison of the propagation of infected and uninfected Vero cells over the course of cultivation on the primary y-axis. On the secondary y-axis the calculated growth rate in h <sup>-1</sup> is displayed for infected and uninfected nuclei. A 60 % medium exchange and infection with LCMV with a MOI of 0.003 FFU/cell occurred 72 hps (dotted line). Error bars represent the standard deviation.....	60
Figure 29: Comparison of Glucose and Lactate concentrations in g/L on the primary y-axis and pH on the secondary y-axis over the cultivation period of infected and uninfected Vero cells. A 60 % medium exchange and infection with LCMV was performed 72 hps (dotted line). Error bars represent the standard deviation.....	63
Figure 30: Comparison of Glucose consumption – and Lactate production – rate in mol/cell/h on the primary y-axis and the molar Lactate / Glucose-yield on the secondary y-axis over the cultivation period of infected and uninfected Vero cells cultivated on 3 g/L Cytodex 1 microcarrier. A 60 % medium exchange and infection with LCMV was performed 72 hps (dotted line). Error bars represent the standard deviation .....	64

- Figure 31: Viral titer of LCMV per mL, produced by Vero cells on 3 g/L Cytodex 1 microcarrier over the cultivation period on the primary y-axis. A 60 % medium exchange and infection with of LCMV with a MOI of 0.003 FFU/nuclei occurred 72 hps (dotted line). On the secondary y-axis the specific Titer in FFU/nuclei is displayed. Error bars represent the standard deviation. .... 64
- Figure 32: Propagation of infected Vero cells on FibraCel discs over the course of cultivation on the primary y-axis. On the secondary y-axis the calculated growth rate in  $h^{-1}$  is displayed. A total medium exchange was performed 144 and 240 hps. On the last medium exchange infection with LCMV with a MOI of 0.003 FFU/nuclei occurred (dotted line). 24 and 48 hps no sampling occurred. Error bars represent the standard deviation. .... 65
- Figure 33: Comparison of Glucose and Lactate concentrations in g/L on the primary y-axis and pH on the secondary y-axis over the cultivation period of infected Vero cells on FibraCel discs. A total medium exchange was performed 144 and 240 hps. On the last medium exchange infection with LCMV with a MOI of 0.003 FFU/nuclei occurred (dotted line). 24 and 48 hps no sampling occurred. 264 hps no pH was measured. Error bars represent the standard deviation. .... 66
- Figure 34: Comparison of Glucose consumption – and Lactate production – rate in mol/cell/h on the primary y-axis and the molar Lactate / Glucose-yield on the secondary y-axis over the cultivation period of infected Vero cells on FibraCel discs. A total medium exchange was performed 144 and 240 hps. On the last medium exchange infection with LCMV with a MOI of 0.003 FFU/nuclei occurred (dotted line). 24 and 48 hps no sampling occurred. Error bars represent the standard deviation.. 67
- Figure 35: Viral titer of LCMV per mL, produced by Vero cells on FibraCel discs over the cultivation period on the primary y-axis in log scale. Cells were infected with LCMV with a MOI of 0.003 FFU/nuclei 240 hps (dotted line). On the secondary y-axis the specific Titer in FFU/nuclei in log scale is displayed. Missing titer values after the infection where lower than the detection limit of the chosen dilution of the assay. Viral titer values were multiplied by a factor of 2.5 for better comparability with titer values of experiments with 80 mL working volume due to the increased working volume of 200 mL. Error bars represent the standard deviation. .... 68
- Figure 36: Comparison of the propagation of infected and uninfected suspension HEK-293 cells in cells/mL over the course of cultivation on the primary y-axis. On the secondary y-axis the calculated growth rate in  $h^{-1}$  is displayed for infected and

uninfected cells. Cells were infected at seeding of $3 \times 10^5$ cells/mL with LCMV with a MOI of $10^{-5}$ FFU/cell. Error bars represent the standard deviation. ....	69
Figure 37: Comparison of Glucose and Lactate concentrations in g/L of infected and uninfected suspension HEK-293 cells over the course of cultivation on the primary y-axis. On the secondary y-axis the pH is displayed for infected and uninfected cells. Cells were infected at seeding of $3 \times 10^5$ cells/mL with LCMV with a MOI of $10^{-5}$ FFU/cell. Error bars represent the standard deviation. ....	70
Figure 38: Comparison of Glucose consumption and Lactate production rate in mol/cell/hour of infected and uninfected HEK293 cells on the primary y-axis against the cultivation period. On the secondary y-axis the molar Lactate/Glucose yield is plotted. The error bars represent the standard deviation. ....	71
Figure 39: Viral titer of LCMV per mL, produced by HEK-293 suspension cells over the cultivation period plotted on the primary y-axis. Infection with LCMV with a MOI of $10^{-5}$ FFU/cell occurred at seeding. On the secondary y-axis the viral titer per cell in FFU/cell is displayed. Error bars represent the standard deviation. ....	71
Figure 40: Supportive graph for comparison of viral titer of different cultivation modes by viral titer [FFU/mL], specific titer [FFU/cell] and viral yield [FFU/FFU] at titer peak. Error bars represent the standard deviation. ....	79
Figure 41: Logarithmic transformed model for the thermal heat inactivation of LCMV in PF26#278-HEK293 .....	98
Figure 42: Certificate of Analysis of Vero cells obtained from ECACC. 1/3 .....	99
Figure 43: Certificate of Analysis of Vero cells obtained from ECACC 2/3 .....	100
Figure 44: Certificate of Analysis of Vero cells obtained from ECACC 3/3 .....	101

## 7.2 List of Tables

Table 1: Specification of volumes used for passaging of adherent cells.....	18
Table 2: 3 <sup>2</sup> -full factorial central composite face experiment design set-up for the determination of an optimal MOI and SCD of adherently growing Vero cells. ....	25
Table 3: DoE set-up for evaluation of cell growth inhibiting factors on Vero cells in microcarrier cultivation.....	28
Table 4: Lower and upper boundaries for predicted viral titers calculated based on the established model and viral titer results in FFU/mL for each sampling point. ....	54
Table 5: Cell density, specific titer and viral yield of Vero cells 96 hpi with LCMV. Cells were seeded with $2 \times 10^4$ cells/cm <sup>2</sup> and infected with an MOI of 0.003 FFU/cell 72 hps. ....	54
Table 6: Excerpt of an overview of data on influenza virus production (Genzel and Reichl, 2009). ....	81

## 7.3 List of Pictures

Picture 1: Phase contrast images of Vero cells over the course of cultivation. ....	45
Picture 2: Phase contrast images of Vero cells on Cytodex 1 microcarrier over the course of cultivation. ....	55
Picture 3: Phase contrast images of comparison of Vero cells with Accutase remains versus Accutase free medium. ....	57
Picture 4: Phase contrast images of propagation of Vero cells on 3 g/L Cytodex 1 microcarrier over the course of cultivation. ....	61

## 7.4 Bibliography

- Ammerman, N.C., Beier-Sexton, M., Azad, A.F., 2008. Growth and Maintenance of Vero Cell Lines, in: Coico, R., Kowalik, T., Quarles, J., Stevenson, B., Taylor, R. (Eds.), *Current Protocols in Microbiology*. John Wiley & Sons, Inc., Hoboken, NJ, USA. doi:10.1002/9780471729259.mca04es11
- Armstrong, C., Lillie, R.D., 1934. Experimental Lymphocytic Choriomeningitis of Monkeys and Mice Produced by a Virus Encountered in Studies of the 1933 St. Louis Encephalitis Epidemic. *Public Health Rep.* 1896-1970 49, 1019. doi:10.2307/4581290
- Aunins, J., Laska, M., Phillips, B., Otero, J., 2011. Chemical engineering perspectives on vaccine production. *Chem Eng Prog* 34–37.
- Barrett, P.N., Mundt, W., Kistner, O., Howard, M.K., 2009. Vero cell platform in vaccine production: moving towards cell culture-based viral vaccines. *Expert Rev Vaccine* 607–618.
- Choi, Y., Chang, J., 2013. Viral vectors for vaccine applications. *Clin. Exp. Vaccine Res.* 2, 97. doi:10.7774/cevr.2013.2.2.97
- Clark, J.M., Hirtenstein, M.D., 1981. Optimizing culture conditions for the production of animal cells in microcarrier culture. *Ann. N. Y. Acad. Sci.* 369, 33–46.
- Côté, J., Garnier, A., Massie, B., Kamen, A., 1998. Serum-free production of recombinant proteins and adenoviral vectors by 293SF-3F6 cells. *Biotechnol. Bioeng.* 59, 567–575.
- Cruz, H.J., Freitas, C.M., Alves, P.M., Moreira, J.L., Carrondo, M.J.T., 2000. Effects of ammonia and lactate on growth, metabolism, and productivity of BHK cells. *Enzyme Microb. Technol.* 27, 43–52.
- Donis, R.O., Chen, L.-M., Davis, C.T., Foust, A., Hossain, M.J., Johnson, A., Klimov, A., Loughlin, R., Xu, X., Tsai, T., Blayer, S., Trusheim, H., Colegate, T., Fox, J., Taylor, B., Hussain, A., Barr, I., Baas, C., Louwerens, J., Geuns, E., Lee, M.-S., Venhuizen, L., Neumeier, E., Ziegler, T., 2014. Performance characteristics of qualified cell lines for isolation and propagation of influenza viruses for vaccine manufacturing. *Vaccine* 32, 6583–6590. doi:10.1016/j.vaccine.2014.06.045
- Durocher, Y., Perret, S., Kamen, A., 2002. High-level and high-throughput recombinant protein production by transient transfection of suspension-growing human 293-EBNA1 cells. *Nucleic Acid Res* 30, E9.



- EMA, 2010. Guideline on quality, non-clinical and clinical aspects of live recombinant viral vectored vaccines.
- Ferreira, T.B., Carrondo, M.J.T., Alves, P.M., 2007. Effect of ammonia production on intracellular pH: Consequent effect on adenovirus vector production. *J. Biotechnol.* 129, 433–438. doi:10.1016/j.jbiotec.2007.01.010
- Genzel, Y., 2015. Designing cell lines for viral vaccine production: Where do we stand? *Biotechnol. J.* 10, 728–740. doi:10.1002/biot.201400388
- Genzel, Y., Reichl, 2009. Continuous cell lines as a production system for influenza vaccines.pdf.
- Josefsberg, J.O., Buckland, B., 2012. Vaccine process technology. *Biotechnol. Bioeng.* 109, 1443–1460. doi:10.1002/bit.24493
- Knipe, D.M., Howley, P.M. (Eds.), 2013. *Fields virology*, 6th ed. ed. Wolters Kluwer/Lippincott Williams & Wilkins Health, Philadelphia, PA.
- Le Ru, A., Jacob, D., Transfiguracion, J., Ansorge, S., Henry, O., Kamen, A.A., 2010. Scalable production of influenza virus in HEK-293 cells for efficient vaccine manufacturing. *Vaccine* 28, 3661–3671. doi:10.1016/j.vaccine.2010.03.029
- Li, S., Locke, E., Bruder, J., Clarke, D., Doolan, D.L., Havenga, M.J.E., Hill, A.V.S., Liljestrom, P., Monath, T.P., Naim, H.Y., Ockenhouse, C., Tang, D.C., Van Kampen, K.R., Viret, J.-F., Zavala, F., Dubovsky, F., 2007. Viral vectors for malaria vaccine development. *Vaccine* 25, 2567–2574. doi:10.1016/j.vaccine.2006.07.035
- Lin, Y.-C., Boone, M., Meuris, L., Lemmens, I., Van Roy, N., Soete, A., Reumers, J., Moisse, M., Plaisance, S., Drmanac, R., Chen, J., Speleman, F., Lambrechts, D., Van de Peer, Y., Tavernier, J., Callewaert, N., 2014. Genome dynamics of the human embryonic kidney 293 lineage in response to cell biology manipulations. *Nat. Commun.* 5, 4767. doi:10.1038/ncomms5767
- Lininger, M., Zuniga, A., Naim, N., 2007. Use of viral vectors for the development of vaccines. *Exp Rev Vaccines* 255–266.
- Logos biosystems, 2014. Luna Automated Cell Counter User manual.
- Merten, O.-W., Schweizer, M., Chahal, P., Kamen, A.A., 2014. Manufacturing of viral vectors for gene therapy: part I. Upstream processing. *Pharm. Bioprocess.* 2, 183–203.
- Microcarrier Cell Culture Principles and Methods, 2013. . GE Healthcare.
- Nova Biomedical, 2001. Nova Stat Profile pHox - Reference manual.

## References

- Ortiz-Riano, E., Cheng, B.Y.H., Carlos de la Torre, J., Martinez-Sobrido, L., 2013. Arenavirus reverse genetics for vaccine development. *J. Gen. Virol.* 94, 1175–1188. doi:10.1099/vir.0.051102-0
- Pham, P.L., Perret, S., Cass, B., Carpentier, E., St-Laurent, G., Bisson, L., Kamen, A., Durocher, Y., 2005. Transient gene expression in HEK293 cells: Peptone addition posttransfection improves recombinant protein synthesis. *Biotechnol. Bioeng.* 90, 332–344. doi:10.1002/bit.20428
- Sigma-Aldrich Co. LLC, 2016. Product Information Sigmacote.
- Sureau, P., 1987. Rabies vaccine production in animal cell culture. *Adv Biochem Eng Biotechnol* 112–125.
- ThermoFisher Scientific, 2014. 5029\_A1110501\_Accutase.pdf.
- Tritsch, G., Moore, G., 1962. Spontaneous decomposition of glutamine in cell culture media. *Exp Cell Res* 360–4.
- Ura, T., Okuda, K., Shimada, M., 2014. Developments in Viral Vector-Based Vaccines. *Vaccines* 2, 624–641. doi:10.3390/vaccines2030624
- Urata, S., Yasuda, J., 2012. Molecular Mechanism of Arenavirus Assembly and Budding. *Viruses* 4, 2049–2079. doi:10.3390/v4102049

## 8 Appendix

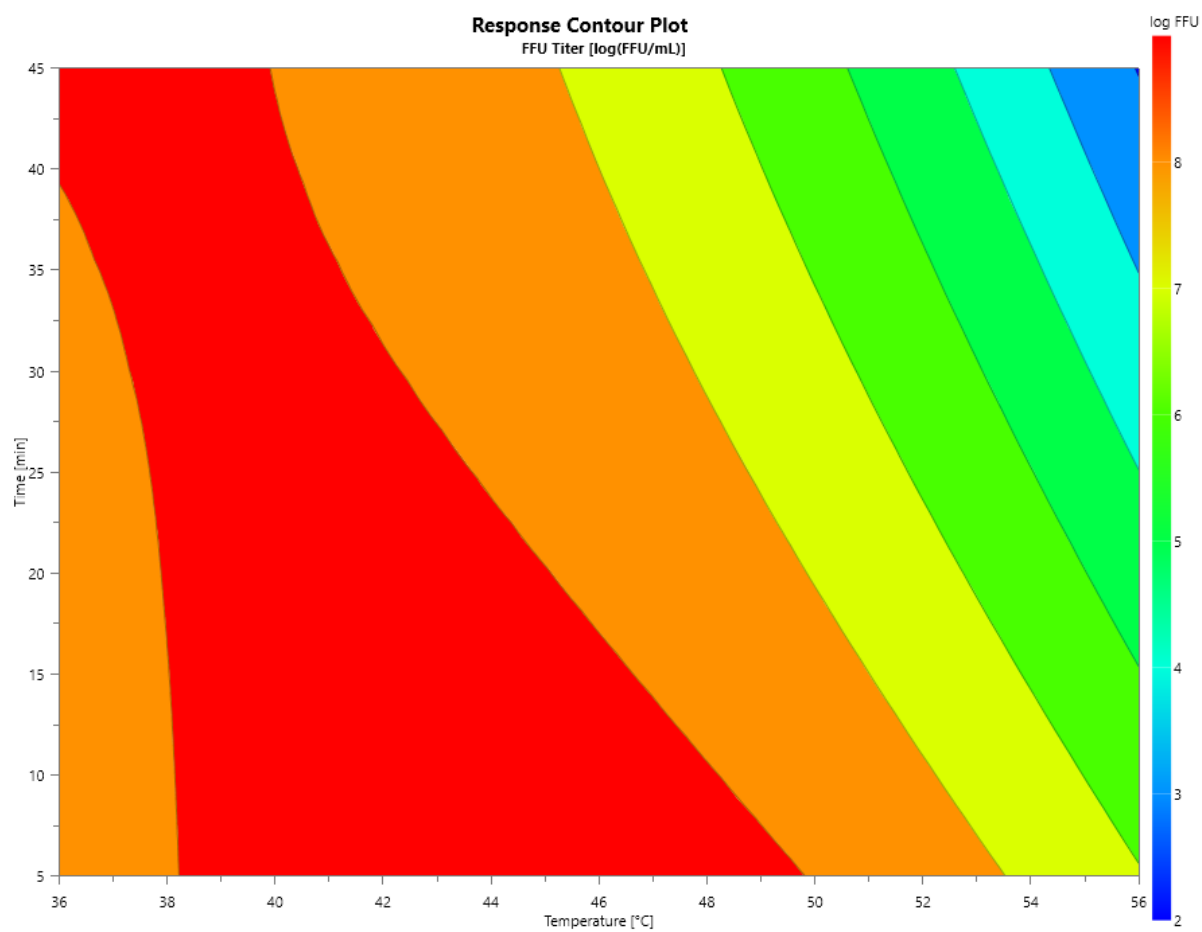




Figure 41: Logarithmic transformed model for the thermal heat inactivation of LCMV in PF26#278-HEK293

	<b>Certificate of Analysis</b>		<b>ECACC</b> European Collection of Cell Cultures
<b>Public Health England</b>		Operated by Public Health England	

**Product Description:** VERO (AC-Free) 08011101

**Lot Number:** 15D003

---

**Test Description:**  
Sterility Testing of Cell Banks. SOP ECC92

**Acceptance Criterion/Specification:**  
All positive controls (Bacillus subtilis and Candida albicans) show evidence of microbial growth (turbidity) and the negative controls show no evidence of microbial growth (clear).  
The criterion for a positive test is turbidity in any of the test broths. All broths should be clear for a negative test result.

**Test Number:** 53445

**Test Date:** 01/05/2015

**Result:** Pass

---

Authorised by  ECACC, Head of Quality      Date 04 JUN. 15

Page 1 of 1

Culture Collections, Public Health England, Porton Down, Salisbury, SP4 0JG, UK  
Tel: +44 (0)1980 612512 Email: culturecollections@phe.gov.uk

Figure 42: Certificate of Analysis of Vero cells obtained from ECACC. 1/3



**Product Description:** VERO (AC-FREE) 08011101

**Lot Number:** 15D003

**Test Description:**

Cell count, viability and confluency of cells on resuscitation from frozen. SOP ECC108

**Acceptance Criterion/Specification:**

were judged acceptable if they meet two of the following criteria:

- >70% viable cells
- $>2 \times 10^6$  total cells/amp
- Cell growth as expected within 2 days.

**Test Number:** 53552

**Test Date:** 04/05/2015

**Result:**  $2.82 \times 10^6$  91.1%

**Test Description:**

Detection of Mycoplasma by PCR using Mycoplasma-specific PCR Primers Validated by ECACC. SOP ECC73

**Acceptance Criterion/Specification:**

Positive controls yield a single 280 bp amplification product. Negative Control yields no amplified product. The criteria for a positive test result is the yield of a single 280bp PCR product.

**Test Number:** 53552

**Test Date:** 04/05/2015



**Result:** Pass

Authorised by *SBrooks* ECACC, Head of Quality Date 04 JUN 15.

Page 1 of 2

Culture Collections, Public Health England, Porton Down, Salisbury, SP4 0JG, UK  
Tel: +44 (0)1980 612512 Email: culturecollections@phe.gov.uk

Figure 43: Certificate of Analysis of Vero cells obtained from ECACC 2/3

 <b>Public Health England</b>	<b>Certificate of Analysis</b>	 <b>ECACC</b> European Collection of Cell Cultures Operated by Public Health England
-----------------------------------------------------------------------------------------------------------------------	----------------------------------------	------------------------------------------------------------------------------------------------------------------------------------------------------------------------------------

**Product Description:** VERO (AC-FREE) 08011101

**Lot Number:** 15D003

---

**Test Description:**  
 Detection of Mycoplasma using a Vero indicator cell line and Hoechst 33258 fluorescent detection system. SOP ECC137

**Acceptance Criterion/Specification:**  
 The Vero cells in the negative control are clearly seen as fluorescing nuclei with no cytoplasmic fluorescence. Positive control (M.hyorhirs) must show evidence of mycoplasma as fluorescing nuclei plus extra nuclear fluorescence of mycoplasma DNA. Positive test results appear as extra nuclear fluorescence of mycoplasma DNA. Negative results show no cytoplasmic fluorescence.

**Test Number:** 53552

**Test Date:** 04/05/2015

**Result:** None detected

---

**Test Description:**  
 Speciation by DNA bar-coding sequencing of the mitochondrial cytochrome c oxidase (COX) sub-unit 1 gene. The availability of published PCR primer sequences for this region has made this the gene of choice for speciation using this method. SOP ECC5

**Acceptance Criterion/Specification:**  
 A HeLa control is run as a standard and must be confirmed as human in order for the test run to be valid.  
 The pass criteria are that the top 5 matches must be the same as the expected species and the percentages matches must be above 95%.

**Test Number:** 53552

**Test Date:** 15/05/2015

**Result:** Pass

---

Authorised by *JBW* ECACC, Head of Quality      Date 04 JUN 15

Page 2 of 2

Culture Collections, Public Health England, Porton Down, Salisbury, SP4 0JG, UK  
 Tel: +44 (0)1980 612512 Email: culturecollections@phe.gov.uk

Figure 44: Certificate of Analysis of Vero cells obtained from ECACC 3/3

## STATUTORY DECLARATION

I declare that I have authored this thesis independently, that I have not used other than the declared sources / resources, and that I have explicitly marked all material which has been quoted either literally or by content from the used sources.

Vienna, October 2017

Philipp Andre

## EIDESSTATTLICHE ERKLÄRUNG

Ich erkläre hiermit an Eides statt, dass ich die vorliegende Arbeit selbständig verfasst, andere als die angegebenen Quellen/Hilfsmittel nicht benutzt, und die den benutzten Quellen wörtlich und inhaltlich entnommene Stellen als solche kenntlich gemacht habe.

Wien, Oktober 2017

Philipp Andre